
Article:
Maksoud, F.J., de la Paz, F.V., Hann, A. et al. (5 more authors) (2022) Porous biomaterials for tissue engineering: a review. Journal of Materials Chemistry B, 40. pp. 8111-8165. ISSN 2050-750X

https://doi.org/10.1039/d1tb02628c

Journal of
Materials Chemistry B

Materials for biology and medicine

Accepted Manuscript

This article can be cited before page numbers have been issued, to do this please use: F. J. Maksoud, F. V. de la Paz, A. Hann, J. Thanarak, G. Reilly, F. Claeyssens, N. Green and Y. S. Zhang, *J. Mater. Chem. B*, 2022, DOI: 10.1039/D1TB02628C.

This is an Accepted Manuscript, which has been through the Royal Society of Chemistry peer review process and has been accepted for publication.

Accepted Manuscripts are published online shortly after acceptance, before technical editing, formatting and proof reading. Using this free service, authors can make their results available to the community, in citable form, before we publish the edited article. We will replace this Accepted Manuscript with the edited and formatted Advance Article as soon as it is available.

You can find more information about Accepted Manuscripts in the Information for Authors.

Please note that technical editing may introduce minor changes to the text and/or graphics, which may alter content. The journal's standard Terms & Conditions and the Ethical guidelines still apply. In no event shall the Royal Society of Chemistry be held responsible for any errors or omissions in this Accepted Manuscript or any consequences arising from the use of any information it contains.

ROYAL SOCIETY OF CHEMISTRY

rsc.li/materials-b

View Article Online
DOI: 10.1039/D1TB02628C

Revision to TB-REV-11-2021-002628.R1

Porous Biomaterials for Tissue Engineering: A Review

Fouad Junior Maksoud[a,†], María Fernanda Velázquez de la Paz[b,†], Alice J. Hann[b], Jeerawan Thanarak[b], Gwendolen C. Reilly[b,c], Frederik Claeyssens[b,c,], Nicola H. Green[b,c,*], Yu Shrike Zhang[a,*]*

[a] Division of Engineering in Medicine, Department of Medicine, Brigham and Women's Hospital, Harvard Medical School, Cambridge, MA 02139, USA
[b] Department of Materials Science and Engineering, Kroto Research Building, North Campus, Broad Lane, University of Sheffield, Sheffield, S3 7HQ, UK
[c] INSIGNEO Institute for in silico Medicine, University of Sheffield, S3 7HQ, UK
[*] Emails: f.claeyssens@sheffield.ac.uk (F. Claeyssens); n.h.green@sheffield.ac.uk (N. H. Green); yszhang@research.bwh.harvard.edu (Y. S. Zhang)

[†] Equal contribution

View Article Online
DOI: 10.1039/D1TB02628C

Abstract
The field of biomaterials has grown rapidly over the past decades. Within this field, porous biomaterials have played a remarkable role in: *i*) enabling the manufacture of complex three-dimensional structures; *ii*) recreating mechanical properties close to those of the host tissues; *iii*) facilitating interconnected structures for the transport of macromolecules and cells; and *iv*) behaving as biocompatible inserts, tailored to either interact or not with the host body. This review outlines a brief history of the development of biomaterials, before discussing current materials proposed for use as porous biomaterials and exploring the state-of-the-art in their manufacture. The wide clinical applications of these materials are extensively discussed, drawing on specific examples of how the porous features of such biomaterials impact their behaviours, as well as the advantages and challenges faced, for each class of the materials.

Keywords
Polymers, Hydrogels, Fabrication Strategies, Bone Scaffolds, Auricular Tissue Grafts, Articular Cartilage Reconstruction, Vascular Regeneration, Pharmaceutical and Therapeutic Applications.

View Article Online
DOI: 10.1039/D1TB02628C

Abbreviations

1,4-BDDMA	1,4-Butanediol Dimethacrylate
3D	Three Dimensional
A-CNC	Aldehyde-Functionalized Cellulose Nanocrystals
ABM	Agent-Based Modelling
AFFP	Allogeneic Fibrin-Fibronectin Protein
Ag	Silver
AID	Average Invasion Depth
AMF	Axial Magnetic Field
Au	Gold
BCP	Bi-Calcium Phosphate
BMPs	Bone Morphogenetic Proteins
BMSCs	Bone Marrow-Derived Mesenchymal Stem Cells
C/T	Chloroform/Toluene
CA-CNC+H-POEGMA	Concentration of Aldehyde-Functionalized Cellulose Nanocrystals
CAD	Computer-Aided Design
CaO	Calcium Oxide
CaP	Calcium Phosphates
CDHA	Calcium-Deficient Hydroxyapatite
CLSM	Confocal Laser Scanning Microscope
CoCr	Cobalt-Chromium
CoCrMo	Cobalt-Chromium-Molybdenum
CPCs	Cardiac Stem Cells
CT	Computed Tomography

View Article Online
DOI: 10.1039/D1TB02628C

CuO	Copper Oxide
CuSO4	Copper Sulfate
DAPI	4',6-Diamino-2-Phenylindole
DECM	Decellularized Cartilage Extracellular Matrix
DLP	Digital Light Processing
DMD	Digital Micromirror Device
EBL	Electron Beam Lithography
ECM	Extracellular Matrix
ECs	Endothelial Cells
EHA80	2-Ethylhexyl Acrylate
FDA	The U.S. Food and Drug Administration
Fe	Iron
FFF	Fused Filament Fabrication
FGF-2	Fibroblast Growth Factor 2
GAG	Glycosaminoglycan
GAS	Glucosamine Sulfate
GECIs	Genetically Encoded Calcium Indicators
GelMA	Gelatin Methacryloyl
H-POEGMA	Hydrogel Poly(Oligoethylene Glycol Methacrylate
H6L	Lattice Solvent Molecules
hACs	Human Articular Chondrocytes
HAp	Hydroxyapatite
HDFs	Human Dermal Fibroblasts
HepG2	Heparin Cells

View Article Online
DOI: 10.1039/D1TB02628C

HF	Hydrofluoric Acid
HG	Hydrogel
HIPE	High Internal Phase Emulsion
hMSCs	Human Mesenchymal Cells
HT	Hydrothermally
HUVEC	Human Umbilical Vein Endothelial Cells
IBOA	Isobornyl Acrylate
IPNs	Interpenetrating Polymer Networks
KPS	Potassium Persulfate
MBG	Mesoporous Bioglass
MEBB	Melt Electrospinning-Based Bioprinting
Mg	Magnesium
MIBL	Masked Ion Beam Lithography
MID	Maximum Invasion Depth
MRI	Magnetic Resonance Imaging
MSC	Mesenchymal Stem Cells
MSNs	Mesoporous Silica Nanoparticles
NaBH4	Sodium Borohydride Solution
NaCl	Sodium Chloride
NaOH	Sodium Hydroxide
NFM	Nanofibres Meshes
NOA	Number of Anastomoses
OCP	Octacalcium Phosphate
P2O5	Phosphorus Oxide

View Article Online
DOI: 10.1039/D1TB02628C

P4HB	Poly(4-Hydroxybutyrate)
PBLG	Poly(Γ-Benzyl-L-Glutamate)
PCL	Poly(ε-Caprolactone)
PDA	Polydopamine
PDMS	Polydimethylsiloxane
PE	Polyethylene
PEG	Poly(Ethylene Glycol)
PEGTA	PEG-Tetra-Acrylate
PEO	Poly(Ethylene Oxide)
PG2	Porous Pullulan/Gelatin
PGA	Poly(Glycolic Acid)
PGS	Poly(Glycerol Sebacate)
PHA	Polyhydroxyalkanoates
PHBHHx	Poly(3-Hydroxybutyrate-co-3-Hydroxyhexanoate)
PHBV	Poly(3-Hydroxybutyrate-co-3-Hydroxyvalerate)
PLA	Poly(Lactic Acid)
PLCL	Poly(L-Lactide-co- ε-Caprolactone)
PLGA	Poly(Lactic-co-Glycolic Acid)
PLL	Poly(L-Lysine)
PMMA	Polymethylmethacrylate
PNIPAAM-Alg	Poly(N-Isopropylacrylamide)-Alginate
PO4	Phosphate
PolyHIPE	Polymerised High Internal Phase Emulsions
Post-OP	Postoperative

View Article Online
DOI: 10.1039/D1TB02628C

PP	Polypropylene
PPF	Poly(Propylene Fumarate)
pPOD	Printable Pharmaceutical Oral Dosage
PPy	Polypyrrole
PR	Positive Resist
PT	Polythiophene
Pt	Platinum
PTI	Poly(Lactic-co-Glycolic Acid)/B-Calcium Phosphate/Icariin
PU	Polyurethane
PVOH	Poly(Vinyl Alcohol)
rBC/Gel	Bacterial Cellulose-Gelatin
REDV	Arg-Glu-Asp-Val
RF	Random Fibre
RGD	Arginine-Glycine-Aspartic Acid
RMF	Radial Magnetic Field
ROSS	Ratio of Successful Sprouts
RP	Radial Pore-Oriented
SA	Sodium Alginate
SEBB	Solution Electrospinning-Based Bioprinting
SEM	Scanning Electron Microscopy
SFF	Solid Freeform Fabrication
SLA	Stereolithography
SLAM	Suspended Layer Additive Manufacture
SMPs	Shape-Memory Polymers

View Article Online
DOI: 10.1039/D1TB02628C

SPNs	Semi-Penetrating Networks
SR-inline-PCI-CT	Synchrotron Radiation Based X-Ray Inline Phase Contrast Imaging-Computed Tomography
SrBG	Strontium-Substituted Bioactive Glass
SSA	Specific Surface Area
TBVL	Total Blood Vessel Length
TBVLS	TBVL Per Initial Sprout
TCP	Tricalcium Phosphate
TE	Tissue Engineering
TEM	Transmission Electron Microscopy
Ti	Titanium
TiAlN	Titanium-Aluminium Nitride
TiO	Titanium Dioxide
TiO2NFs	Titanium Nanofibres
TMS	Trimodal Mesoporous Bioactive Glass Scaffolds
TN	Titanium Nitride
UHMWPE	Ultra-High-Molecular- Weight Polyethylene
VMMX	Volume-Stable Collagen Matrices
VN	Vanadium Nitride
VP	Vat-Polymerization
VSCM	Volume-Stable Collagen Matrices
β-TCP	B-Tricalcium Phosphate
μCT	Micro-Computed Tomography
μSLA	Micro-Stereolithography

View Article Online
DOI: 10.1039/D1TB02628C

Table of Contents

1. Introduction 11
2. Choice of Porous Materials 12
2.1. Polymers 12
2.1.1. Polymer Selection 12
2.1.2. Polymers and The Host Tissue 13
2.2. Hydrogels 16
2.3. Ceramics 19
2.4. Glass 20
2.5. Calcium Phosphate 22
2.6. Hydroxyapatite 25
2.7. Metals 26
3. Fabrication Strategies 28
3.1. Templating and Salt-Templating 28
3.2 Emulsion Templating 31
3.3. Freeze-Drying 34
3.4. Patterning 36
3.4.1. Cleanroom Techniques 37
3.4.2. Post-Treatment 38
3.5. Electrospinning 40
3.6. Bioprinting 43
3.6.1. Stereolithography Apparatus and Digital Light Processing 44
3.6.2. Inkjet Bioprinting 44
3.6.3. Laser-Assisted Bioprinting 45
3.6.4. Extrusion-Based Bioprinting 45
3.6.5. Electrospinning-Based Bioprinting 45
4. Applications 45
4.1. Bone Tissue Engineering 46
4.2. Auricular Tissue Engineering 48
4.3. Articular Cartilage Regeneration 53
4.4. Reconstructive Tissue Engineering 56
4.5. Vascular Regeneration 59
4.6. Pharmaceutical Applications 62
4.6.1. Drug Screening 63

View Article Online
DOI: 10.1039/D1TB02628C

4.6.2. Gene Therapy 64
4.6.3. Growth Factor and Drug Delivery 64
5. Conclusions 65
Acknowledgment 67
References 68

View Article Online
DOI: 10.1039/D1TB02628C

1. Introduction

The use of materials has long been of interest within the clinical field. Knowledge has been incorporated from several areas, including physical sciences, engineering, life sciences, and computer sciences, to generate the field of biomaterials science. The ultimate objective of these biomaterials is to enable tissue repair and regeneration, and eventually re-establish the structure and/or function of native tissues. A biomaterial should mimic the body, not necessarily in structure, but certainly in functionality (1).

Porous biomaterials have been demonstrated to *i*) be manufacturable into complex three-dimensional (3D) structures, *ii*) replicate mechanical properties similar to the host tissues; *iii*) form interconnected structures to enable transport of macromolecules and ingress of cells; and *iv*) behave as tissue-compatible implants, tailored to either interact or not with the host body (1). This review offers an overview of porous materials (*e.g.*, hydrogels, ceramics, polymers, glass, calcium phosphates (CaP), hydroxyapatite (HAp), and metals), their relevant features, promising manufacturing techniques, and the clinical applications that have been addressed by porous biomaterials.

Generally, 3D structures encompass pores at the nano-, micro-, and macroscales. Each pore size can act to improve the biological function of the implant. Macropores (100-500 μm) should be interconnected and allow surface cell attachment, tissue ingrowth, and vascularization (2). Micropores (<100 μm) and nanopores (<100 nm) (3) allow further delivery of biomolecules and ions. Various fabrication techniques, at different stages of development, are available for creating multiple pore scales in an interconnected cellular framework, *i.e.*, a hierarchical porosity, for a range of porous biomaterials. Widely used fabrication techniques include templating and salt-templating, freeze-drying, patterning, post-treatment, 3D bioprinting, emulsion, and electrospinning, among others. In particular, rapid prototyping techniques are commonly used in tissue engineering over conventional techniques due to the advantage of being able to develop computer-controlled designs *a priori*. Based on computer-aided design (CAD), some additive manufacturing techniques, such as stereolithography (SLA)/digital light processing, selective laser sintering, and fused filament fabrication are also being used to successfully produce interconnected macro- and microstructures (4,5).

This review aims to introduce and report the latest developments in the rapidly expanding field of porous biomaterials for tissue engineering applications. There are many excellent reviews of porous biomaterials for specific applications in existence; however this review will provide a broad overview, in order to demonstrate the extensive applications of this important category of biomaterials and wide benefits to the field of tissue engineering and regenerative medicine (6–10). We will first present the choices of porous biomaterials that have been successfully manufactured onto bio-based constructs, including their origin, advantages, and limitations. Secondly, we will describe the principles and capabilities of the manufacturing techniques used to fabricate porous scaffolds that mimic the prospective host tissues. Lastly, we will discuss some key applications of these porous biomaterials, their current challenges, and future opportunities.

2. Choice of Porous Materials

View Article Online
DOI: 10.1039/D1TB02628C

A wide variety of materials and their blends are available and can be selected according to Ashby diagrams (11). Material choice is driven by the need to mimic the conformation, configuration, and mechanics of the target native tissue, for both the macro and microcomponents. Porous materials offer variable local structures that cannot be found in bulk; they work as the framework for neo-tissue formation, whilst allowing and even facilitating cells to interact within the material and the body's environment.

The next step is manufacturing a successful porous construct. The most important elements to consider can be divided into the physical and the chemical/biological properties. Physical features include pore geometry, pore size, pore homogeneity and distribution, porosity, interconnectivity, hydrophobicity, and mechanical properties (compressive and tensile strengths, equilibrium modulus, fatigue properties, among others). Chemical characteristics influence a material's cytocompatibility and bioactivity, enhancing cell adhesion, proliferation, migration, and differentiation. Other characteristics to take into account are rheological properties, degradability, and immunoreactivity. In this section, examples from the most commonly used materials and their porous features are discussed.

2.1. Polymers

The chemical structure, configuration and conformation of the monomers and the connection between the polymer chains define the mechanical and chemical properties of a polymer. For this reason, polymers are suitable for use in a wide range of biomaterials and tissue engineering areas. Additionally, polymers can be used in a solid, liquid, and gelled state. For example, poly(ethylene glycol) (PEG) can be manufactured as a bulk material, or as a gel-like one, which makes it versatile for blending as a hydrogel (12) or bulk polymer (13). Porous polymers coming from both natural and synthetic sources have been proposed for soft and hard tissue applications; the most important features and applied examples can be found below.

2.1.1. Polymer Selection

Through tailored manufacturing techniques, a wide variety of macro and micro morphologies can be obtained, as shown in **Fig. 1A**. Among the most important factors to consider when choosing the right polymer are their rheological and mechanical properties, their interaction with water, their crosslinking mechanisms, degradation properties, and cell interactions, illustrated in **Fig. 1B**.

Thermoplastic porous materials have been proposed for cardiac (14,15), corneal (16), urogynecological (17), chondral (18,19), neuronal (20), and vascular applications (20–22), among others. Thermoset elastomers are often stiffer and have been studied for bone (23,24), maxillofacial prostheses (25,26), and dental applications (27,28). Promising elastomeric biomaterials include poly(glycerol sebacate) (PGS) (29,30), poly(ε-caprolactone) (PCL) (31), and silicone/polydimethylsiloxane (PDMS) (32–34). These materials are malleable, and mimic native soft tissues mechanical properties; they are cost-efficient and they have shown positive interactions with cellular environments, not only facilitating cell proliferation within the scaffolds but allowing differentiation to occur (35,36).

View Article Online
DOI: 10.1039/D1TB02628C

A particular sub-group of thermoset polymers, *i.e.* shape-memory polymers (SMPs) have gained special attention as resorbable materials (37), wound dressings/scar management (38,39), and drug carriers (40,41). For example, citric acid-based elastomers were developed with shape-memory effects sensitive to anatomical temperatures for the controlled release of drugs (42). Even though SMPs are commonly proposed for soft tissue engineering, the versatility of some materials have enabled the use of SMPs for tissue engineering applications requiring stiffer materials. For example, PCL has been proposed as a perivascular wrap which is mouldable at body temperature, and allows the scaffold to mimic the patient's venous geometry (43). In a similar research direction, porous PCL-SMP scaffolds were developed as "self-fit" cranio-maxillo facial bone (44) and femoral defects (44,45).

Finally, conjugated polymers are polymers with a backbone that alternates single- and double-bonds, which creates delocalized π-electrons which makes them electrically conductive (46). As they are softer than metals, these polymers have been used to form porous matrices for neural probes (47), ocular drug delivery systems (48), and to support bone regeneration (49). Moreover, conjugated polymers have found a niche market in bioelectronics; they are easy to manufacture and possess tailored sol-gel structures whilst maintaining the benefits of their optical and electronic properties (50). For example, the biocompatibility of porous and non-porous polypyrrole (PPy) tri-layer actuators were tested *in vivo* (51). The porous material (pore size: 150 μm) encouraged tissue growth; however, the pores promoted delayering of the actuator, releasing debris in the host tissues. Similar pore sizes have been explored with polythiophene (PT)-PCL scaffolds, showing good osteoblast cell adhesion and proliferation (52). Nonetheless, PPy has proved to excel for controlled drug release (53–55). Similarly, polyaniline has been mixed with soft polymers such as silicone (56) and polyhydroxyalkanoates (PHAs) (57) as antimicrobial drug carriers for tissue engineering. In particular, poly(3-hydroxybutyrate-co-3-hydroxyvalerate) (PHBV) is a PHA with antibacterial properties and can be used as a coating for metal porous scaffolds for bone regeneration applications, as shown in **Fig. 1C**.

The intermolecular forces between the polymeric chains define the elasticity and associated mechanical properties of the material (*e.g.*, tensile and compressive strengths, toughness, failure strain). Graphs in **Fig. 1D** compare the compressive strengths and stiffness of various materials used as biomaterials, specifically as porous structures. As observed, mechanical properties of polymers vary as the porosity changes, allowing porous polymers to be used in multiple tissue engineering applications.

2.1.2. Polymers and The Host Tissue

Polymers with low protein adsorption and positive cell adhesion usually show a reduced immune response. Polymeric materials are also able to offer cell binding motifs and promote cellular interactions, important for other tissue engineering applications, such as bone tissue engineering (58). Biocompatible porous materials include synthetic polymers (59) or natural polymers. The latter ones can be further categorised into polysaccharide-based polymers (*e.g.*, chitin, chitosan, alginate, glycosaminoglycans (GAGs) such as chondroitin sulfate (18,60)) and protein-based polymers (*e.g.*, collagens (61), gelatin (62–64), silk (26,65–67)).

View Article Online
DOI: 10.1039/D1TB02628C

Biodegradable polymers are used as temporary structures that are broken down by hydrolytic or enzymatic processes, or a combination of both. Degradation processes can happen at the surface of the material, the bulk, or as a mixture. **Fig. 1B** shows the most important elements to take into consideration when manufacturing and processing porous polymers aimed for clinical research.

Porous natural polymers usually degrade through the action of enzymes and are mainly used for sutures and patches for wound healing and post-surgery wound care (68,69). For example, Wang *et al.* built a 3-layered "sandwich" structure scaffold with gradient pore size (167 μm on the outside layers and 87 μm as inner layer) and achieved superior wound healing in an *in vivo* murine model *via* increased granulation tissue formation and wound re-epithelialization (69). Similarly, highly porous (70-95%) hyaluronic acid constructs for cutaneous tissue repair have been jet-spun; the centrifugal forces expel a polymer melt that is subsequently stretched by a combination of the collector's quick rotation and the air flow (70). Their porosity was controlled by rehydration, as they observed water absorption decreased directly proportional to the hydration time; and were tailored to keep 80% of their integrity after 1 week. Silk is another natural polymer widely used as biomaterial. Indeed, the Kaplan group highlighted the amazing potential of silk for biomaterials in an early high impact review (71). Recently this group has also been working on porous silk constructs for tissue engineering and Bosio *et al.* have reported gel-spun degradable microtubes with pores of ~20 μm for microvascular grafts (65). They noticed that cell numbers were low for the first 14 days, but scaffolds maintained their mechanical properties when blended with low concentrations of poly(ethylene oxide) (PEO). To offset the cellular reactions, tubes with pores between 60 and 80 μm were functionalized with Arg-Glu-Asp-Val (REDV) peptides and showed an improved cell adhesion (66).

The main degradation mechanism for synthetic degradable polymers in water is *via* hydrolytic breaking of labile chemical bonds in their polymer backbone. The most commonly used porous synthetic polymers are polyesters (including polyester-based polyurethanes (PU)), for both weight- and non-weight-bearing applications. For example, poly(glycolic acid) (PGA), poly(lactic acid) (PLA), and PCL have been proposed as porous nerve guide conduits. The three materials have different degradation times *in vivo*. PGA will start degrading a few hours after implantation and normally degrades along a week to a month timescale (63) PLA remains in the body for up to 6 months, while PCL can take 1-2 years to degrade (72,73). Despite supporting cell growth, most synthetic polymers are hydrophobic and can release acidic byproducts while degrading (74); natural polymer coatings such as zein (75) and chitosan (76), as well as fibroin and gelatin have been proposed to improve cell adhesion and growth onto synthetic polymers (64,77).

Polymeric materials have already shown significant clinical successes. Biostable polymers are non-degradable materials frequently used in musculoskeletal repair and encapsulated cell therapies. PE has a successful track record for bone implants (78–80) and was recently investigated for cardiovascular applications, *e.g.*, heart valves (81,82). Ultra-high-molecular-weight polyethylene (UHMWPE) is commonly used as an articulating material in total hip/knee replacements due to its chemical inertness, high biostability and compatibility with the joint space. Also, novel applications of this material have raised interest in the biomedical field. For example, UHMWPE porous aerogels (porosity 94-97% and pores 2-5 μm) showed tailorable mechanical properties, which could benefit cell interactions (83). Homogeneous and larger pore sizes (80-700

View Article Online
DOI: 10.1039/D1TB02628C

μm) have been proposed to mimic the trabecular bone's properties, using salt-leached UHMWPE scaffolds, with resulting mechanical properties within the lower ranges of the target tissue (84).

Contrastingly, polypropylene (PP) is generally used for the regeneration of soft tissues. PP meshes have been previously used for hernia and pelvic floor repair (85), however, they have shown undesired inflammatory reactions (86). Recently, scaffolds have blended PP with a dopamine-functionalized polysaccharide derived hydrogel to form PP-co-(OCMC-DA/CMCS) abdominal meshes minimising abdominal adhesions, whilst supporting the deposition of collagen around the mesh and its integration with the abdominal wall (87).

Recent studies have explored the encapsulation of cells, drugs, and biomolecules within both degradable and non-degradable porous polymeric membranes. For example, porous nanocomposites and silicone have been used to deliver nucleic acids and support drug delivery techniques (88).

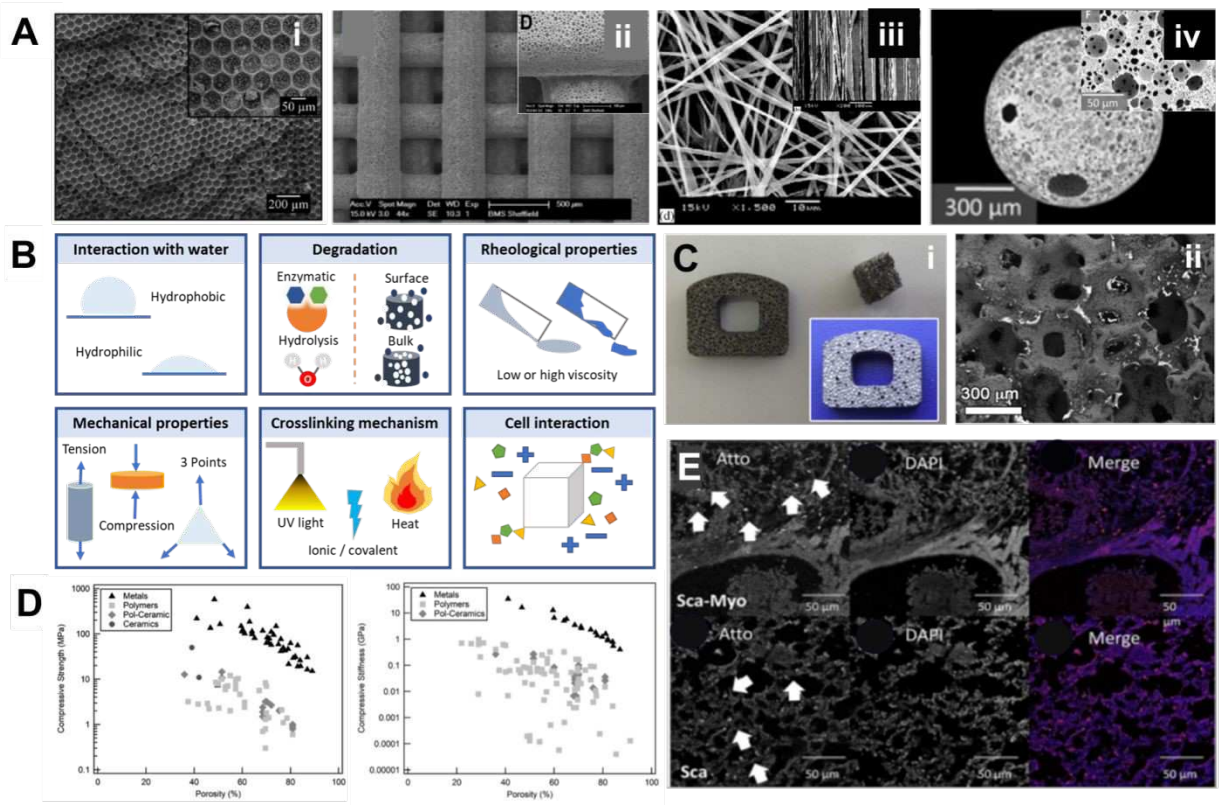

Fig. 1. *Polymer materials have numerous origins, resulting in a wide variety of materials rich in different properties. A) SEM pictures of: i) Monodisperse, interfacial initiated poly(1,4-BDDMA) foams with 5 mol % of the water-soluble initiator KPS with pore sizes of around 70 μm (top left). ii) IBOA+UV-234 'woodpile' scaffold. iii) AMF and RMF electrospun fibres. iv) Modulated particle diameter of model compositions and pore diameter of model compositions (top left). B) Some of the important factors to take into account when designing and manufacturing a polymeric biomaterial. C) i) Porous Ta TM cross-section coated with a PHBV 10% w/v emulsion and its SEM micrograph ii). D) Data compiled from existing literature showing compressive strength versus porosity and compressive stiffness versus porosity for 3D-printed biomaterials of all architectures for various material types. E) Histological assessment of PHA/PCL porous scaffolds seeded with cardiac stem cells (CPCs). Views [nuclear (DAPI), and label (Atto) presented in grayscale, and fused shown in colour (Atto-red, DAPI-blue)], indicating CPC retention (H, K, N) within the scaffold and myocardium (white arrows). Reproduced from Open Source from Ai (89), Aii (90), E (14), and with permission of Elsevier from Aiii (20), Aiv (23)), C:i-ii (24) and D (91).*

View Article Online
DOI: 10.1039/D1TB02628C

Abbreviations: *AMF: Axial Magnetic Field; (1,4-BDDMA): 1,4-Butanediol Dimethacrylate; Cpcs: Cardiac Stem Cells; DAPI: 4',6-Diamino-2-Phenylindole; IBOA: Isobornyl Acrylate; KPS: Potassium Persulfate; PCL: Poly(ε-Caprolactone); PHA: Polyhydroxyalkanoate; PHBV: Poly(3-Hydroxybutyrate-Co-3-Hydroxyvalerate); RMF: Radial Magnetic Field.*

2.2. Hydrogels

Hydrogels are formed from crosslinked hydrophilic polymers, and can hold large amounts of water (92). They can form single or multiple polymeric networks. When two polymers are combined these can be defined as double or dual networks and, depending on the constituent polymer structures, they can be classified as semi-interpenetrating polymer networks (semi-IPNs, combining a crosslinked and a linear polymer) or interpenetrating polymer networks (IPNs, combining two crosslinked polymers), as displayed in **Fig. 2A** (93). Hydrogels have emerged as popular materials within regenerative medicine due to their ability to mimic a highly hydrated 3D soft tissue environment (**Fig. 2B**) with a variety of external and internal geometries (**Fig. 2C**). The porosity, pore size and pore shape of a hydrogel can be varied both by materials formulation (*e.g.*, the amount of water within the hydrogel) and the manufacturing technique and balancing these can yield hydrogels with interesting internal pore geometries. **Fig. 2D** shows the range of pore morphologies obtained from directional freezing *via* freeze-casting aerogels at different dispersion and weight ratios and demonstrates that radically different pore geometries can be obtained (sponge-like, columnar, or lamellar). The directionality within the internal structure of the hydrogel results in an anisotropic stress-strain response of this material upon compression (**Fig. 2E**). This generates tuneable characteristics including mechanical properties such as resistance to tension and compression, related to material memory and point of break (**Fig. 2F**). These factors influence degradation rates and molecule diffusibility, as well as making them an attractive option for controlled cell and drug delivery, and cell encapsulation (94).

Hydrogels allow for passive diffusion of oxygen, nutrients, and other water-soluble molecules but an important challenge arises from their inability to support diffusion throughout larger-scale constructs, with levels often falling below those required for viable tissue engineering solutions (95). Various methods have been developed for the fabrication of hydrogel constructs with macroporous architectures, designed to enhance the viability of cells within the scaffolds (**Fig. 2G**). However, the pores often collapse due to the generally weak mechanical properties and high-water content of the material. Although increasing crosslinking and polymer concentration may lead to increased mechanical stability of the porous structure, this may give rise to undesirable changes within the microenvironment and resultant mechanotransduction processes that may alter the differentiation of the cultured cells (96). Furthermore, denser polymer concentrations may be seen to interfere with cells' extracellular matrix (ECM) deposition and migration (97,98).

Gelatin is low-cost, non-immunogenic, and degradable, making it an attractive option for the development of biomaterials. Gelatin also contains cell-binding motifs such as the arginine-glycine-aspartic acid (RGD) peptide sequence, which promotes attachment and viability of encapsulated cells (99). Modification of gelatin with methacrylic anhydride to form gelatin methacryloyl (GelMA) has become increasingly popular, as it allows for the production of a photocurable hydrogel with tunable physical and chemical properties whilst maintaining the biocompatibility of gelatin (100,101). The latter feature has opened the opportunity for hydrogels to be used as inks for bioprinting techniques. Billiet *et al.* demonstrated the printing of cell-laden GelMA hydrogels for the production of mechanically stable scaffolds (63). High concentrations

View Article Online
DOI: 10.1039/D1TB02628C

of GelMA (10-20% w/v) showed high printability and allowed for the fast-physical gelation and an excellent 3D shape fidelity resulting in a 100% interconnected pore network. Finally, GelMA has also been explored for its ability to permit physical diffusion and allow for transport of biological molecules through the hydrogel, aiding cellular mechanisms (102).

Alginate is another biodegradable and biocompatible polysaccharide and can be naturally derived from seaweed. You *et al.* produced alginate scaffolds with various levels of porosity varying the contact angle between strands whilst using sequential strand deposition (103). This methodology usually uses automatic dispensing systems, and sometimes tends towards pneumatic dispensing mechanism (also known as bioplotters) that deposit strand-like materials on a surface and are useful for 2D and 3D scaffolds, in a process similar to fused filament fabrication (FFF). Researchers found that a 2% w/v sodium alginate-based hydrogel with a polyethylenimine crosslinker was optimal for maintaining the structure. Optimisation of the calcium ion concentration (used as the crosslinker) produced a mechanically stable, porous scaffold with controlled degradation rates. However, unlike gelatin, alginate lacks cellular adhesion sites, limiting its uses for cell culture. The same group recently fabricated similar porous structures but using a blend of gelatin and sodium alginate to overcome the poor cellular adhesion to alginate (104).

Additive manufacturing can also create micro- and nanoporous hydrogels. Suspended layer additive manufacture (SLAM) has been developed as an alternative to the high costs of 3D printing. SLAM allows low-viscosity hydrogels (between 0.25% and 1.0% w/v) to be extruded at room temperature, preserving their newly formed structure by submersion in a self-healing fluid-gel supporting agarose matrix (105). Biodegradable hydrogels such as poly(*N*-isopropylacrylamide-co-vinylpyrrolidone-co-methacrylate-polylactide) have been used in conjunction with mannitol as a porogen, to facilitate the healing response by encouraging rapid cellular infiltration. Positive cell infiltration and macrophage polarisation was promoted a few days after the injection (106) (**Fig 2H**).

More viscous hydrogels can be processed using techniques that use hydrogels as colloids, *e.g.*, emulsion-templating and freeze-drying (107). For example, GelMA-PEO emulsions created a microporous hydrogel which could then be used as a photocrosslinkable bioink to form highly interconnected and hierarchical pores, and support cell proliferation and spreading (94,108–110). Similarly, vascular grafts were manufactured from PCL-gelatin by combining electrospinning and freeze-drying methods for the controlled release of heparin (111).

View Article Online
DOI: 10.1039/D1TB02628C

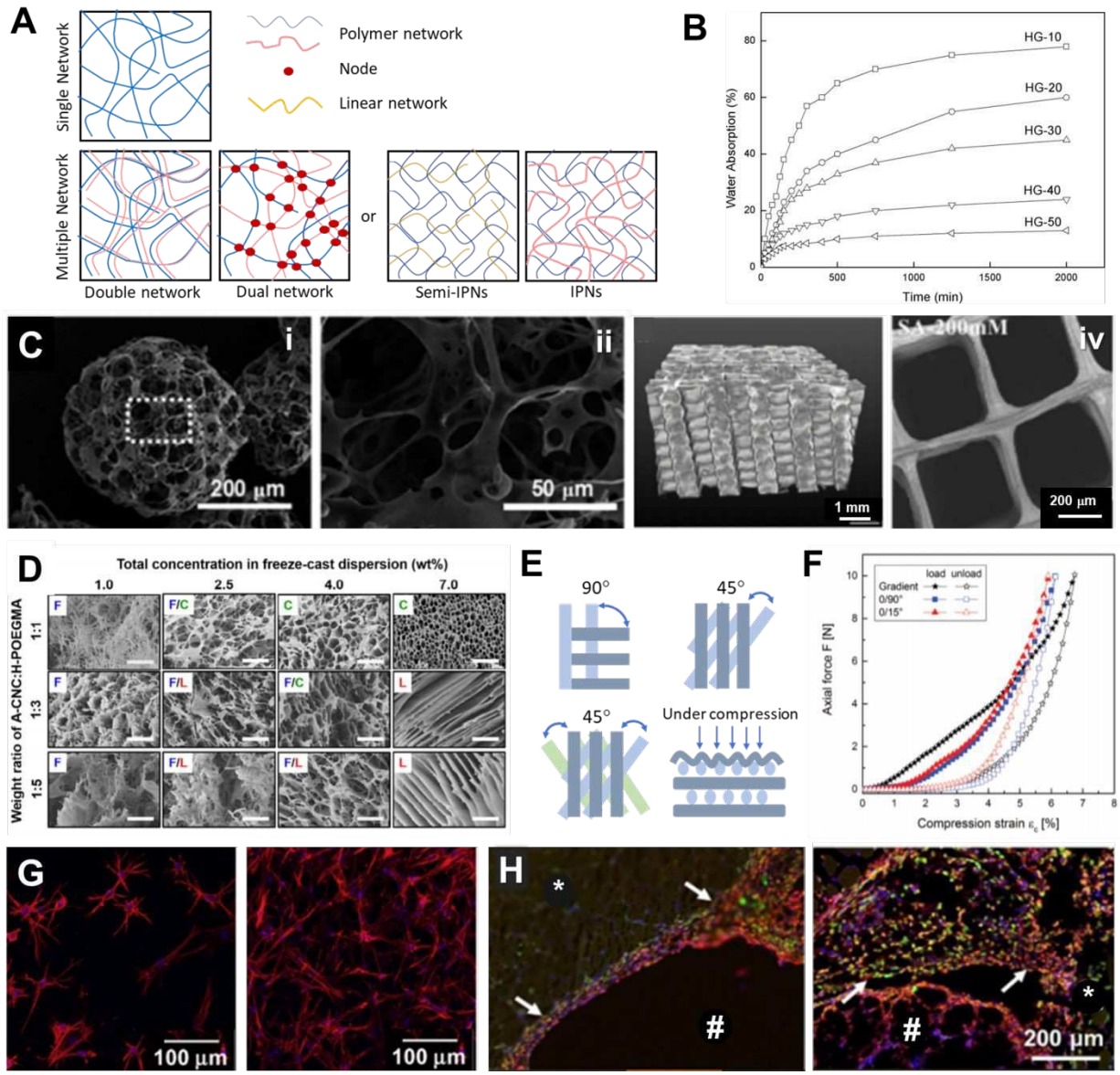

***Fig. 2**. Porous hydrogels are a source of biomaterials with a wide range of chemical and mechanical properties. A) Hydrogels can be formed by single polymer networks, or multiple networks formed by combining linear polymers and/or crosslinked polymer networks. The connection between strands can be a chemical of a physical crosslink. B) Time-dependent rewetting data of HG-10, HG-20, HG-30, HG-40, and HG-50, for different compositions of cellulose-soy protein hydrogels. C) (i-ii) Scanning electron micrographs of porous PBLG microspheres fabricated at a gelatin concentration of 6.5% w/v. iii) SR-inline-PCI-CT-based 3D reconstruction of cross-section of porous hydrogel scaffolds (SA-100 mM). iv) SEM images of SA-200 mM scaffolds (n = 10, *p < 0.05). D) Representative SEM images of aerogels cross-section (the XY-plane perpendicular to the ice-growth direction) with morphologies ranging from fibrillar (F) to columnar (C) to lamellar (L) and their combinations, dependent on A-CNC:H-POEGMA weight ratio and CA-CNC+H-POEGMA. Scale bars are 20 µm. E) The arrangement of the walls on hydrogel scaffolds defines an angle directly related to their behaviour under compression, dictating their point of break and material memory. F) Mechanical response of gradient and non-gradient (0/15° and 0/90°) scaffolds to axial compression load and unload with 1 µm s^{-1} in the axial z -direction at 37 °C up to 10 N. G) Morphology of fibroblasts within differently functionalized PEG-based matrices and in collagen gels at day 1 and week 2. H) Macrophage polarisation 3 days after hydrogel injection. *: muscle, #: hydrogel, Arrows: foreign body capsule. CD206 (green)/CD68 (red) staining at the hydrogel/muscle interface. Reproduced with permission of Elsevier, from: B (112)), C:i-ii ((113), C:iii-iv (103), D (114), F (112), G (99), and H (106).*

***Abbreviations:** A-CNC: Cellulose Nanocrystals; H-POEGMA: Hydrogel Poly(Oligoethylene Glycol Methacrylate); CA-CNC+H-POEGMA: Concentration A-CNC; CD: M2 Macrophages; HG:Hydrogel; PBLG: Poly(Γ-Benzyl-L-Glutamate); PEG:*

View Article Online
DOI: 10.1039/D1TB02628C

Polyethylene Glycol; SA: Sodium Alginate; SEM: Scanning Electron Microscopy; SR-Inline-PCI-CT: Synchrotron Radiation-Based X-Ray Inline Phase-Contrast Imaging-Computed Tomography.

2.3. Ceramics

Porous bioceramics, or bioceramic foams, are versatile advanced materials with distinctive applications in the biomedical fields (115). This remarkable class of ceramics is used in biomedicine to fix and rebuild the impaired tissue of musculoskeletal systems (116). These materials are classified based on their responses to the biological environment, for instance, alumina and zirconia are bioinert, while CaP ceramics are bioactive and bioresorbable (117). They are widely used as orthopaedic implants, in maxillofacial surgery, and as dental inserts, and research is being undertaken to further extend these uses.

Porous bioceramics are used in a variety of clinical applications, depending on the chemical properties at the pore surfaces and the pore sizes within the material. The pore surface properties vary based on their composition (*e.g.*, silicon dioxide, alumina, and titanium dioxide (TiO_2)), state (crystalline, amorphous, or semi-crystalline,in the case of glass-ceramics), and treatments (existence or the absence of hydroxyl groups or silanol) (2). **Table 1** lists the applications of porous ceramics corresponding to the pore characteristics.

Table 1. *The applications of porous ceramics related to the pore characteristics.*

Pores property	**Different applications**	
Typical size	0.001 μm	Filtration and separation (118)
	0.02 μm	Reverse osmosis membrane (119)
	0.2 μm	Microbe immobilisation (120)
	10 μm	Fine foaming (121)
Surface chemistry	Nitrogen and oxygen surface groups	Catalyst support (122)
	Protein function groups	Adsorption and absorption (123)
	Activated carbons	Enzymes immobilisation (124)

Porous bioceramics are used as bone implants at non-load-bearing sites and require an open interconnected porous network (>100 μm) (**Fig. 3**), to encourage tissue ingrowth and mechanical interlocking. For example, porous HAp ceramics with approximately 70% interconnected porosity allow sufficient ingrowth to be used as implants for bioactive fixation (125) (**Fig. 4**). The porous network also allows nutrient delivery and removal of waste through proper vascularization. Bioresorption can take place with bioactive glass, HAp, and tricalcium phosphate (TCP), and slow bioresorption would potentially allow eventual replacement of the implant with new living tissue (2).

View Article Online
DOI: 10.1039/D1TB02628C

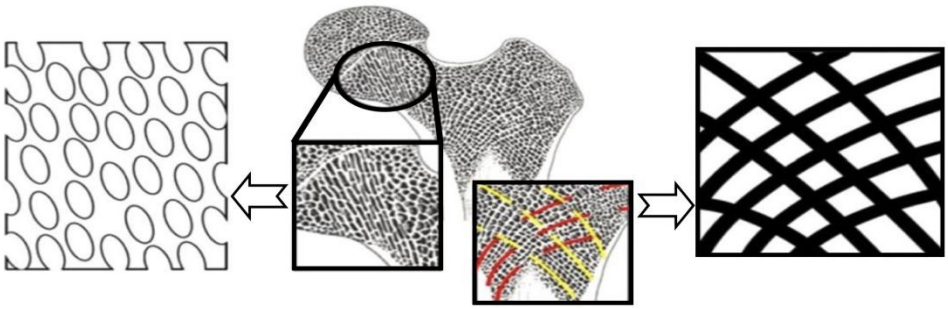

Fig. 3. *A diagram of native human bone morphology (centre) and a potential network of channels (right) and macropores (left) that can be integrated in the implant structure to mimic natural bone architecture. Reproduced with permission of Springer Nature, from (126).*

For drug delivery use, porous ceramics need a hierarchical porosity to achieve rapid transport, high selectivity, fast uptake, and release (127). This can be achieved by creating a range of pore sizes, *i.e.*, bimodal or trimodal size distributions (127). For example, mesoporous silica nanoparticles (MSNs), particularly MCM-41 and SBA-15 have been widely implemented in controlled drug release systems (128,129). Other examples include inorganic porous materials such as zirconia, alumina, and titania (130). For instance, a recent study prepared a bimodal mesoporous silicon oxycarbide ceramic, functionalized with amino groups, and studied its release kinetics for Tenofovir, an antiviral drug used to treat human immunodeficiency virus (HIV) and chronic hepatitis B infections. The resulting porous bioceramic showed an increased drug loading rate and a favourable adsorption process (131).

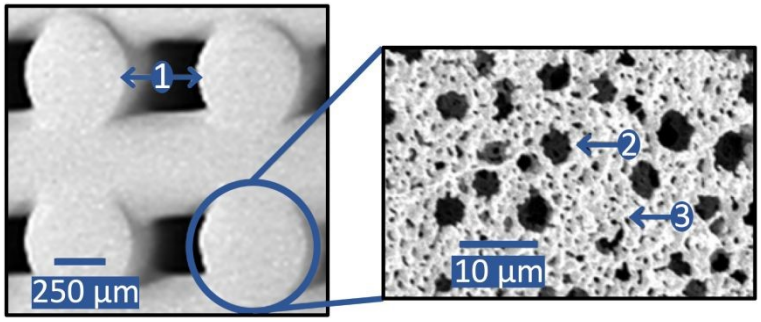

Fig. 4. *Ceramic scaffolds may contain pores on multiple length scales to facilitate bone in-growth such as this HAp lattice with three levels of porosity. The macropores (1), micropores (2), and submicron pores (3) can be controlled by the processing (132,133). Reproduced with permission of John Wiley and Sons.*

Abbreviations: *HAp: Hydroxyapatite.*

2.4. Glass

Glasses have an amorphous structure whereas glass-ceramics, commonly the result of the partial crystallisation of glasses, possess an arranged organised structure (134). Bioactive glasses and glass ceramics, despite their different preparation methods, have a common set of properties, such as the ability to degrade at a controllable rate and to release ions. Glasses can be obtained from different sources and they are classified accordingly as metallic, chalcogenide, or oxidic. The last category contains materials obtained from various oxides such as silicon dioxide, phosphorus

View Article Online
DOI: 10.1039/D1TB02628C

oxide (P_2O_5), boric anhydride, sodium oxide, aluminium oxide, germanium dioxide, with the main typical glass forming elements being silicon, phosphorus, and boron (134).

The first bioactive glass system produced in 1969, Bioglass® or 45S5 (135), was prepared by a melt-quenching method that involves melting high-purity oxides. These glasses consist of a silicate network with network-modifiers, such as sodium oxide and calcium oxide (CaO). Their major disadvantage was their fully dense structure which limited their clinical use. However, the melt-quenching method is still the most reliable for certain compositions such as phosphate and borophosphate glasses that have shown great potential in biomedical applications (136–140) due to their good bioresorbable properties (134). Phosphate-based glasses are chemically similar to the inorganic phase of human bone and have high solubility which can be tailored by varying the composition (139). Borophosphate glasses have better thermal and mechanical properties than pure phosphate glasses (141). **Fig. 5** shows bioactive glasses and glass–ceramics for orbital socket surgery.

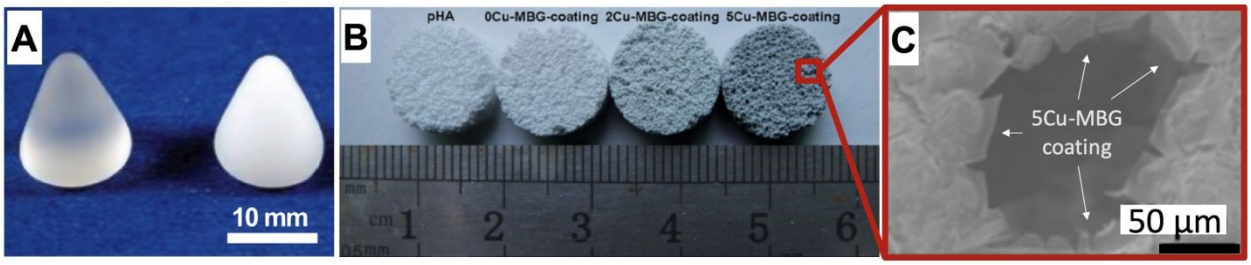

Fig. 5. *(A) Conical orbital implants (anterior diameter 10 mm, posterior diameter 3 mm, length 12 mm) made of 45S5 Bioglass® (left), Biosilicate® I glass–ceramic (centre) and Biosilicate® II glass–ceramic (right) (142). (B, C) MBG-coated porous HAp scaffolds for possible use as orbital implants: on the left, photograph showing the outward appearance of the HAp devices with different MBG coating (containing 0, 2 and 5 mol.% of CuO), on the right, morphology of porous HAp coated with 5 mol% Cu-doped MBG (132). Reproduced with permission of Springer Nature, from: A (142), B & C: (132).*

Abbreviations: *Cuo: Copper Oxide; Hap: Hydroxyapatite; MBG: Mesoporous Bioactive Glass.*

Another well-known, low-temperature, and low-cost preparation method used to obtain bioactive glasses and glass-ceramics, is the sol-gel route. This method has become popular due to the ease of obtaining porous materials with high surface area, various shapes and structure types, *e.g.*, crystalline or amorphous. It is noted that at ambient temperature, the sol-gel route gives control over the porosity through fibres, films, or nanoparticles (134).

Currently, much research effort is directed towards 3D structuring of porous self-supported bioglasses, also known as textured monoliths (134). Many of the resulting strategies typically require a sacrificial template that creates the macroporosity; synthetic foams are key in this approach (143,144). The template can be removed by dissolution (145) or thermal decomposition (145,146). Using F127, methylcellulose, and PU sponge as templates mixed in a specific sequence Tang *et al*. synthesized a trimodal mesoporous bioactive glass scaffold (TMS) (147). This material included macropores (200-500 µm) with a high pore interconnectivity, cell-sized micropores (<10 µm), and mesopores with entrapped active and drug release properties (approximately 7.5 nm). Beyond synthetic sacrificial templates, natural templates are gaining attention due to their innate, sophisticated architecture. Biomolecules (148), plants (149) or pollen (150) have successfully been employed as templates, generally in combination with the sol-gel process (151). Nanofibrous structures synthesized by electrospinning have also been explored to obtain nanofibrous scaffolds

View Article Online
DOI: 10.1039/D1TB02628C

and have gained increasing interest since they resemble the native ECM. Sol-gel techniques have generated nanofibrous scaffolds with fibre diameters 10 times thinner than those obtained by electrospinning, using a 3D bacterial cellulose aerogel as a sacrificial template (152). Depending on the intrinsic order of the employed template, final structures ranging from disordered foam-like textures (125,153–155) to ordered opal-like (156) complementary lattices can be obtained. Recently, bioglass self-supporting monoliths, hosting well-aligned ordered macropores were obtained by an ice structuring-based method, either employing sol-gel (157) or preformed bioglass precursors (158).

Aside from the numerous strictly inorganic structures, advanced hybrids of bioglass-biopolymer are being developed. These new hybrid composites aim to achieve better cell adhesion, proliferation, differentiation, and organization in a normal tissue setting while being degradable at an adequate rate. Bioglass-biopolymer composites can be combined with specific drugs or nanoparticles (*e.g.*, silver or gold) to improve the system's medical or mechanical properties. The most commonly employed biopolymers in tissue engineering research are proteins (*e.g.*, collagen, albumin, silk fibroin), natural polysaccharides (*e.g.*, chitosan, alginates, hyaluronic acid, starch), and PHAs (159,160) (*e.g.*, poly((R)-3-hydroxybutyrate), hydroxy valerate copolymer, PHBV (161), and synthetic poly(*α*-hydroxy esters) (*e.g.*, PLA, PGA, and their copolymers).

Much effort is being put into developing methods for rapid prototyping of bioglass and bioactive glass composites. Pires *et al.* reported that additive manufacture using several formulations of $CaO{\cdot}P_2O_5{\cdot}TiO_2$ glass generated promising temporary scaffolds for low load-bearing bone tissue regeneration (162). In another study, Wu *et al*. proposed an easy method to prepare hierarchical and multifunctional MBG scaffolds with controllable pore architecture, excellent mechanical strength, and mineralization ability for bone regeneration, by a modified 3D-printing technique using poly(vinyl alcohol) (PVOH) as a binder (163). Moreover, 45S5 Bioglass® (45S5) or strontium-substituted bioactive glass (SrBG) was incorporated into PCL and fabricated into 3D bioactive composite scaffolds utilizing additive manufacturing technology (164). The composite scaffolds (PCL/45S5 and PCL/SrBG) could be reproducibly manufactured with a scaffold morphology closely resembling that of PCL scaffolds but with higher compressive Young's modulus at similar volumetric porosity (~75%).

2.5. Calcium Phosphate

CaP from natural and synthetic sources has been extensively studied as a biomaterial as it is the basis of the composition of the mineral phase of the human bone (165–168) and has well-demonstrated osteogenic potential. CaP is resorbable *in vivo* as demonstrated in the early 90's by Ripamonti (**Fig. 6A-B**). Bone mineral contains mostly calcium and phosphate together with several trace elements. Diffraction patterns have indicated carbonate, magnesium (Mg) and sodium are present within these trace elements. Therefore, bone apatite crystals can be conceived as carbonated-apatite nanocrystals (169).

A selected mixture of CaPs as ceramics and cements: HAp, biphasic phosphates, and tricalcium phosphate agents (mainly *β*-tricalcium phosphate (*β*-TCP)), have been proposed in dental applications (**Fig. 6C**), and as ear and eye implants (170,171). When manufactured as porous materials they have also been used as drug carriers and antibacterial agents (**Fig. 6D**) (172).

View Article Online
DOI: 10.1039/D1TB02628C

Although they have comparably low compressive strengths compared to *in vivo* bone (**Fig. 6E**), they have good cell compatibility (**Fig. 6F**), facilitate protein adhesion, have tailorable biodegradability, osteoconductivity and the ability to improve osteoinductivity. These last two characteristics have attracted attention since 1991 when Ripamonti introduced the intrinsic osteoinductive properties of CaPs (172,173). This feature has been observed *in vivo* where further inflammation in the body could enhance osteoinductive pathways, and which would allow CaPs to be used without the addition of bone morphogenetic proteins (BMPs) (**Fig. 6G**) (174).

CaPs have only recently been proposed as porous materials, with interconnected voids at the macro- and micropore level (175,176). Specifically, research groups have explored different architectures and microstructures (**Fig. 6H**), aiming at environments that are suitable for bone cells, while also supporting the formation of new nerves and blood vessels.

Even though surfactants and porogens have been widely used to create pores in CaP, recent studies have also investigated biomimetic foaming (simulating host tissues) and 3D-printing methods, to better control the reproducibility and architectural detail of scaffolds; examples can be observed in **Fig. 6I**. Biomimetic foaming creates free porogen-solvent interconnected structures, and can be achieved through freeze-drying (177,178), electrospinning (179,180), and Pickering emulsions (181). In addition to the geometric features, cells forming neo-tissues have shown preference to differentiate on topographic details (rough surfaces) and chemically active (polar) surfaces. For example, ectopic bone and a more accelerated bone formation was observed on calcium-deficient hydroxyapatite (CDHA), *i.e.*, CaP that can hydrolyze by itself to form a cement (182). CDHA scaffolds with inherent rough surface were compared with 3D-printed sintered ones, the later ones being associated with smooth and clean prints (176). New areas of study are also exploring self-setting co-extruded ceramics. These material-hybrid inks offer bioactive surfaces plus the benefit of hardening at room temperature using hydrothermal treatments. In addition, they preserve an interconnected nano-structural architecture, capable of supporting mesenchymal cell adhesion and proliferation (183).

The micro/nanoscale porosity and the specific surface area (SSA) determine the overall interconnection of the structure. Optimal SSA values between 30-40 m^2/g have been identified in successful ceramic microstructures with high porosities (64-76%) (176,184). Surface geometry can also impact both cell attachment and cell proliferation. Barba *et al*. demonstrated that spherical concave macropores were superior to prismatic convex macropores, even after switching between foaming and 3D-printing techniques (176). Spherical macropores provided mineral niches, where calcium and phosphate ions were slowly released, attracting relevant proteins and growth factors whilst enhancing material resorption, as supported by biphasic CaP-foamed scaffolds (185) and interconnected CaP constructs for metastatic cell studies (186).

Porosity and pore size have been shown to significantly affect the rate and type of degradation, as well as the osteoinductive properties. On CDHA foams, ectopic bone has replaced the scaffold, whereas in sintered CaPs, pores have been coated by new bone, sometimes blocking the movement of molecules (176). In a previous publication (174), the same group identified that new bone formation concentrates at the centre of the scaffold, possibly linked to the fast diffusion of ions. To improve homogeneous distribution of new bone formation, low-temperature powder-based inkjet methods have been proposed as a novel method of solid freeform fabrication (SFF)

View Article Online
DOI: 10.1039/D1TB02628C

(187). With this methodology, a sliced computational model of the structure is loaded into the printer and the nozzle then jets a liquid solution into a thin layer of powder onto a platform. When the first layer is built, the platform is lowered down and the jet injects the next layer, until the construct is finished, and excess loose powder is removed. By varying pore sizes, layer thickness, and printing orientations, Farzadi *et al*. found a uniform distribution of cells through their one-dimensional (x-axis) and lower-wall-thickness printed scaffolds (187).

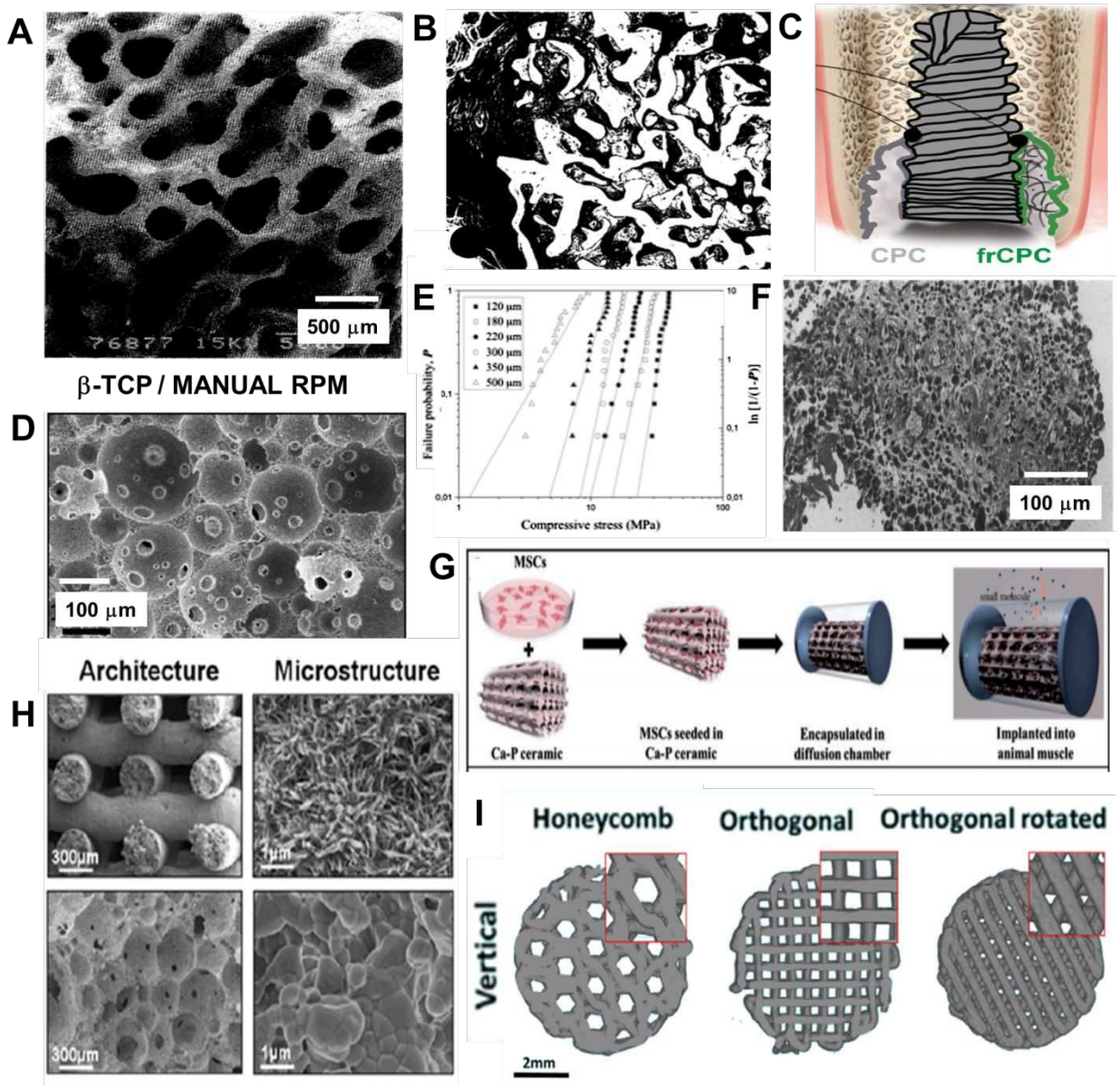

Fig 6. *Manufacturing & application evolution of CaPs. A-B showed early characterisation of CaPs in the 1990s, and the discovery of its biological properties. A) Conservation of macroporosity from bone apatite. B) New crystals inside the microporosity of CaP ceramic after 1 year implantation in cortical mastoidal bone of a dog. C) Graphical abstract of fibre-reinforced CaP cement to stabilise dental implants. D) SEM image of porous 70% w/v β-TCP scaffolds emulsified by manual speed (more variables presented in original paper). E). Weibull plot of the compressive strength stress data for BCP-7Sr3Ag with different pore sizes. Straight lines are best fits to data using the Weibull probability function. F) Light micrograph of exudate in a pore of a canal-wall prosthesis removed from a chronically infected middle ear. G) MSCs isolated from rat's bone marrow, cultured with CaP in a diffusion chamber, then implanted in the dog's muscle for 6 months. H) SEM of CDHA-Foam and CDHA-Rob-450 groups showing similar*

View Article Online
DOI: 10.1039/D1TB02628C

architecture, open and interconnected, prismatic, convex macropores. The microstructure of the CDHA scaffolds consisted of the typical network of entangled, needle-like nanocrystals, whereas the sintered ceramics showed polyhedral smooth crystals. I) Virtual reconstructions from μCT data of scaffolds printed with different patterns. Vertical view from the printing plane. Reproduced from Open Source from: D (188), G (189), with permission of Elsevier from: A (190), B (191), D & H (176), E (192), F (171), I (183).

Abbreviations: *AFFP: Allogeneic Fibrin-Fibronectin Protein; BCP: Bicalcium Phosphate; B-TCP: Beta-Tricalcium Phosphate; Cap: Calcium Phosphate; CDHA: Calcium Deficient Hydroxyapatite; Mct: Micro-Computed Tomography; MSC: Mesenchymal Stem Cells; SEM: Scanning Electron Microscope.*

2.6. Hydroxyapatite

HAp ($Ca_{10}(PO_4)_6(OH)_2$) is one of the most commonly found forms of CaPs (**Fig. 7A**). It is a popular choice for bone substitutes as it is a key component of the mineralized phase within the bone and is highly biocompatible (193). HAp is generally used as a powder-precursor, either in its pure form or as a composite with other materials such as CaPs (194), polymeric materials (195), and ion substitution (196), to obtain more desirable internal and superficial characteristics. Despite its beneficial bioactive properties, HAp's poor mechanical strength and slow degradation rates limit its use in its pure form and the majority of studies employ it within composites.

HAp composites have been created using both natural and synthetic sources. For example, HAp scaffolds derived from cuttlefish have been used due to their inherent well-interconnected porous structure (**Fig. 7B**) (197), whilst silk fibroin/HAp composites have been processed and blended to create a flexible but stable structure (198). The fibrils create a heterogeneous interconnected structure that could be further enriched with growth factors **(Fig. 7C**). HAp's compatibility has also proved effective for the attachment and differentiation of osteoblasts seeded on freeze-cast porous HAp scaffolds (**Fig. 7D**) (199).

Cox *et al.* were able to show that within HAp/PVOH composites, flowability, and hence printability was increased by decreasing the HAp content (200); however, a reduction in bioactive properties was observed. Good printability is desirable, as it allows the creation of specific macroporous architectures with controlled and high-resolution interconnected pores. High printing resolution is associated with a decrease in interparticle voids, leading to stronger bonds between particulates, evidenced in the mechanical properties of printed HAp/PVOH constructs. Furthermore, novel printing techniques (as sintering and depowdering techniques), can also eliminate the use of solvents which could occlude the pores (5,200) and negatively impact on cell viability (201,202).

The benefits of HAp composites as drug carriers have been explored by Han *et al*., who prepared functionalized HA/poly(L-lysine)/polydopamine (PLL/PDA) scaffolds with enhanced bioactivity by embedding BMP in the polymeric coating. Masson's trichrome staining evidenced the potential of coated HAp scaffolds as protein delivery systems (**Fig. 7E**) (203).

View Article Online
DOI: 10.1039/D1TB02628C

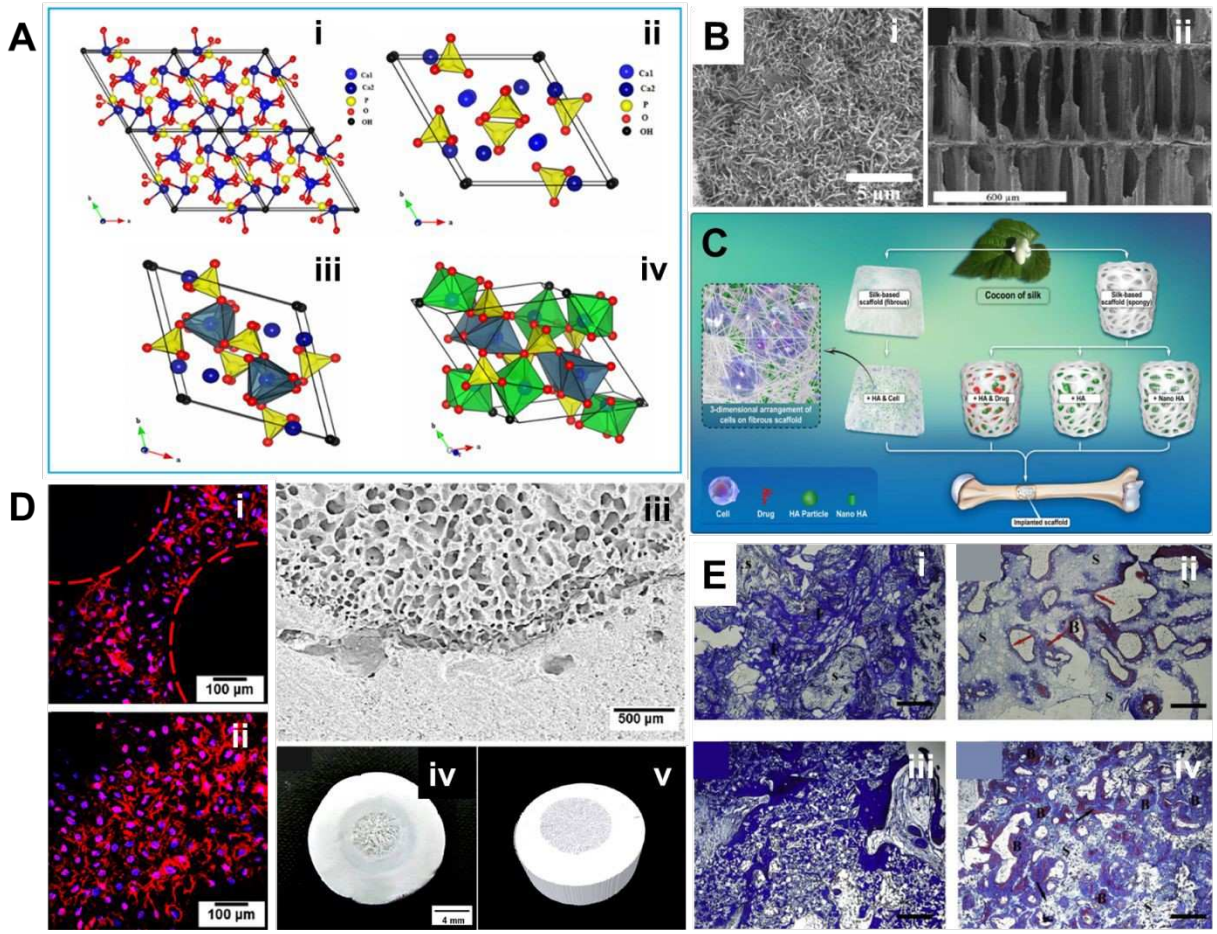

Fig. 7. *A) i) Projections of: the unit cell of HAp; ii) the arrangement of octahedrons [Ca(1)O_6] in the HAP structure; iii) the sequence of octahedral [Ca(1)O_6] and tetrahedral [PO_4] in the HAp structure; and iv) the sequence of octahedral and tetrahedral [PO_4] in the HAp structure. B) i) HAp scaffold derived from cuttlefish bone displaying interconnected channelled structure maintained after HT conversion. ii) Porous HAp scaffolds and nanostructures of CaP deposited on the scaffolds assisted by H6L molecules with a concentration of 0.5 mM. C) Different types and applications of bioceramics made by silk and HAp. D) Porous part and i) dense part ii) pre-osteoblast cells cultured on a porous HAp bone-like scaffold iii). Optical image. iv) and v) reconstructed µCT images with initial HAp contents of 15% initial and 40% outer volume (v/v), respectively. E) Masson's trichrome staining of HA-BMP2 scaffolds after 12 weeks of implantation. i) Bare HAp scaffold; ii) HA-BMP2 scaffold; iii) HA-PLL/PDA scaffold; iv) HA-PLL/PDA-BMP2 scaffold. Scale bars: 0.5 mm. Reproduced from Open Source: D (199), and with permission from Elsevier: A (204), Bi (197), Bii (205), D (198), and E (203).*

Abbreviations: *BMP: Bone Morphogenic Protein; Hap: Hydroxyapatite; H6L: Lattice Solvent Molecules; HT: Hydrothermally; Mct: Micro-Computed Tomography; PDA: Polydopamine; PLL: Poly L-Lysine; PO_4: Phosphate.*

2.7. Metals

Metals are the most commonly used scaffolds for load-bearing implants, especially in orthopaedic surgeries. They can be used in cardiovascular surgery, maxillofacial surgery, and as dental materials (206). Widely used metals and alloys for clinical applications include stainless steel, titanium and its alloys, cobalt-based alloys, cobalt-chromium (Co–Cr) alloys and tantalum-based alloys (207). The first stainless steel alloy used clinically contained chromium and nickel, making it stronger and more corrosion-resistant than steel (206). Co–Cr alloys have been used in artificial joints due to their excellent wear-resistance property. Titanium (Ti) is distinguished for its lightweight, along with its alloys, they are known for their excellent tensile strength and pitting

View Article Online
DOI: 10.1039/D1TB02628C

corrosion-resistance and have been used in applications such as dental and intravascular restoration wiring (208)) and as porous Ti (Ti_6Al_4V) for bone reconstruction (209,210). The precious metals such as gold (Au), silver (Ag), platinum (Pt), and their alloys are typically used in dentistry as they hold good castability, ductility, and corrosion-resistance. Tantalum is often used for X-ray markers for stents. The flexibility of amorphous alloys like zirconium-based alloys makes them good candidates for miniaturised metal implants. Biodegradable metals such as iron-based (Fe) or Mg-based alloys are now used for implant material (1),(211),(212),(213)).

When it comes to stainless steel, it is mainly used in fixed surgical implants. The most commonly used alloy is 316L (316 low-carbon steel) due to its excellent biocompatibility, as it forms a thin protective chromium oxide layer on its surface avoiding corrosion. It is cheap, easily available, has excellent fabrication properties, is biocompatible, and has great strength (214,215). However, when exposed to complex body fluids containing chloride ions or reduced sulphur compounds, stainless steel implants release toxic elements such as nickel and chromium. In this regard, one method developed is to coat the alloy with transition metal nitrides such as Ti-nitride (TN), vanadium nitride (VN), and TiAlN, to act as a protective coating against wear and corrosion (216,217). Another major concern is the presence of toxic nickel upon which many patients are sensitive. Research is also going on in the direction of developing nickel-free stainless steel by replacing it with nitrogen (214).

Furthermore, Co–Cr alloys exhibit excellent mechanical properties and corrosion resistance. They are usually used as components in modular prosthetic devices such as hip or knee joints, particularly in the ball and socket joint where movement is needed (209). Recently, Co–Cr–Mo alloy as a porous structure has been proposed to prevent orthopaedic implant infections (218), and has also been used in conjunction with UHMWPE to improve its corrosion- and wear-resistance (219).

On the other hand, Ti is a perfect material for surgical implants thanks to its strong corrosion-resistance coupled with lightweight and excellent biocompatibility. Ti alloys are used in craniofacial implants, dental implants, joint replacement parts for hip, knee, shoulder, spine, elbow, and wrist, and bone-fixation materials such as nails, screws, nuts, and plates, among others (209). It is well-noted that Ti–6Al–4V is the most commonly used alloy in prosthetic devices. These materials are compatible with imaging techniques such as computed tomography (CT) scanning and magnetic resonance imaging (MRI). Research on Ti alloys is also focused on developing porous structures to allow penetration of the vascular system for the total integration of metal and bone (220,221). A novel Ti alloy with low enough Young's modulus to avoid stress-shielding but high enough to suppress spring back has been developed to be used as spine-fixation implants so that it can be bent to match with the curvature of the patient's spine. Such alloys include Ti–Cr, Ti-Mo, Ti–Zr–Cr, Ti–Zr–Mo, and Ti–Zr–Mo–Cr (222,223). Then comes the nickel-Ti alloy, or Nitinol, which is a smart material with shape-memory and superelastic properties, excellent biocompatibility, and considered highly stable in the body. It has an elastic modulus closer to that of bone than other metal and metal alloy implant materials. Nitinol finds applications in orthodontics, in the treatment of bone fractures, and as bone suture anchors for attaching soft tissues such as tendons and ligaments to the bone, and as reinforcement of blood vessels. Adding copper to Nitinol has demonstrated better fatigue and modified shape-memory properties in both bulk and porous structures (214,224).

View Article Online
DOI: 10.1039/D1TB02628C

Mg alloy AZ91D has a lower corrosion-resistance than Ti and Co–Cr alloys. However, AZ91D resembles more to the bone in terms of its mechanical properties such as tensile strength, elongation to fracture, and Young's modulus (206). This makes them suitable as biodegradable biomaterials since they readily dissolve in corrosive solutions.

Finally, Fe-based alloys are also used, but exclusively in temporary implant applications. They have higher strengths and Young's moduli than Mg-based alloys (225).

3. Fabrication Strategies

As shown in Ashby diagrams comparing natural with synthetic materials (see for example (226) and (11)), the range of materials available for tissue-engineering applications is quite narrow; the mechanical properties need to be soft yet tough, a balance that is difficult to achieve. However, there is still the possibility of tuning the physical and chemical features of those limited candidates and here is where manufacturing techniques play an important role. Biofabrication strategies include all technologies adapted or designed specifically for biomaterials, which seek to modify the chemical arrangement, state of matter, and/or architecture of materials to make them suitable for the micro- and macro-environments in the body. Biofabrication techniques for porous materials are: *i*) stimuli-induced techniques to introduce pores into the material(s); *ii*) material-material interaction techniques to create pores; and *iii*) moulding or printing techniques to build porous constructs. The most promising techniques are summarized and illustrated in **Fig. 8A**.

3.1. Templating and Salt-Templating

Templating is commonly used to fabricate biomaterial constructs with controlled pores in the μm-to-nm range, with the template used to obtain tailored morphologies and geometries. To create a porous scaffold a porogen, which acts as the removable or pore-forming phase, is introduced to a non-templating phase. The sacrificial phase can be removed through mechanical stimuli or porogen-dissolution, resulting in the formation of pores (227). The size, geometry, and orientation of pores can be controlled through a careful choice of the porogen, impacting the overall internal phase volume, degree of porosity, and interconnectivity of the scaffold. This method can be used to improve physical properties of 3D scaffolds such as strength and stiffness (228). A general overview on the steps involved in templating is illustrated in **Fig. 8A**.

Salt-templating methods are commonly used for biomedical applications as the porogen or removal phase is a salt that: *i*) can be easily dissolved without affecting the porous structure; *ii*) does not leave toxic residues; *iii*) is cost-effective and easy to implement; *iv*) and does not generally react with the functional groups of the other material(s). Sodium chloride (NaCl) crystals have been used as default porogens with sizes between 100-300 μm, and at concentrations of 20-50% w/v, easily removed with water. As this exceeds the saturation concentration, the salts can be found in the solid state and dissolved after crosslinking, even if crystalized within the polymeric matrix. Additionally, techniques such as microfluidics (229), freeze-drying (230,231), and post-crosslinking coating (232,233) have been implemented to further control the morphology of the

View Article Online
DOI: 10.1039/D1TB02628C

pores, commonly affected by swelling/deswelling ratios in hydrogels and shrinking ratios on bulky materials.

Poly(*N*-isopropylacrylamide)-alginate (PNIPAAM-Alg) hydrogel porous constructs have been used to analyse swelling/deswelling rates at different porosities and pore sizes, concluding that at higher porosities, these porous materials reach the equilibrium swelling state 15 times faster than non-porous ones (234). The effect of NaCl weight ratios on the surface of the scaffolds can be observed in **Fig. 8B** where porosity and pore interconnectivity increased with an increasing NaCl ratio. Moreover, hydrogels crosslinked through covalent chemical interactions of water-soluble polymers are neither instantaneous nor rapid, hence their formation is considered time-dependent. Therefore, the swelling time and ratio are their most important features. This interaction defines the diffusion of water molecules into and out of the material, which explain their behaviour in aqueous environments including the human body (235). By decreasing the time to reach the equilibrium swelling state, the mechanical properties of the resulting material can be modified and improved to match the desired usage, especially their pore. Furthermore, an increased porosity results in an increased surface area and leads to a more homogeneous coating, positive cytological effects, and unique cell topologies (236),(235),(236). The advantages of increased swelling ratios in salt-templating have been explored by coating SMPs with acrylic acid and *N*-hydroxyethyl acrylamide for vascular applications (41). Coated SMPs were able to absorb up to 5 times more fluid than uncoated ones, whilst supporting cellular adhesion. Contrastingly, Na^+ ions have been shown to affect the number of crosslinkable reactive groups impacting the degree of crosslinking and degradation rates. Large pores (>200 μm) linked to high porosities (>65%) allow water and fluids to go through, easing the washing stage (237). Thus, the balance between porogen grain size and concentration, and mixing method need to be tailored to both material and application. An alternative is salt-leaching using powder, which is a solvent-free, low-temperature/pressure technique that generates high-porosity (70-80%) structures without collapsing and shrinking, and with attractive macropores for cell migration (238).

One of the main disadvantages of salt-leaching is the lack of control on orientation and homogeneous distribution of salt crystals. For that reason, recent experiments propose salt-templating as part of a dual-pore manufacturing technique. For example, Mohanty *et al*. designed a PVOH polymer base to construct a 3D structure with defined macropores (239). Additionally, the hydrogel solution contained NaCl to create random micropores (**Fig. 8C-E**). They successfully controlled the overall geometry of the construct and offered different paths for fluids and molecules to travel through the scaffold.

Other salts have also been used on single-salt-leaching or dual-pore methods. For instance, copper sulfate ($CuSO_4$) was chosen due to its hydrophilicity, allowing it to be rapidly removed from processed structures. Additionally, in water it dissociates into Cu^{2+} and SO_4^{2-} ions, promoting a change in colour and allowing a more ready confirmation of porogen removal. Jakus *et al*. 3D-printed poly(lactic-*co*-glycolic acid) (PLGA) and $CuSO_4$ constructs and evaluated their "elevated porosity", confirming the excellent mechanical properties that PLGA is known for. Furthermore, the adhesion of human mesenchymal cell (hMSC), viability, and proliferation were significantly improved (**Fig. 8F**) (240). Sugars have also been explored as leaching elements. For example, Pashneh-Tala combined sucrose leaching with both subtractive and additive manufacturing techniques to produce inherently porous 3D structured materials from poly(glycerol sebacate) (241). These scaffolds exhibited a high internal porosity (up to 77%) and supported fibroblast ingrowth.

View Article Online
DOI: 10.1039/D1TB02628C

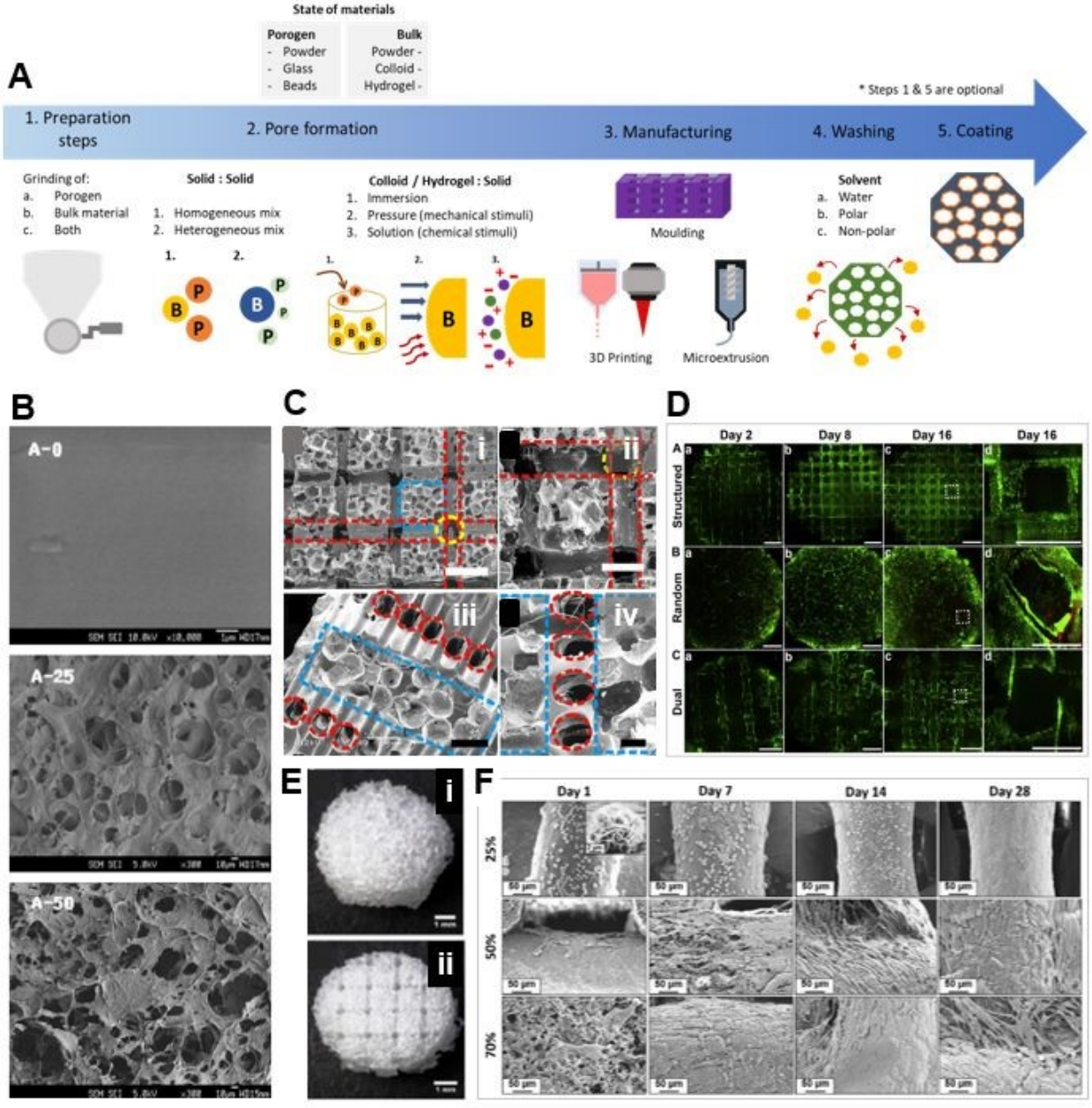

Fig. 8. *A) Common steps used for salt templating. The top part shows various states in which both porogen and bulk materials can be used and the bottom, the different manufacturing procedures proposed by research groups. B) Surface morphologies of an alginate matrix with various NaCl weight ratios. C) SEM images of fabricated dual-pore scaffolds (structured pore size 400 μm × 400 μm, distance between structured pores 800 μm; random pore size 300–600 μm): i) Top view showing structured pores and an array of random pores; and ii) its magnification. iii) Cross-sectional view of structured and random pores, and iv) its magnification. Dashed lines: yellow — structured pores in z-direction; red — structured pores in x or y-direction; blue — random pores area. Scale bars: i. 1 mm; ii-iii 500 μm; iv. 250 μm. D) Live/dead staining of HepG2 cells: Top view on i. structured, ii. random, and iii. dual-pore scaffolds on day 2, 8, and 16. (Green — live; red — dead). Scale bars: a,b,c: 1 mm and d: 350 μm. E) Resulting fabricated porous PDMS scaffolds: i) Salt mould replicated random pore scaffold with pore size of 300–600 μm. ii) PVOH mould replicated dual-pore scaffolds with structured pores of 400 μm× 400 μ random pores of 300–600 μm. F) Representative scanning electron micrographs of human MSCs on 25, 50, and 70% w/v F-PLGA 1, 7, 14, and 28 days after seeding. Reproduced with permission of Elsevier from: B (234), C-E (239), and F (240).*

View Article Online
DOI: 10.1039/D1TB02628C

Abbreviations: *HepG2: Heparin Cells; MSCs: Mesenchymal Cells; PDMS: Polydimethylsiloxane; PLGA: Poly(Lactic-co-Glycolic Acid); PVOH: Polyvinyl Alcohol; SEM: Scanning Electron Microscopy.*

However, this technique uses solvents to aid the creation of macro and micro-structures or enhance their chemical and mechanical properties. These solvents may occlude pores by corroding or altering the features of the solid phase, leading to poor interconnectivity (228,242). Consequently, sol-gel deposition and emulsion-templating are more commonly used for biomaterials. The latter will be discussed in the next section.

Sol-gel deposition is a technique that uses a colloidal suspension of precursor molecules, known as the 'sol', which is typically thermally treated to form a gel. The result is a tailored micro- and/ or nanostructure on both the surface and internal phase of the scaffolds (228). Armstrong *et al*. combined sol-gel deposition with layer-by-layer deposition of a cell-laden bioink, in order to inject a precise mix of growth factors, copolymers, and cell types, whilst simultaneously controlling the mechanical properties of the matrix using 3D printing (242). Despite the early success of printing techniques, there are limitations when the printing parameters also need to accommodate cell survival environments, as the temperature of the material inside and outside of the nozzle should promote cell survival and viability, whilst maintaining the material's ideal viscosity. In the same study, the group reported that sol-gel deposition in combination with 3D printing enhanced physical and rheological characteristics, and long-term fidelity of pluronic-co-alginate hydrogels. Similarly, Bechara *et al*. reported on the fabrication of PCL nanowires using a solvent-free nano-templating technique (243). Solvent-free templating is especially advantageous as it will not compromise the intrinsic bioactivity of scaffolds, such as mechanical strength and biodegradability.

3.2 Emulsion Templating

Emulsions can be used as versatile templates for porous structures (227,244). As shown in **Fig. 9A**, emulsions are immiscible liquids, with one phase dispersed in the other as visible droplets, and possibly additional intermediate phases (244). Emulsions can be divided into water-in-oil (W/O) and oil-in-water (O/W). Emulsions are thermodynamically unstable systems and their stability thus can be understood as their resistance to the sequence of consecutive stages of destabilisation (245), defined by the physical and chemical interaction between the ingredients involved in the emulsion. When the material is solidified and the internal phase (*i.e.*, the one forming the droplets) is removed, an arrangement of pores is left behind. When the droplet phase volume is high (<74%) this enables production of interconnected porous materials via polymerisation of the continuous phase of the emulsion. These materials are termed polymerised high internal phase emulsions (polyHIPEs). **Fig. 9B** shows the most common fabrication techniques that use emulsions. A recent review by Dikici *et al*. summarises in particular the emergent use of polyHIPE-based scaffolds for tissue engineering (10).

One of the biggest advantages of these techniques is that they enable tunability of the pore size, distribution, porosity, and interconnectivity (**Fig. 9C**). This can be achieved by the addition of initiators, surfactants, and solvents, coupled with manufacturing parameters such as mixing techniques (mixing paddle geometry and speed), temperature, times of emulsification, and further crosslinking. Polymerisation of the monomers occurs around the emulsion droplets, and pore size is controlled by the size of the emulsion droplets up to the micron scale (227). For acrylate and

View Article Online
DOI: 10.1039/D1TB02628C

styrene-based emulsions, ultraviolet light or heat are commonly used to induce polymerisation while alginate emulsions have been produced by crosslinking with Ca^{2+} (90,246,247).

Current polymer and hydrogel emulsions seek to enhance both the mechanical properties and the 3D pore features. At higher internal phase volumes (>74.048%) emulsions are referred to as HIPEs and have an increased porosity that has proven successful for cartilage (90,248), nerve (249), vascular (250), and bone (23,251) regeneration. Also, more complicated structures have been attempted by the combination of manufacturing techniques. For example, Johnson *et al*. successfully used an emulsion-based ink to fabricate scaffolds using micro-stereolithography (μSLA) (**Fig. 9D**) by combining emulsion synthesis with laser-based additive manufacturing setups (227). Additionally, Dikici *et al*. produced barrier membranes by combining PCL-based emulsions with electrospinning (31). **Fig. 9E** shows the impact of different pore sizes on cell morphology cultured on PCL-based scaffolds. Cells tended to spread as in flat surfaces in the scaffolds with the larger pore size (31). This method produced polymer matrices with consistent morphology as well as good mechanical properties. The method has demonstrated excellent reproducibility and can be used to manufacture scaffolds for 3D cell culture (252). Additionally, the 3D printing resolution of these scaffolds can be fine-tuned via inclusion of photo-absorbers in the photocurable resin (90), indicating a potential route for using these resins in commercial SLA setups (253). Currently, it is still a real challenge to scale up very high-resolution structures to an industrial level, which makes it still time consuming to achieve microstructures with controlled porosity (227).

The surface of these materials can be functionalised *via* air plasma treatment, which increases cell adhesion and bioactivity of scaffolds by rendering them hydrophilic. Moreover, Hsiao *et al.* used this method to improve the process of making hydrogel from nanoemulsion-based inks and 3D printing (254). With oxygen-permeability and rapid photopolymerisation, the researchers were able to print the hydrogel with high fidelity by SLA. The gel was developed to spread evenly during the printing process, allowing the production of mechanically stable scaffolds with a homogeneous interconnected morphology. However, the relation between the internal phase volume and strength/Young's modulus is inversely proportional, and as such it may not be possible to optimise both the porosity and mechanical properties of the material.

The use of two-phase aqueous emulsions is another emulsion templating technique that can be used to produce porous scaffolds (255). This method allows the development of scaffolds either by photopolymerisation or bioprinting. GelMA and PEO solutions have been used to make biocompatible scaffolds for tissue engineering, regenerative medicine, and drug delivery (94,108,109). The size of PEO droplets and the physical properties were properly controlled during the fabrication along with the bioprintable capability of the emulsion. The scaffolds offered larger pore sizes which lead to desired interconnected structures. With this technique, a high biocompatibility of GelMA bioprinted scaffolds has been achieved with various types of cells, including a high viability, proliferation rate and metabolic rate, as previously discussed and illustrated in **Fig. 9C**.

With promising results on *in vitro* experiments using emulsion templates, it is likely that emulsion-templated scaffolds will have a significant impact on tissue engineering in the coming years. However, as emulsions can be sensitive to change in internal and external variables,

View Article Online
DOI: 10.1039/D1TB02628C

challenges remain in finding the appropriate manufacturing formulations and techniques, as well as a balance between desired mechanical properties and architectural designs.

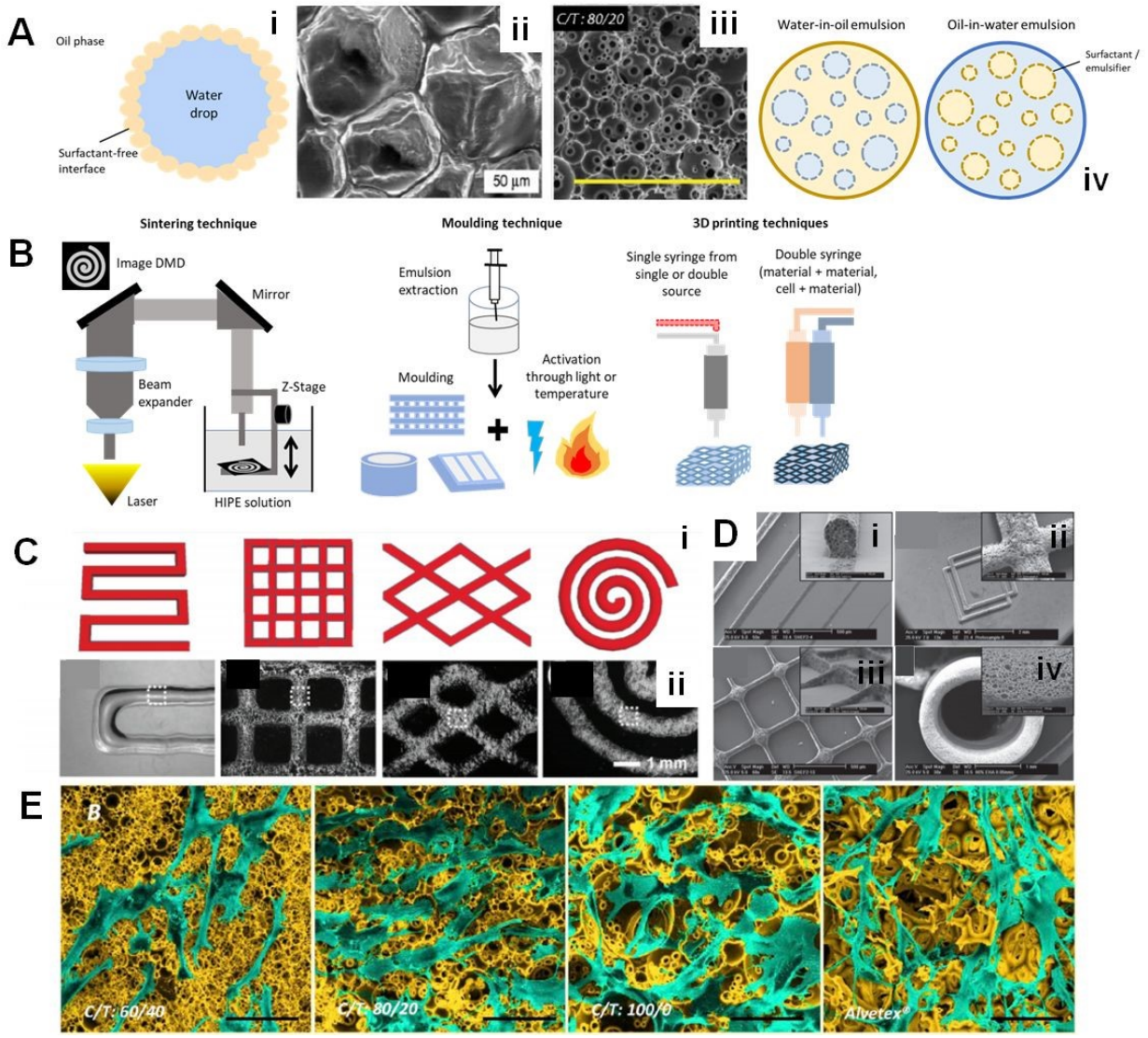

Fig. 9. *Emulsion techniques and successful applications are displayed herein. A) The origin of emulsions can be through Pickering 1907's surfactant-free formulation, with a structure i) and SEM image like ii). However, the use of surfactant is also used to obtain structures as displayed in iii) and imaged in iv). ii) is showing 2-ethylhexyl acrylate and silica nanoparticle emulsion (S4-a1.8). iii are SEM images of PCL-C/T, 5 days after polymerisation (scale bars: 100 µm). B) Several techniques have used emulsions as raw material for bioengineering constructs, the most common protocols include sintering, moulding and 3D printing. C) Extrusion bioprinting of the aqueous two-phase emulsion bioink. i) Designed patterns. ii) Optical micrographs of corresponding bioprinted i,v) standard GelMA hydrogel patterns and ii–iv,vi–viii) porous GelMA hydrogel patterns at i–iv) low magnification and v–viii) high magnification. D) SEM images of EHA80 polyHIPE structures produced by microstereolithography at different speeds i); overlapping squares with the intersection of squares in the intersection ii); grid at 17× magnification (inset shows side view of the grid pattern at 194 × magnification, clearly showing the open porous nature of the structure) iii); tube created by photopolymerisation of HIPEs while translating in the z direction (inset shows detail of the top surface of the tube) iv). Scale bars: i) and iii) 500 µm; ii) 2 mm; iv) 1 mm; all insets 100 µm. E) SEM images of 4-day cultured HDFs on C/T:60/40, C/T:80/20, C/T:100/0 and Alvetex®, respectively. SEM images were false-coloured for clear visibility of the cells on the scaffold surface. (yellow: scaffold, turquoise: cells (scale bars: 50 µm). Reproduced from Open Source: Aiii and E (31); and with permission of Wiley from: Aii (256), C (94), and D (227).*

View Article Online
DOI: 10.1039/D1TB02628C

Abbreviations: *C/T: Chloroform/Toluene; EHA80: 2-Ethylhexyl Acrylate; GelMA: Gelatin Methacrylate; HDFs: Human Dermal Fibroblasts; PCL: Poly(ε-Caprolactone); SEM: Scanning Electron Microscope.*

3.3. Freeze-Drying

Freeze-drying can be used to generate polymeric porous biomaterials. This method is looked at as a physical manufacturing procedure that depends on the phase characteristics of the polymer and the solvent involved, while the pore size is dependent on the concentration of the polymeric solution (257). Typically, freeze-drying consists of three main steps: *i*) freezing stage, *ii*) primary drying stage, then *iii*) secondary drying stage (258). During the freezing stage, the temperature is reduced so that the solvent freezes. Water is often the main solvent, though a mixture of alcohol and water can be used. The water present as free water will undergo a freezing process, but the bound water which is associated with the polymer will remain in its liquid state throughout the process (259,260). During the primary drying stage, the frozen solvent is removed by sublimation. Finally, during the secondary drying stage, the bound water is removed by water desorption enhanced by the application of heat to achieve a certain required moisture level.

The drying process is highly dependent on the material response to heat. Thermo-stable materials can be processed with a wide range of drying techniques. However, material decomposition is a challenge for thermo-stable materials and necessitates the application of complementary drying techniques.

Most liquids freeze by crystallisation, noting that controlled crystallisation can produce crystals with tailored sizes and structures. The process requires control of the temperature, heating/cooling rate, and the total process time, as well as the solution's concentration (261). The solvent is then removed through sublimation by lowering the pressure and adding heat, though the operating temperature must be lower than the eutectic point; the last point where solid and liquid phases coexist (262,263).

High-porosity scaffolds (up to 98% porosity) are fabricated by freeze-drying polymer solutions over leachable templates. In these cases, a high effective porosity is achieved, large pores are well-interconnected and very few isolated pores are present in the structure which requires three main steps: *i*) preparation of leachable templates (*e.g.*, by fusing salt and sugar); *ii*) freeze-drying the polymeric solution; *iii*) leaching the template. The introduction of leachable templates leads to a higher porosity and connectivity between the pores. This technique reduces the amount of implanted polymer while increasing the SSA for tissue growth (264). Furthermore, the pore morphology is critical for cell growth and function (265). In their study, Haugh *et al.* showed that pore size is dependent on two main factors: freezing temperature and an annealing step, where temperatures are raised to increase the crystallisation rate (257) (**Fig. 10**). The pore size decreases with lower freezing temperatures, while the annealing step resulted in an approximately 40% increase in the pore size.

View Article Online
DOI: 10.1039/D1TB02628C

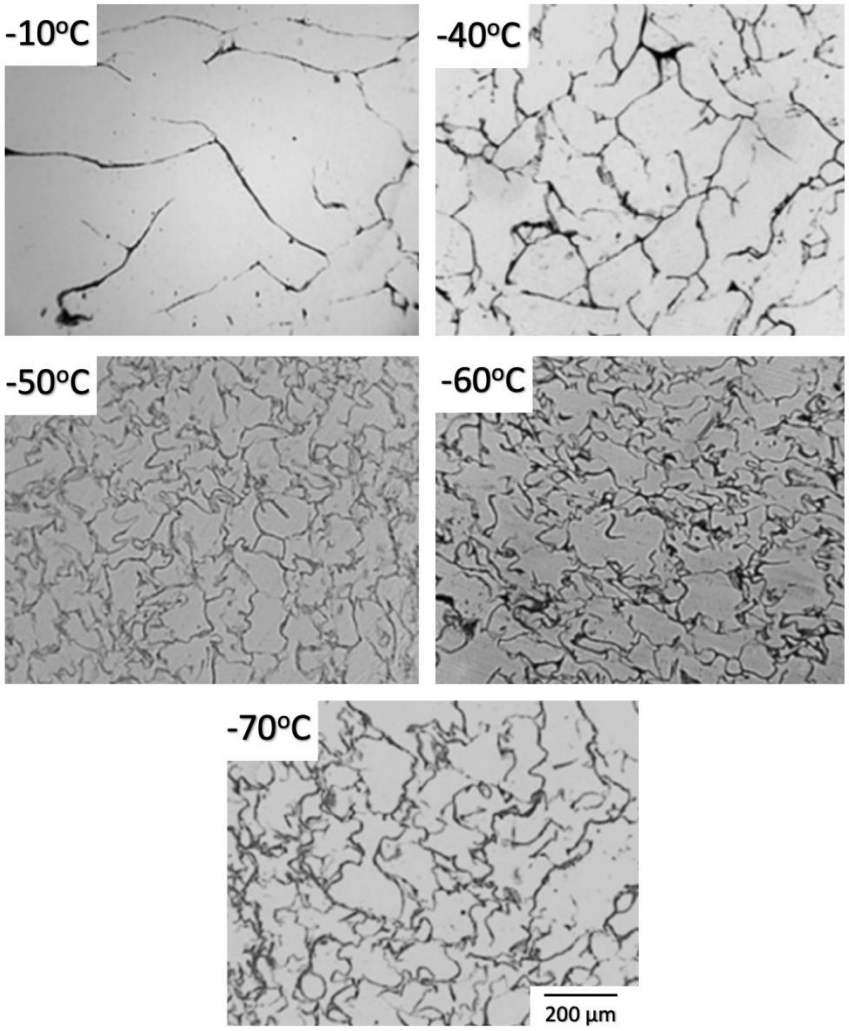

Fig. 10. *Digital images of stained scaffold sections at different freezing temperatures (T_f) captured at 125x magnification. The pore size decreases with the reduction of T_f. It is remarked that for a temperature below -50 ºC the mean pore size does not change substantially. Reproduced with permission of Mary Ann Liebert from (257).*

Wu *et al.* showed that increasing the polymer concentration decreases the porosity resulting in lower water adsorption (163). Furthermore, they studied the effect of crosslinking agent amount on the pore size of the gelatin porous scaffold. They remarked that the pore size decreased as the crosslinking agent amount increased (**Fig. 11**).

View Article Online
DOI: 10.1039/D1TB02628C

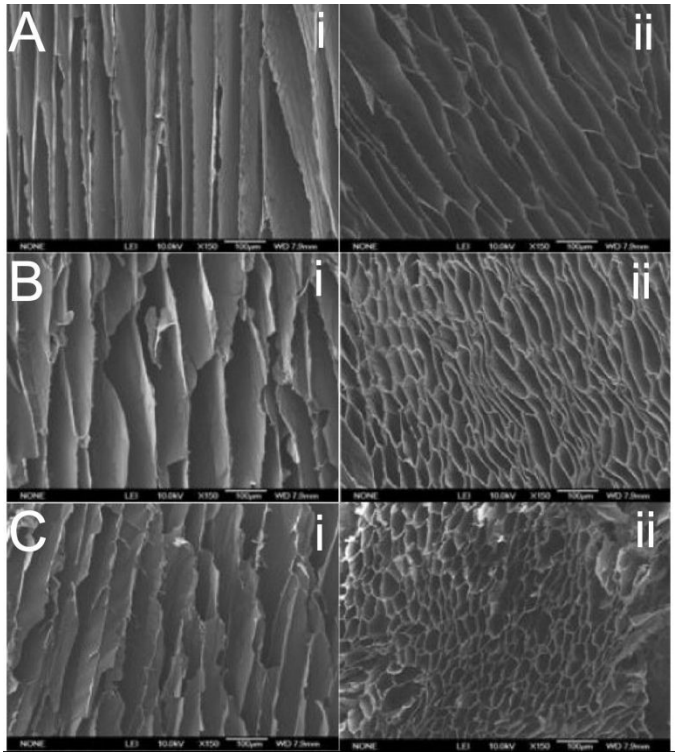

Fig. 11. *SEM images of cross-sections of gelatin scaffolds (A-i, B-i and C-i) with increasingly added amounts of crosslinking agents (A:0.1%, 0.3%, and 0.5% w/v). (A-ii, B-ii and C-ii) are the SEM images of vertical sections of such scaffolds. The effect of increasing the amount of agents applied is clear as the pore size is substantially reduced with increased amounts of crosslinking agents (from A to C). Reproduced with permission of Elsevier from (266).*

The properties of the 3D scaffolds are critical for tissue growth and compatibility. For instance, some surfaces are hydrophobic which is not conducive for cell adhesion. Modifications to the surface's properties are introduced to the produced scaffold. Pretreatment techniques can include applying ethanol, alkaline, or plasma treatment (267–269). Yet, these pre-wetting methods can only be applied to scaffolds that will be used immediately, with polymer degradation being observed if structures are immersed for long periods in these harsh solutions. Chen *et al.* introduced a new method to alter properties of a 3D porous material by filling the pores with a collagen solution (270). Centrifugation is applied to remove the excess of the solution to obtain a uniform coating layer. This method is very efficient in improving the structure's surface properties such as wettability, promoting effective cell seeding, and the resulting scaffold is easy to store.

3.4. Patterning

The introduction of topographical and chemical patterns to biomaterial surfaces is key to controlling the cell response, with a variety of patterning techniques used to introduce various topographical cues, *i.e.*, sizes, shapes, and chemical patterns that enhance the cellular activities (271–273).

Patterning techniques can be divided into two categories: *i*) cleanroom techniques founded on traditional microfabrication methods, and *ii*) non-traditional techniques, not dependent on cleanroom methods.

View Article Online
DOI: 10.1039/D1TB02628C

3.4.1. Cleanroom Techniques

It has been possible to develop techniques that allow for good consistency at the micro and nanoscale resolution in topographical patterning (272). These mainly use masked ion beam lithography (MIBL), photolithography, or electron beam lithography (EBL) to create an appropriate pattern that is then transferred to the scaffold by a chemical etching process.

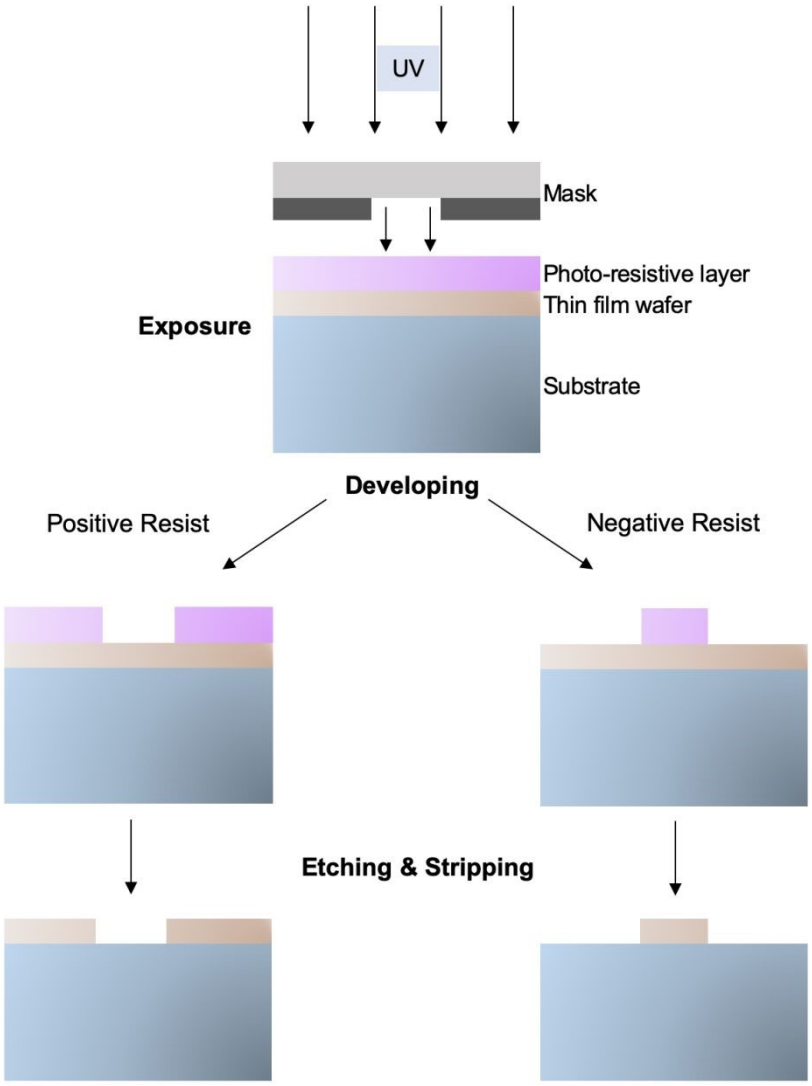

Fig. 12. *Schematic representing the patterning process using lithography. The process starts by cleaning the surface followed by wafer preparation. Then, the photoresist layer is applied over the wafer. Removal of well-patterned areas is done by the exposure of the surface to radiation/ion-beam/laser through a patterned mask to get the intended pattern. This latter step is the main differentiation between various lithography techniques. The last two steps, namely etching and stripping, consist of removal of wafer and PR by treating the surface with the convenient chemicals. Reproduced with permission of Elsevier from (274).*

Abbreviations: *PR: Positive Resist.*

In MIBL the surface is covered with a nickel mesh which defines the pattern to be applied to the surface. The entire surface is exposed to the ion beam except areas "masked" by mesh. MIBL is not frequently used, though it can create topographical features on non-standard materials

View Article Online
DOI: 10.1039/D1TB02628C

(*e.g.*, polymethylmethacrylate (PMMA)) allowing additional material selection (275). In parallel, photolithography employs a photoresist layer which is removed by exposure to intense light. The exposed surfaces then undergo chemical etching, before the resist is removed by organic solvents, inorganic acids (*e.g.*, hydrofluoric acid (HF)), or plasma etching (274). This method is limited by the materials that can be used (*i.e.*, silicon, glass, or quartz) and its low throughput (276). **Fig. 12** represents the general lithography process steps.

Similarly, EBL is analogous to photolithography, but uses a focused beam of electrons, which enhances the resolution of this method (order of nanoscale patterns) compared to the aforementioned lithography techniques (277). However, the same limitations related to the throughput and etching step apply to the EBL technique.

On the other hand, surfaces can be modified with patterns of biologically active chemicals or by introducing a patterned intermediate layer, which affects the chemical properties of the surface. Similar to topographical patterning, photolithography (278) and EBL (279) can be used to introduce chemical patterns. Bryant *et al.* studied photopatterning to suit well-defined cell types (280). They found that porous hydrogels could be patterned for various specific applications using this technique. For example, Myung *et al.* designed an artificial cornea including a micropatterned skirt region by photochemical patterning of a hydrogel scaffold (281).

Jing *et al.* introduced large pores to bacterial cellulose hydrogel using a laser-patterning technique. Then a sequential chemical modification of the membrane was achieved to enhance its activity using gelatin and HAp, respectively. The produced scaffold showed good substrate-cell activity for bone tissue engineering applications (282). The types of possible chemical modifications are discussed in the chemical treatment section below.

3.4.2. Post-Treatment

The ability of any scaffold to support and develop a tissue is dependent on properties such as porosity, pore size, interconnectivity, and wettability, among others. Surface treatment techniques are used to alter the scaffold's surface properties. These modifications can be introduced by physical treatment, chemical treatment, coating, or printing treatment methods (283,284)(285),(283,284).

Physical treatments can be *via*: *i*) solvents to remove contaminants; *ii*) surface-roughening to increase the surface area; and *iii*) heat-treatment to enhance the mechanical properties.

On the other hand, the chemical treatment is more engaged to change the chemical properties of the surface. This technique serves to modify many surface-related factors such as biodegradation properties, hydrophobicity, antistatic properties, barrier properties amongst others. It is critical to alter such properties to meet the tissue's adequate conditions. Chemical methods can be divided into three main categories: *i*) functionalising chemical groups; *ii*) incorporating functional groups; and *iii*) grafting functional monomers/polymers (284).

View Article Online
DOI: 10.1039/D1TB02628C

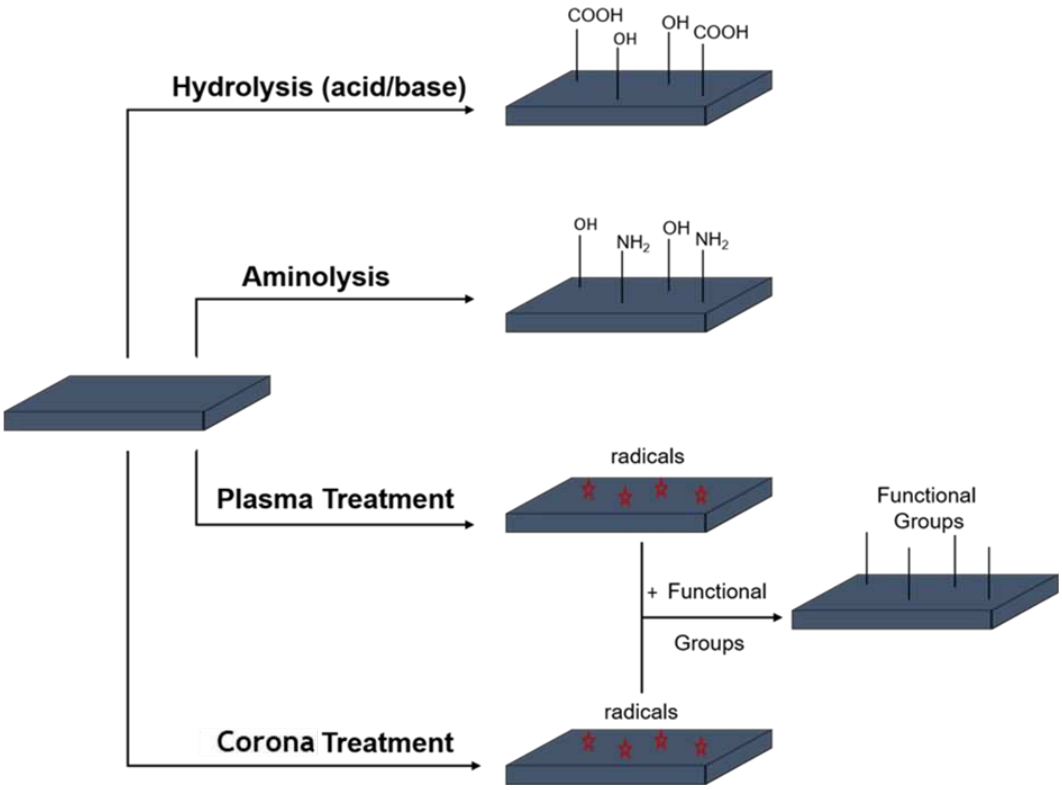

Fig. 13. *Scheme representing various types of chemical treatment for surface modification. Hydrolysis and aminolysis consist of the introduction of hydrophilic groups to the surface. Plasma and corona treatments aim at incorporating functional groups to change properties of the surface, yet they pass through the radical formation step before new functional groups are added to the surface.*

When functionalising through chemical groups the aim is to introduce hydrophilic groups such as carboxylic acid, hydroxyl, and amino groups. to the surface to enhance its hydrophilicity. The sample is hydrolysed by adding a strong base (*e.g.*, sodium hydroxide) to format two surface moieties: carboxylic acid (-COOH) and an hydroxyl group (-OH) (268,286,287). Alternatively, aminolysis can produce free amino groups (288,289). However, this method may affect the degradation rate and other mechanical properties of the surface. Moreover, the use of strong bases can cause an irregular surface etching (290).

The incorporation of functional groups process applies methods such as amination, oxidation, nitration, and halogenation. Functional groups can be added by applying several techniques such as flame treatment, plasma, radiation, and corona treatment. As illustrated in **Fig. 13**, this technique includes radical formation followed by the addition of functional groups to the surface under study. Similarly, radiation treatment plays an important role, where high-energy radiation is applied to break bonds and release free radicals. These alterations of the surface's chemical properties serve to enhance the biocompatibility of the material, by providing a more favourable surface for cell attachment (285).

Plasma treatment can be used to modify the surface chemistry without altering its bulk properties. This technique can be used to enhance hydrophilicity, structure, and roughness so that the intended cell-surface compatibility is achieved. In this method, the sample is exposed to low-pressure gas (*i.e.*, air, ammonia, oxygen, or argon), the gas is ionised and then hits the surface with

View Article Online
DOI: 10.1039/D1TB02628C

very high velocity (291). The surface can incorporate functional groups such as hydroxyls (-OH), aldehydes (-CHO), carboxylic acids (-COOH), and amino groups ($-NH_2$) that enhance the cell-substrate interaction (283,284). A drawback of this technique is that the introduced properties can be lost over time, in particular in polymers where the surfaces have the tendency to reconstitute themselves *via* hydrophobic recovery (290,292).

Notably, corona treatment is the most widely used atmospheric pressure plasma technique. This technique applies a high voltage to an electrode with a sharp tip. This leads to the formation of radicals such as ozone as illustrated in **Fig. 13**. In addition, the very high energy applied near the surface causes chemical bonds to break down. The free radicals present react and recombine with the broken bonds at the surface, modifying its properties. For instance, adding polar groups enhances the affinity to cells, adhesion, and wettability (293–296).

The aforementioned methods present a glance at the various types of surface post-treatment techniques. For example, Castilho *et al.* post-treated printed scaffolds by applying an acid solution which would lead to a series of chemical reactions that enhanced the mechanical properties of the porous medium under study (297). Bertol *et al.* applied different post-processing conditions to 3D-printed scaffolds (298). Immersion of scaffold in binder and Ringer's solution lead to an enhancement in mechanical properties. On the other hand, the immersion of the scaffold in phosphoric acid for example decreased the porosity, which is unfavorable for tissue applications. A wide range of chemical/physical treatments are present in the literature to enhance the chemical and mechanical properties of scaffolds prepared for each specific application.

3.5. Electrospinning

Electrospinning is an extrusion-based method for the fabrication of nanofibers from polymers. It is widely used within tissue engineering for the production of fibrous scaffolds, with heterogeneous and interconnected pores. Some of its advantages can be found in **Fig. 14A**, particularly the high surface to volume ratio and the high tensile strength. A brief explanation on the mechanism of electrospinning is shown in **Fig. 14B**. In conventional electrospinning polymer solutions are used while also molten polymers can be used at elevated temperatures; this is known as melt electrospinning (299).

The role of tissue microenvironments and the ECM have repeatedly been proven to be highly influential in guiding cell morphology (300), attachment (301,302)), proliferation (303), and differentiation (304), where minor changes in structure and surface chemistry (conductivity/charge) can allow for significant changes in cell behaviour (305,306). Electrospinning has the capacity to produce nanometre-diameter fibres and may be able to mimic this microstructure and physical cues to promote differentiation and survival of surrounding cells. With careful control of parameters, fibres can achieve a consistent and reproducible level of fibre diameter and alignment. Examples of this can be found in **Fig. 14C**. where four different fibre arrangements produce completely different morphologies, hence their application.

However, due to the electrostatic attractions induced within the fibres, they generally are deposited with a high packing density, reducing pore size and impeding the infiltration of cells deeper into the scaffold. Several methods have tried to increase this pore size, such as salt-leaching

View Article Online
DOI: 10.1039/D1TB02628C

or ultrasonication, which has been shown to loosen the more densely packed fibres and increase infiltration and viability of cells (307,308). Jeong *et al*. used RGD peptide-modified alginate and PEO at different humidity levels (**Fig. 14D**) to increase the mat thickness and decrease the fibre diameters, increasing the pore size to up to 300 nm, with enhanced fibroblast infiltration and proliferation.

Wet electrospinning can also produce high porosity scaffolds. Here a polymer is spun into a low-viscosity liquid to produce a structure with increased pore size. Chen *et al*. used this method to create a 3D fibrous scaffold of PLGA, with pore sizes in the 5-40 μm of range (309). Furthermore, this method allowed the creation of 3 out of the 4 layers of the articular cartilage, and the successful proliferation and early differentiation of hMSCs (**Fig. 14E**).

Macroporous PCL electrospun vascular grafts have been tested *in vivo* with no evidence of aneurysm or calcification, showing their potential to support the regeneration of neovessels (**Fig. 14F**) through controlled material degradation (310). Cell penetration was also improved by using patterned collectors, which increased the pore size but more importantly the pore size distribution, which allowed fibroblast infiltration to a depth of 250 μm, compared with 30 μm for conventional meshes. Cell response to the patterned collectors can be observed in **Fig. 14G** (311). Another study created nanofiber scaffolds with precisely controlled diameters using customized glass moulds and gas-foaming with aqueous sodium borohydride ($NaBH_4$) solution. This resulted in cell penetration throughout 10 mm of the expanded scaffolds, compared to only surface level infiltration on unexpanded scaffolds (312).

View Article Online
DOI: 10.1039/D1TB02628C

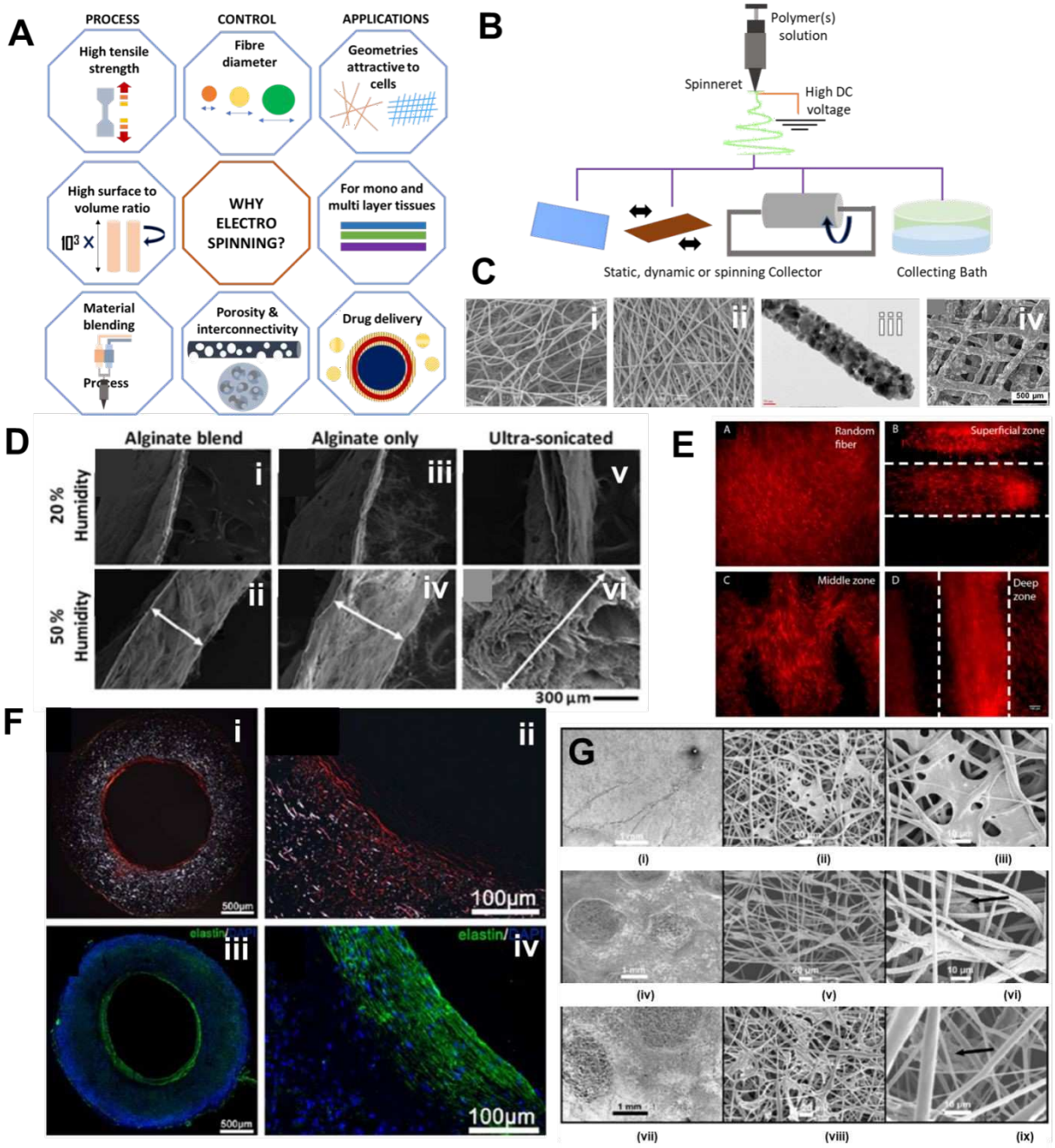

Fig. 14. *A) Relevant characteristics that place electrospinning as a promising material in tissue engineering during the manufacture, characterisation and application of electrospun matrices. B) The main elements of electrospinning are the syringe that feeds a single or multiple polymers/hydrogels, a source of high voltage and different types of collectors. C) Illustration of electrospinning setups: collected from liquid bath i) and conventional flat platform ii). iii) TEM images of TiO_2 NFs and iv) is the morphological characterisation of the PCL/HAp composite scaffolds. D) SEM photomicrographs of cross-sectional sliced mats of (i-ii) alginate/PEO/Pluronic F127-blended nanofibres, (iii-iv) alginate only nanofibres following PEO/Pluronic F127 extraction, and (v-vi) ultrasonicated alginate only nanofibres fabricated at 20% and 50% humidity conditions. E) Immunostaining of collagen type I on hMSCs seeded scaffolds after 21 days of culture in chondrogenic medium: i) RF scaffolds and (ii-iv) sections of the scaffolds, as labelled. The scale bar in iv (100 µm) applies to all panels. The dashed lines in panels ii and iv delineate the collagen fibre orientation. F) ECM deposition. Sirius red staining showed that collagen (red fibres) was distributed in the neo-tissue and into the graft wall i). ii) was the magnified image of i), while collagen distribution in the native blood vessel was shown iii) and its magnified graft iv). G) Cell response on electrospun scaffolds prepared by patterned collectors: compared to the conventional electrospun scaffold i), the scaffolds prepared by patterned collectors were having zones with a lower fibre density of 10-fold increased porosity (iv-vii), and as a result, fibroblasts infiltration was relatively enhanced (ii-iii: normal, v-vi: and viii-ix patterned.*

View Article Online
DOI: 10.1039/D1TB02628C

Reproduced from Open Source: C:i-ii (309), E (313); with permission from Elsevier: Ciii (314), Civ (315), G (311); with permission of RSC: D (307); and with permission from Wiley: F (310).

Abbreviations: *ECM: Extracellular Matrix; hMSCs: Human Mesenchymal Cells; PCL/HAp: Poly(ε-Caprolactone)/Hydroxyapatite; PEO: Polyethylene Oxide; RF: Random Fibre; SEM: Scanning Electron Microscopy; TEM: Transmission Electron Microscopy; TiO_2 NFs: Titanium Dioxide Nanofibres.*

3.6. Bioprinting

Bioprinting can provide high accuracy and reproducibility in 3D biomaterial fabrication, which is a substantial advantage compared to other applied methods (316,317). Bioprinting consists of different printing techniques such as SLA and digital light processing that are used in vat-polymerization (VP) bioprinting in addition to other techniques such as inkjet bioprinting, laser-assisted bioprinting, extrusion bioprinting, and electrospinning-based bioprinting (318,319). These different techniques are illustrated in **Fig. 15**.

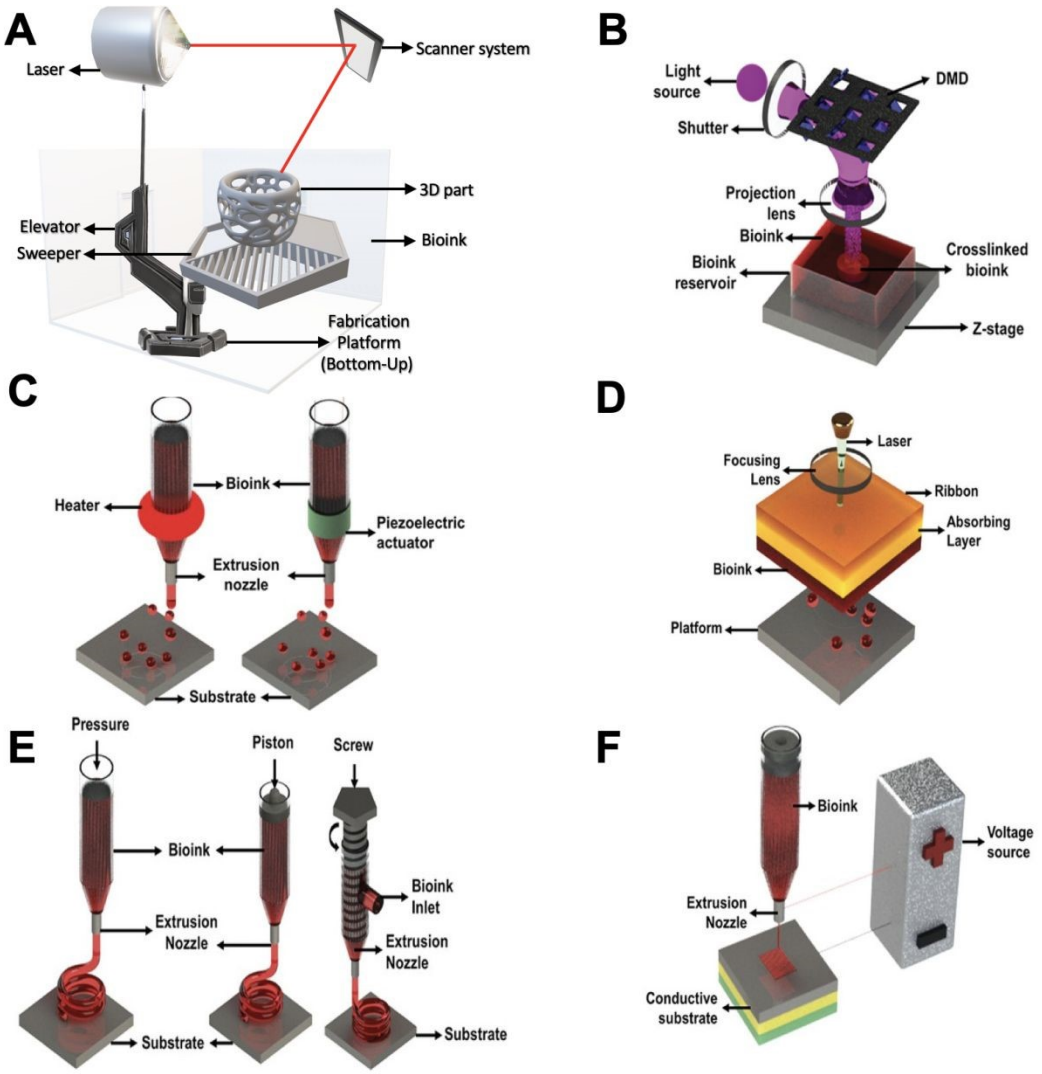

Fig. 15. *Scheme presenting the different applied 3D bioprinting techniques. A) SLA and B) DLP techniques make use of light to selectively change the state of fluid to solid in the reservoir. C) Inkjet bioprinting that is analogous to 2D ink printers while*

View Article Online
DOI: 10.1039/D1TB02628C

replacing ink by bioink and papers with a 3D platform. D) Laser-assisted bioprinting is analogous to the inkjet technique except that it uses laser to make finer deposition for the bioink over the platform. E) Extrusion bioprinting is a technique where the deposition of bioink is done through a mechanical-base manner. F) Electrospinning-based bioprinting makes use of electrospinning techniques through applying high voltage in the bioink deposition process (318,319). Reproduced with permission of Wiley Online Library from (318,319).

Abbreviations: *DLP: Digital Light Processing; SLA: Stereolithography; VP: Vat Polymerisation.*

3.6.1. Stereolithography Apparatus and Digital Light Processing

SLA uses layer-by-layer photocrosslinking to fabricate 3D structures by a spatially selective state-change of fluid in the reservoir (320). The first medical application was the reconstruction of high precision, detailed cranial tissue with (321). A 2D pattern is projected on the bioink reservoir (**Fig. 15A**), allowing the formation of the intended 3D structure. As the method uses light, no shear stress is applied and cell viability is maintained. Importantly, this method is considered high resolution, with the ability to generate 3-μm features in a 100-μm-thick hydrogel (322). SLA is one of the additive manufacturing techniques defined by VP (**Fig. 15B**). A version of SLA, termed as μ-SLA, aims to produce (sub)micrometre-resolution printing *via* the bespoke laser-based SLA set-ups, allowing the printing of complex micro-geometries.

In DLP, the cross-sectional area from each layer of the computed model is oftentimes printed by projecting light onto a digital micromirror device (DMD), containing up to one million micro-mirrors, or a liquid-crystal device. This projects a 2D pattern into the resin reservoir, enabling the solidification of an entire layer in a single exposure. Afterwards, the platform is translated in the y-axis and the process is repeated until the completion of printing (323,324). DLP printing has a remarkable printing speed that can reach 0.05 m/s and an acceptable resolution of 1 to 2 μm with a layer thickness of 1 to 10 μm (325). This is achieved by eliminating the interfacial interfaces, and materials printed with inclusion of cells have shown superior cell viability (>85%) (325).

Both SLA and DLP processes involve a layer-by-layer deposition of photocurable resins, supported by a static bed (323). However, DLP allows for parallelisation of the photocuring process which results in faster printing, and a more efficient operation at a wider range of wavelengths. The efficiency of DLP methods also rely on their ability to use customised resin reservoirs and small volumes of photoreactive resin (326).

3.6.2. Inkjet Bioprinting

Boland *et al.* patented inkjet bioprinting in 2003 (327). The concept is analogous to 2D inkjet printing, with the ink replaced by bioink and paper by a 3D platform, allowing the formation of 3D structures (328). As illustrated in **Fig. 15C**, the deposition of bioink is controlled by changing the extrusion nozzle size *via* thermal or piezoelectric actuators. The deposition of bioink will eventually build the intended 3D structure. This technique is considered a low-cost, simple, rapid, high cell-viability, and high-resolution bioprinting method (329–331). Gao *et al.* used a bioprinter, to deposit eight materials and crosslink bioprinted units to create a mechanically strong and suitable structure for bone and cartilage applications (329). Yoon *et al.* innovatively combined

View Article Online
DOI: 10.1039/D1TB02628C

inkjet bioprinting and spray-coating techniques producing bioprinted tissues that showed very high cell proliferation, in addition to a remarkable cellular activity (332).

3.6.3. Laser-Assisted Bioprinting

Duocastella *et al.* first introduced laser-assisted bioprinting to the tissue-engineering field (333). Similar to inkjet, this is a direct-writing technique but importantly it uses a high-intensity pulsed laser to print the bioink. This method has a set-up as shown in **Fig. 15D**, consisting of two parallel surfaces called the ribbon and the acceptor surface. The transparent ribbon material (typically glass or quartz) has the bioink coated on top of a thin layer that absorbs the laser light (*e.g.*, a 10- to 20-nm-thick layer of gold). The printing occurs when a laser is focused at a certain specific pixel of the ribbon, the absorbing layer vaporizes and impels a small droplet of bioink due to the increase in pressure. The impelled droplet deposits on the acceptor surface. This method maintains a very high cell viability in addition to its very high resolution. However, it is still not a frequently used technique due to its high cost and the need for further optimisation studies (334–336).

3.6.4. Extrusion-Based Bioprinting

Zein *et al.* introduced the extrusion-based mechanism for 3D bioprinting (337). **Fig. 15E** illustrates the two main techniques used: pneumatic and mechanical driven extrusion. Pneumatic systems, which can be a valve or valve-free, use pressure to inject bioinks onto a platform (338). Mechanical systems can be controlled by a piston or by a screw. The aforementioned systems serve to inject bioinks that will deposit and form a 3D structure. The extrusion-based technique can be used for high-viscosity bioinks and is a continuous and not droplet-deposition method, however there is a moderate impact on the viability of cells due to the high shear stresses imposed in this technique (330,338,339).

3.6.5. Electrospinning-Based Bioprinting

Melt electrospinning-based bioprinting (MEBB) is another form of electrospinning, where a high voltage is applied to melt the polymer coupled with the solidification process. This process can achieve a high level of control and resolution. MEBB showed the ability to deposit fine fibres up to 650 nm, which may be utilised to increase the resolution of bioprinting. **Fig. 5F** shows the setup consisting of a robotic stage where the electrospinning equipment is set, an extrusion system, a pneumatic regulator, and a high-voltage source. This method can either apply a continuous or discontinuous deposition of inks (340–343).

4. Applications

Human tissues are porous in nature. This porosity ranges from the nanometre scale, to allow the diffusion of oxygen and metabolites through the ECM, up to the millimetre-scale, seen within the trabecular bone (344). The organisation of pores in native tissue is complex and hierarchical, playing a vital role in its mechanical properties and biological functionality. Each tissue has a different arrangement depending on its function and location in the body.

View Article Online
DOI: 10.1039/D1TB02628C

Mimicking these structures is key for the development of successful scaffolds for clinical applications. Initially it was often not possible to use synthetic materials for larger-scale organ/tissue repair due to the limitations of diffusion and poor integration with the host tissue that resulted in poor cell infiltration, necrotic cores, fibrotic capsule formation, and subsequent graft failure. However, recently, the potential to control the pore size, interconnectivity, and porosity has led to the possibility of viable scaffolds for implantation.

4.1. Bone Tissue Engineering

In bone replacement scaffolds, porosity and material topography play imperative roles in helping modulate osteogenesis and neovascularization. High and variable porosities and pores larger than 100 μm are ideal for nutrient diffusion, the development of the osteons, and mineralisation (147). Diverse geometries and surface topologies can be observed in **Fig. 16A**. However, by increasing the previous features, a decrease in the mechanical strength of the porous structure can impact their performance, as bones support for high-load-bearing regions.

Due to their notable mechanical properties, metals were the first materials to be considered suitable for bone regeneration, in particular in load-bearing applications. However, they are intrinsically bioinert and diverse efforts have been made to promote their biocompatibility, bioactivity, and enhance their osteoconductive and/or osteoinductive characteristics. For example, micro-/nanoporous Ti scaffolds have been surface-modified to improve osteoblast attachement and differentiation (345). A more recent study developed 3D-printed porous Ti (Ti6Al4V) scaffolds with pores around 600 μm and reported favourable bone ingrowth and fixation stability (**Fig. 16B**). Improved bioactivity was achieved by an alkali acid-heat treatment and simulated body fluid (SBF) immersion (346). In a third approach, 3D-printed stiff Ti scaffolds were coated with polyamide, and demonstrated to trigger bone regeneration in *in vivo* sheep trials (**Fig. 16C**) whilst maintaining their load-bearing structural role (347).

CaPs, although showing great promise in terms of biocompatibility and osteoconductivity, are heavily limited by their low toughness and poor fracture resistance. Various studies have demonstrated enhanced properties obtainable from CaPs with the addition of structural coatings (through sol-gel or electrodeposition) or by using ECM proteins, such as type I collagen, which forms a critical component of the bone (348,349). Inzana *et al.* recently produced macroporous collagen-CaP scaffolds using a low-temperature inkjet 3D-printing methodology (350). Their results showed that the fabricated scaffolds had greater mechanical strength as well as allowing for increased bone regenerative capacity within a critically sized murine femoral defect. As an alternative proposal, octacalcium phosphate (OCP) has been doped with Fe^{3+} to enhance affinity and cell growth, whilst promoting angiogenic differentiation through its controlled release (347,351). The final porous structure and pore orientation can be found in **Fig. 16B** (351).

Synthetic biocompatible or/and biodegradable polymers such as PLA, PCL, and PEG are commonly used in bone scaffolds due to their customisable chemical, physical, and mechanical properties. Polymer composite scaffolds have shown to improve osteogenic abilities; for example, the addition of PEG into porous PLA scaffolds supported growth of mineralising osteoblasts (80). Through 3D-printing technologies, a PLGA/TCP/Icariin (PTI) scaffold was manufactured and

View Article Online
DOI: 10.1039/D1TB02628C

showed a stable structure with enhanced angiogenesis properties when implanted in a necrotic rabbit model (352). Additionally, the composite had a controlled degradation whilst maintaining its structure. The relation between the mechanical properties and degradation rates are reported in **Fig. 16D**.

Other common materials popular due to their mechanical stability include MBG, which has been demonstrated to be biocompatible and osteoinductive (339,353,354). Zhang *et al.* manufactured MBG scaffolds containing strontium forming a highly porous scaffold with increased biological activity. Strontium, a trace element found within human bone, promotes osteoblast differentiation and inhibits the osteoblasts' bone-resorbing activities (354). Their study used 3D-printed slurries made of Sr-MBG and PVOH with compressive strengths of ~8-9 MPa, comparable to that of trabecular bone, as well as a good apatite-forming ability in the osteoblast-like cell line MC3T3-E1. Whilst the use of slurry-based inks may bypass the use of toxic solvents, the process is restricted by long drying times between layer deposition, limiting their use for the larger and more complex scaffolds that may be necessary within bone engineering. A similar glass approach was developed using chitosan-diatomite composites (silica) where high porosities (82-90%) and pores larger than 200 μm exhibited high compressive moduli and early mineralisation (355). The different pore and interconnected morphologies can be observed in **Fig. 16E**. Finally, having in mind the importance of both mimicking the porous structure of the bone, and bearing the mechanical load from the host tissue, a trimodal MGB scaffold was manufactured with meso-, macro-, and nanopores enriched with BMPs, was demonstrated to perform successfully for medullary cavity reunion (189).

It is clear that the macro- and microstructures of the constructs play an important role in the modulation of osteoblast survival and osteogenic mechanisms. This growth is complemented by the long-term support of the structure. However, challenges in bone regeneration remain in defining clear parameters for the balance of physical, mechanical, chemical, and biological features.

View Article Online
DOI: 10.1039/D1TB02628C

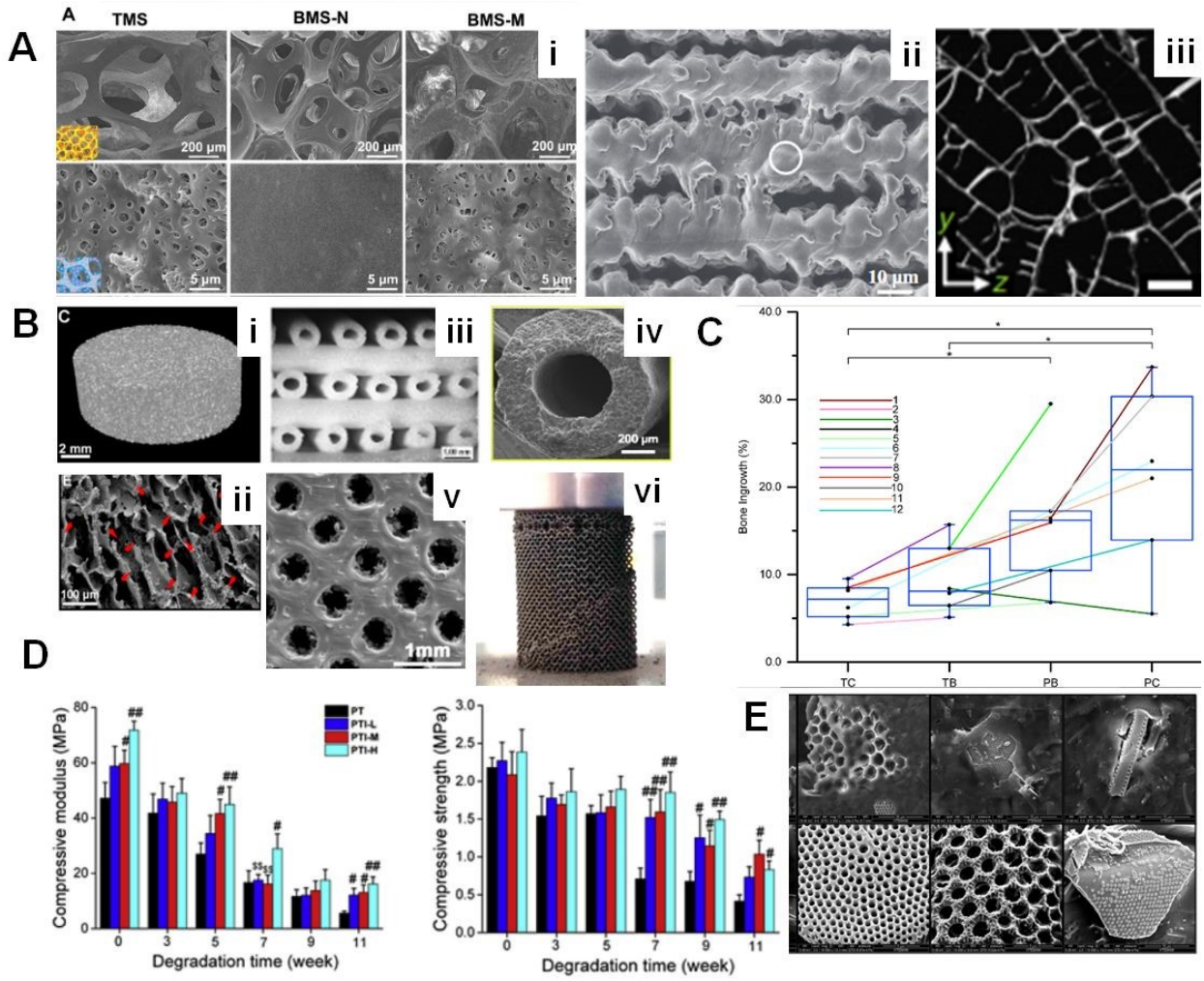

Fig. 16. *A) i) Structural analyses of trimodal MGB scaffolds: SEM images of the macroporous networks (upper row) and surface topologies (bottom row). ii) SEM images of the LTi-1 Ti porous scaffolds. iii) Scaffold pore architecture guides cell migration in vitro. Here, a perpendicular to the direction of directional freezing during production. B) μCT images i) and SEM internal structure ii) of an iron-doped OCP/PLGA scaffold for potential cancerous bone regeneration. iii-iv) The characteristics of the ceramic 3D-printed hollow-pipe-packed BRT-H scaffolds. Channels = 500 μm. v) Micrographs of 3D-printed porous Ti6Al4V specimens for mechanical in vitro test. vi) Failure modes observed in unfilled samples of porous Ti structures. C) Bone ingrowth observed in four scaffold groups (Ti control: TC; Ti biomimetic: TB; Polyamide biomimetic: PB; and Polyamide control: PC). Samples are plotted in the order of decreasing stiffness: TC – stiff, TB and PB – matching the moduli of trabecular bone, PC – most compliant and anisotropic. Box plots are superimposed onto the same graph. D) Mechanical changes in volume and mechanical properties during degradation of PLGA/TCP/Icariin: PTI) scaffolds in vitro. E) SEM of biosilica incorporated chitosan scaffolds with 100x (1 mm), 250x (500 μm), and 1000x (100 μm) magnification. Reproduced from Open Source: Aiii (356), C (347); with permission from Elsevier: Ai (147), Aii (345), B:i-ii (351), B:iii-iv (357), Bv (346), Bvi (358), D (352), and E (355).*

Abbreviations: *BRT-H: Silicate Bioceramic; MBG: Mesoporous Bioglass; μCT: Micro-Computed Tomography; PTI: PLGA/TCP/Icariin: Poly(Lactic-co-Glycolic Acid)/β-Calcium Phosphate/Icariin; SEM: Scanning Electron Microscopy.*

4.2. Auricular Tissue Engineering

The externally visible part of the ear, which is mainly constituted from elastic cartilage, is termed the auricle and is mainly responsible for collecting and converging sound to the middle ear (362). Auricular damage therefore not only affects the aesthetic appearance of the individuals but also compromises their hearing capabilities (359). The medical concerns around auricular

View Article Online
DOI: 10.1039/D1TB02628C

malformations emerged back in 1920s, while in 1930s, the need for the development of scaffolds that are biocompatible and stable to reconstruct the auricle area was clearly stated (360). This opened the door to research in the area where both the autologous surgical procedure and reconstructive scaffold development were studied in detail.

Aside from the difficulties finding suitable autologous tissue (361), many issues were faced when using autologous costal cartilage. These include the need for several surgeries to complete the reconstruction of the compromised donor site, significant pain after surgery, pneumothorax risks, and the fact that the results are not always optimal even when performed by an expert (362). This had shifted the research attention towards alternative approaches and spiked interest in tissue engineering using biomaterials. Some of the main approaches followed in auricular tissue engineering are shown in **Fig. 17** and will be explained in the following section.

Among the many alternatives developed, implanting and growing a constructive scaffold on the back of a mouse is one of the most famous (363). In the first work based on this methodology, a copolymer PLA and PGA scaffold was seeded with primary chondrocytes and then implanted subcutaneously. New cartilage started to grow from the explanted tissue after 12 weeks. This was the beginning of many studies based on this methodology (364–375). The interested reader may refer to other reviews for more details (376,377).

Strategies differed from an *in vivo* method where, after scaffold implantation, the surrounding tissue provides cells for new tissue development, to other approaches that improve this tissue formation *in vitro* or *ex vivo* by combining the scaffolds and cells (367,378).

Many biomaterials, both synthetic and natural, have been explored for the development of scaffolds with an architecture similar to that of the auricle. Moreover, many polyesters such as PU (379), PGA (368), PCL (364,375,380–382), and PLA (383) were part of the biodegradable synthetic biomaterials used in auricular tissue engineering. Other synthetic biomaterials used for scaffold development comprise biostable inert materials, including PE (365,378). On the other hand, many natural biomaterials have been investigated including alginate (375), nanocellulose (373), and a mixture of alginate and silk (384).

View Article Online
DOI: 10.1039/D1TB02628C

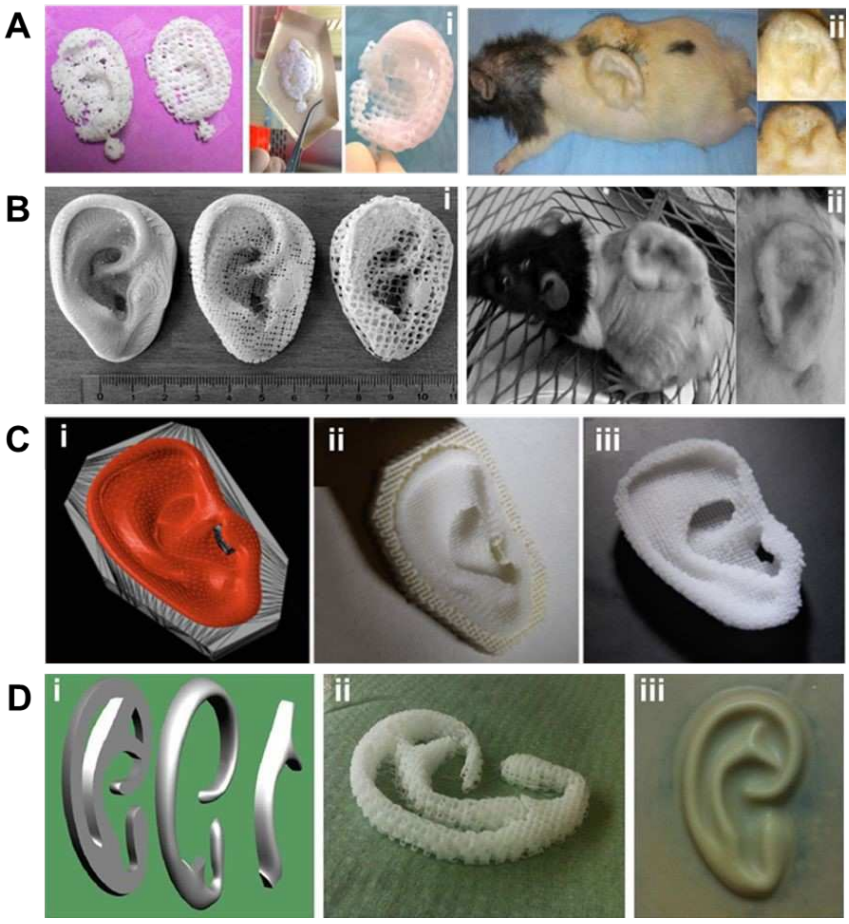

Fig. 17. *Some of the main strategies for auricular tissue engineering. A) i) Random and pore ear scaffolds before, during, and after seeding. Random and spherical pore ear scaffolds (left). Scaffold in Sylgard® mould (mid). Scaffold seeded with chondrocytes in a collagen-hyaluronic acid hydrogel (right). ii) Ear scaffolds after subcutaneous implantation. Posterior surface up on right dorsum, anterior surface up on left dorsum (left). Anterior face surface details (right upper) and anterior oblique view highlighting excellent projection (right lower) (385). B) Printed PU auricular prostheses with varying degrees of porosity; i) starting from left to right: non-porous PU; microporous PU; and macroporous PU. ii) Ear scaffolds after subcutaneous implantation (386). C) 3D-printed complex anatomical structures based on PCL with PVOH support of the right ear. i) CADs showing permanent (red) and sacrificial (grey) components. ii) Printed structures showing PCL (bright white) and PVOH (off-white). iii) PCL scaffold after sacrificing PVOH support (387). D) i) Modular approach where each module exhibits decreasing cross-sectional diameter and allowance of adequate oxygen gradient. i) Assembled modular construct printed in PCL ii) that displays satisfactory aesthetic appearance under rubber 'skin' (388).*

Abbreviations: *PCL: Poly(ε-Caprolactone); PU: Polyurethane; PVOH: Polyvinyl Alcohol.*

During *in vivo* implantation, the scaffold needs to be stabilised, which is why metals, such as Ti, have been used in the process (389). Comparing the collagen scaffolds manufactured in a PDMS mould both with and without the Ti framework, it could be seen that a distorted and flattened geometry was obtained when the metallic framework was not used, unlike the relatively unchanged geometry when Ti was deployed (389). Another study combined the use of Ti framework with polymer meshes developed using electrospinning and implanted in mice, which demonstrated a new cartilage formation that retained its shape with time due to the metallic framework (364). It should be noted here that although this approach has its advantages in stabilising the structure during the formation of the neocartilage, another surgery will be needed to remove the metallic framework.

View Article Online
DOI: 10.1039/D1TB02628C

Manufacturing scaffolds with an appropriate geometry is possible using many biofabrication strategies to accurately reproduce the geometry of the designed mould (384,390,391). Additive manufacturing was the technique of choice in many studies (375,380–382). Additionally, bioprinting was used for the same purpose where hydrogels, or bioinks, are used for 3D construct manufacturing. Several studies have also reported methods that combine more than one strategy in the same process, such as the manufacturing of polymeric scaffolds to serve as the mechanical support for the structures that are bioprinted (375,380–382). In such studies, additive manufacturing was used to produce PCL scaffolds, which in turn were bioprinted with alginate that contained chondrocytes, or were deposited with the plain alginate, specifically in their pores, after being seeded with a rabbit's auricular chondrocytes (382). Comparing the two approaches, it was reported that bioprinting the cells on the PCL produced scaffolds with better levels of GAG, and collagen type II, as well as increased cell viability levels compared to the strategy where cells were seeded onto alginate. Furthermore, better regeneration was observed upon performing the implant in a rabbit's ear when the cells bioprinted on PCL were used, as opposed to the partial regeneration observed when using the PCL scaffolds seeded onto chondrocytes. Other methodologies based on combining different biofabrication strategies were also reported. Moreover, the combination of PCL supportive structure and the selective dispensing between the decellularized cartilage-based ECM polymer filaments or alginate along with auricular chondrocytes was also stated (375). Using this methodology, GAGs and collagen type II, which are the hallmark of cartilaginous tissue, were observed following 8 weeks of the *in vivo* experiment of the subcutaneous implant in mice.

One of the challenges facing is finding an appropriate cell source to develop a cartilaginous framework (392). Many approaches had been evaluated for this purpose where one of the most common is the use of chondrocytes isolated from the patient. However, many concerns such as the dedifferentiation of chondrocytes, along with the limited availability, have urged research to move in an alternative direction. Moreover, combining bone marrow-derived mesenchymal stem cells (BMSCs) with primary articular chondrocytes in different ratios was one of the alternative approaches proposed by Kang *et al.* for ear cartilage engineering (305). It was reported that, for new cartilage tissues to form *in vitro*, at least 30% of chondrocytes viability is required. Consequently, cells were used in different ratios for culturing of PGA fibrous nonwoven scaffolds, and it was reported that a smaller construct size was obtained when fewer chondrocytes and BMSCs were used relative to different conditions. After 8 weeks cultures with more than 30% of chondrocyte viability were comparable to chondrocyte controls in terms of GAG, collagen type II deposition, as well as mechanical properties. Morrison *et al.* investigated a similar approach where the combination of BMSCs and collagen type I hydrogel was tested (372). Thermal gelation was applied to the cells encapsulated in the hydrogel, and the implantation took place in nude mice. Comparing the results obtained using this approach to 100% chondrocyte and 50:50 ratio of chondrocytes to BMSC after one and three months, significant resorption was reported but a lower expression of GAGs especially for the 50:50 ratio. The previously reported studies shed light on the interesting approach of using animal stem cells from bone marrow combined with many cartilage sources, but it is still not validated in humans, which means that notably more work needs to be done in order to use such approaches clinically (393). Human cell sources have also been investigated, where a combination of stem cells derived from the human adipose, and scaffolds derived from small intestine submucosa had been previously reported (394).

View Article Online
DOI: 10.1039/D1TB02628C

Up until now, the tissue engineering approaches reported were validated both *in vitro* and *via* using different animal models (379,384,390). Different conditions and materials were tested on small rodents where a partial scaffold is implanted subcutaneously; however, the use of the reported results to develop a full-size human scaffold model is still very limited. It is only recently that the very first human clinical trials were reported (383). In this study, patients affected with microtia had been treated using different approaches based on their case **Fig. 18**. Data from a μCT scan of the patient's ear was used to construct a 3D model. A negative mould was then prepared using a 3D-printing technique that produced a master of the ear. The scaffolds consisted of two PGA nonwoven fibre layers that surrounded a PCL inner core and were coated with bonded PLA. The microtia cartilage was used for the collection of the autologous cartilage biopsies, and in vitro expansion and isolation of the chondrocytes was performed. In the first surgery, the implantation of a skin expander was necessary to obtain enough skin to cover the implant in the second surgery. Before the re-implantation occurred, *in vitro* culturing of the scaffolds seeded with chondrocytes took place for 12 weeks. The implantation of this in vitro cultured scaffold took place in the second surgery and the skin expander provided extra skin to cover the construct. The patient developed a mature cartilage and benefitted from an adequate aesthetic reconstruction as reported by the authors when referring to the follow-up at 2.5 years after surgery. This significant advancement in the field still needs to be coupled with more details on the function of the ear, and a discussion on the middle and inner ear structures development, since microtia and anotia patients often suffer from other complications in the middle and inner ear. Additionally, the focus of such studies should not be centred only on the aesthetic aspect, but rather on restoring the hearing function of the patient as part of functional therapy.

Auricular tissue engineering has evolved significantly over the last few years, but challenges still need to be addressed to make a real breakthrough in the field. As a poorly vascularised tissue, it struggles to promote transfer of molecules and nutrients. The generation of skin to cover the implant, which takes extensive time and needs to be done in a more efficient and timely manner. However, the preliminary clinical trials show great promise and could be the next alternative therapy to autologous tissue.

View Article Online
DOI: 10.1039/D1TB02628C

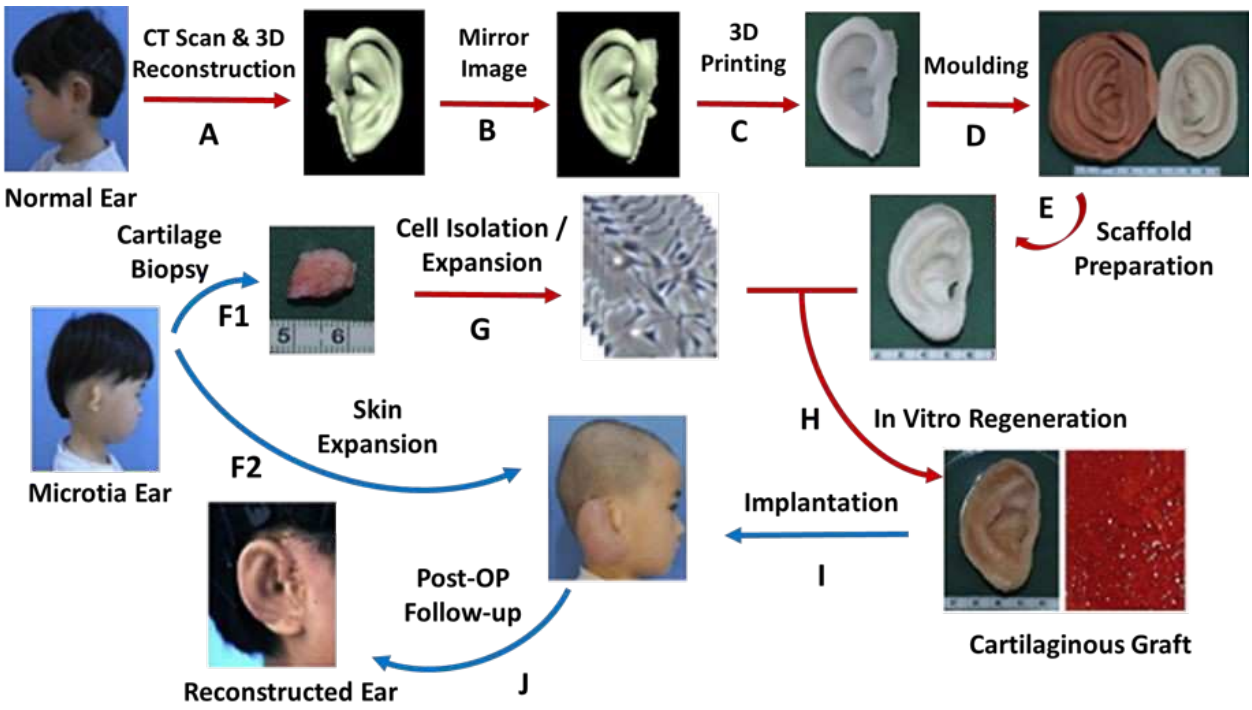

Fig. 18. *Schematic representation of a human auricle reconstruction using human ear-shaped cartilage developed through tissue engineering. Adapted with permission (383). Arrows in red refer to lab procedures while arrows in blue are surgical procedures.*

Abbreviations: *3D: Three-Dimensional; CT: Computed Tomography; Post-OP: Postoperative.*

4.3. Articular Cartilage Regeneration

While cartilage is innervated, it lacks blood vessels, making healing and regeneration difficult. Therefore, for effective chondral regeneration biomaterials must offer a spatial frame for new cell proliferation, migration and differentiation. Due to concomitant diseases associated with the loss of cartilage, most of the biomaterial proposals for chondral regeneration have focused on articular cartilage. This tissue is formed by 4 layers that differ in fibre composition, orientation and organization, which influence the cell concentration and morphology. Early approaches have intended to reproduce a single matrix that can be used for regenerating one or all layers, whilst novel approaches include graded and multi-layer scaffolds that resemble the host tissue, as shown by the complex designs in **Fig. 19A** and **Fig. 19B** (395–397).

Due to the viscoelastic nature of the native tissue, materials as hydrogels, colloids and soft polymers are commonly used for chondral regeneration as they can bear and recover from load cycles, through biphasic viscoelastic behaviour (where the internal tissue fluid pressure interacts with the load through a slow stress-relaxation process) (398). Eftekhari *et al.* reviewed the most common materials used for this application and highlighted that hydrogels have good degradation rates and encourage ECM production but lack mechanical stability and positive cell adhesion (399). On the contrary, polymers have good mechanical strengths and strains to failure, but most cause immunoreactivity and present complications for degradation. However, as a middle ground, both materials are mostly biocompatible, and good for drug and cell delivery. Challenges for any proposal in this area remain on encouraging a hyaline-like tissue formation.

View Article Online
DOI: 10.1039/D1TB02628C

The geometrical configuration of the implant/scaffold is important in two ways: it provides a stable temporary frame for the formation of neotissues, and it helps the transfer of fluids, molecules and cells. The compressive and tensile moduli of human articular cartilage have been reported as 0.079 ± 0.039 to 13 ± 4.2 MPa, and 0.76 ± 0.13 to 54.6 ± 37.6 MPa respectively. Olubamiji *et al.* studied the various molecular weights associated with pore size, orientation, and spacing on PCL scaffolds and their influence on the mechanical properties of the material. By independently varying pore size and spacing the porosity of the scaffolds differed significantly; however, it was barely affected by pore orientation. Nonetheless, even with mixed pore configurations, the scaffolds did not collapse and their mechanical properties were still close to those in the host tissue (400).

This is not the case for natural polymers and hydrogels, which struggle to keep solid structures. Mechanical properties of silk-fibroin-chitosan freeze dried porous scaffolds were tailored obtaining compressive moduli close to that the native tissue (401). The compressive moduli of sodium alginate-gelatin constructs have been tuned to reflect those found *in vivo* by varying the thickness, slice gaps and scaffold size. Kankala's populated scaffolds can be observed in **Fig. 19C** (402).

Pore geometry and orientation have been shown to impact cell differentiation. Electrospun oriented nanofibers showed a higher level of GAGs and type II collagen compared with microfibres, and were better suited for the superficial layer of the articular cartilage (403). Preference for nanofibres has been confirmed by Chen *et al.* who incorporated glucosamine sulfate (GAS) to their PCL/GAS nanofibres and studied the release of ECM in them (404). Other macromolecules have been incorporated into electrospun nanofiber meshes to enhance cell recognition and adhesion including amino groups from chondroitin sulfate, one of the most important GAGs found in cartilage (18), and illustrated in **Fig. 19D**.

Biomaterials should also address the biological environment. Hydrogels, both IPNs and SPNs, have been extensively used as they retain molecules and cellular bodies, and can be tailored to disintegrate to various rates. Additionally, they can be enriched with drugs, macromolecules, and growth factors (402,405).

Zhao *et al.* photocrosslinked a chitosan-alginate-based scaffold, porous through salt-leaching (406). They took advantage of the biocompatibility, low immunogenicity and biodegradability of the chitosan and improved the cell adhesion through the addition of gelatin. They observed cell adhesion and proliferation rates increased for 14 days; this differentiated behaviour promotes the production of type II collagen, also found on chondrocytes seeded on channelled constructs obtained from collagen sponges (407) and decellularized porcine articular cartilage (408).

The latest proposals are hybrid scaffolds where the inherent inflammatory effect from synthetic materials is balanced by the addition of natural ones in-formula or as a coating through hydrogen bonding, ionic interactions, and chemical or mechanical crosslinking (409–411).

View Article Online
DOI: 10.1039/D1TB02628C

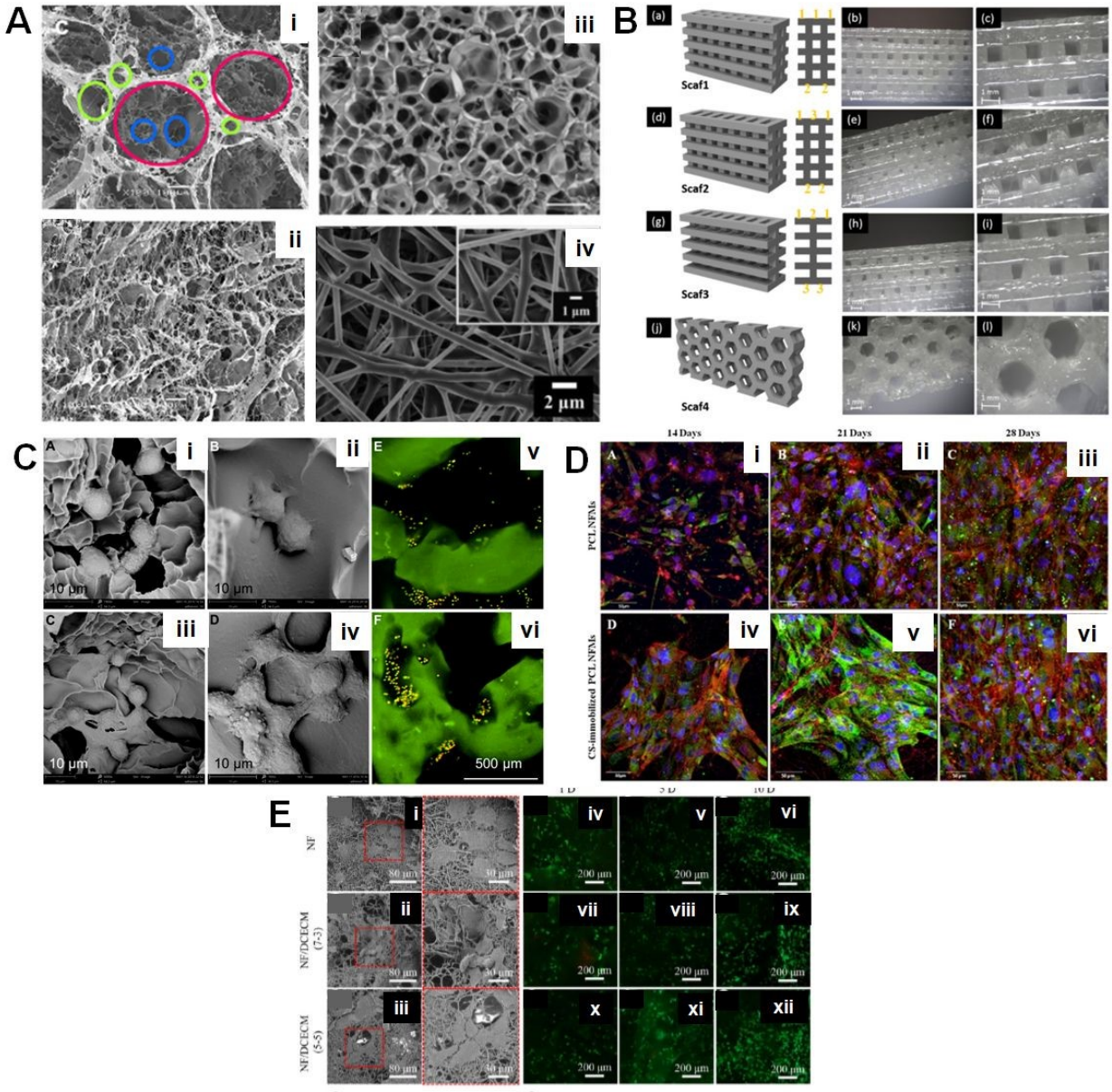

Fig. 19. *A) SEM micrographs of: i-ii) Top surface of 400 mm-3D funnel like collagen sponge. Red circles, green circles, and blue circles indicate large surface pores, small surface pores, and inner bulk pores, respectively. iii) Heat-treated lactose-crosslinked fish gelatin-based porous scaffolds. iv) Nanofibrous GAS-PCL mats. B) Layered gelatin/PLLA scaffold models and their structure after the printing process. Samples prepared for mechanical tests. C) Chondrocytes distribution on 3D-printed sodium alginate-gelatin scaffolds. i-iv) SEM images showing the adhesion of chondrocytes after i) 1, ii) 3, iii) 5, and iv) 7 h. v-vi) CLSM images showing the distribution of cells over the scaffolds at different magnifications. D) Confocal microscopy images of hACs seeded onto i-iii) PCL-NFMs and iv-v) chondroitin sulfate-immobilized PCL-NFMs along the time course of the experiment (i.e., 14, 21, and 28 days). Cytoskeleton evidenced by phalloidin is shown in red, nuclei are stained blue for DAPI and vinculin is stained green. E) Cell morphology and cell viability assay of 3D nanofibre DCECM scaffolds. i-iii) SEM images of chondrocytes seeded on the scaffolds after 3 days of culturing. iv) Cell adhesion rate on all three scaffolds. v-xii) Confocal microscopy images of live/dead cell staining of the scaffolds seeded with chondrocytes after 1, 5, and 10 days of culturing, respectively. Reproduced from Open Source: C (402); with permission from Elsevier: Ai-ii (407), Aiii (410), Aiv (404), B (412), D (413); and permission from ACS: E (19).*

Abbreviations: *CLSM: Confocal Laser Scanning Microscope; DAPI: 4',6-Diamidino-2-Phenylindole; DECM: Decellularized Cartilage Extracellular Matrix; GAS: Glucosamine Sulfate; Hacs: Human Articular Chondrocytes; NFM: Nanofibres Meshes; PCL: Poly(ε-Caprolactone); PLLA: Polylactic Acid; SEM: Scanning Electron Microscopy.*

View Article Online
DOI: 10.1039/D1TB02628C

4.4. Reconstructive Tissue Engineering

Although there are still many challenges in the production of complex artificial organs, there are a few applications that have already found their ways through to the clinic, such as skin grafts, trachea, and hernia repair implants (414–416).

Many different biomaterials are available for use in reconstructive medicine. Hsieh *et al.* reviewed one of the most popular techniques for the development of porous materials for reconstructive surgery, 3D printing, and reported that porous scaffolds could be printed with long-term fidelity and controlled mechanical properties, with the aid of computational models and CAD for presurgical planning and the implantation of patient tailored constructs (417). In addition to the reproduction of robust complex structures, scaffolds have been ameliorated through coatings, and molecule or drug delivery systems (416,418).

Although there has been a huge advancement in 3D-printed materials for reconstructive surgery in the last 10 years, some challenges still need to be overcome: *i*) the biological transition from inert to biofunctional/mature materials ready for implantation); *ii*) a technological jump, as there are only few matches between materials and manufacturing techniques; and *iii*) the regulatory gap between reliability and safety related to upscaling (419).

Reconstructive tissue engineering has shown success in the repair of the largest organ, the skin. 3D printing has been used to produce chitosan-based porous (400 μm) scaffolds, that provided successful cell adhesion and proliferation in both *in vitro* co-cultured structures (fibroblasts and keratinocytes), and *in vivo* in diabetic rats' wounds (420). Similarly, porous pullulan/gelatin (PG2) scaffolds manufactured through particulate leaching and controlled degradation showed good *in vivo* results in mice for healing kinetics, wound bed-body immersion, and scarring. **Fig. 20Ai** shows the internal porous structure that supported wound-healing (421). The effect of porosity has also been explored in silk fibroin (SF) scaffolds with a mixture of micro and nanopores that supported neogenesis and collagen matrix formation of fibrous microstructures for dermal tissue reconstruction (**Fig. 20Aii**) (67). However, enhancing innervation and vascularisation of the constructs has yet to be addressed. To support angiogenesis, gelatin-sulfonated silk constructs were 3D-printed and supplemented with fibroblast growth factor 2 (FGF-2). Successful granulation and wound healing were observed; vascularisation aided by the FGF-2 (422). Joseph *et al*. also confirmed the benefits of supplementing their PCL-gelatin scaffolds with growth factors and human urine-derived stem cells (423).

Surface modifications have also shown positive results on dermal flaps. Electrospun PU-PLLA constructs surface modified with acrylic acid were studied both *in vitro* and *in vivo* with enhanced cell proliferation rates and a greater angiogenic response in comparison with uncoated membranes (227). Similarly, cellulose-gelatin emulsions were used to increase the natural polymer's bioactivity and cell penetration (**Fig. 20Aiii**), accelerating the wound healing process (424). A treatment on pressure sores has been robustly developed on fibrin/alginate porous scaffolds combined to a plasma polymerised PDMS membrane which is intended to aid chronic pressure sores treatment. The hybrid membrane increased its material stability whilst still enhancing cell infiltration and proliferation, illustrated in **Fig. 20B** (425).

View Article Online
DOI: 10.1039/D1TB02628C

Challenges still remain as current manufacturing techniques are unable to fabricate large flaps of artificial skin with full vascularisation, and tissue engineered skin with functional structures (*e.g.*, sweat glands and hair follicles) has still not been generated successfully (426).

Vascularisation and innervation of implants have also been studied on their own. PLL/PLGA porous scaffolds that have been shown to induce neuro-vascular interactions were co-cultured in a system supplemented with genetically encoded calcium indicators (GECIs) (427). The study allowed the research group to monitor functional activity of the neural and vascular network in complex constructs (428). From the neural perspective, wall morphology has an impact on the material's resistance. The influence of the cross-sectional morphology of porous PLGA conduits were studied through modelling and mimicking a force stimulus. They developed a comprehensive study on porosity, number of layers and their arrangement. As a means to study vascularisation of scaffolds, Kong *et al.* assembled a tissue flap into a vascular pedicle, using the body as a bioreactor (429). By connecting their early vascularised construct to a human capillary network, they could track the tissue cells' behaviour, and the angiogenic process. The proof of concept allowed them to understand what other parameters and supplements would impact the healing process, compared to the native human abdominal skin.

Tissue engineering has also been employed to reconstruct genitourinary and gastrointestinal tissue. As shown in **Fig. 20B*i-ii***, hollow collagen hyaluronic with platelet-rich plasma doped constructs can be tailored for use as ureter-like tubular and bladder-like scaffolds due to the natural collagen's chemical composition and the scaffold's ability to withstand fluid pressures (430,431). In a similar context, abdominal tissue regeneration has also taken advantage of porous solutions. A radial pore-oriented collagen scaffold (RP-Composite) was tested in rabbit diaphragmatic hernias. The pore size and orientation (**Fig. 20C**) impacted in the pressure resilience, but denoted overall better results than on commercially available scaffolds (432). Similarly, pectin-based 3D porous scaffolds with tailored degradability and the possibility to be used as cell carriers were studied for use in peritoneal adhesions due to their potential antiadhesive effects (**Fig. 20C*ii, iv***) (433). Finally, porous poly(L-lactide-co-ε-caprolactone) (PLCL) scaffolds have been proposed for vaginal tissue engineering due to their elastic modulus and biocompatibility, evidenced by the cellular results on epithelial and stromal cells (434).

Fibroblasts have shown a positive alignment with polymeric fibrils, with a potential for surgical and reconstructive biomedical applications. Soft tissue augmentation can also make use of porous structures, as shown by a study with volume-stable collagen matrices (VSCM) that suggested a short inflammatory phase and full integration with adjacent soft connective tissues, illustrated in **Fig. 20D.**

Additive manufacturing has also found a niche in soft tissue reconstruction, specifically breast tissue, which faces current challenges in guiding the regeneration of both adipose and fibrous tissue in large sections. CAD models tailored to a patient's scan have helped to study the mechanical properties of the host tissue. These models have been used to create simulated external frames composed of geometrical arrangements that mimic the original tissue and provide a stable interconnected frame. Additionally, each line of the net has an internal porosity (1.25-2.5 mm), that allows the construct to be used as molecule/cell carrier (**Fig. 20D*iv***) (435). The benefits of

View Article Online
DOI: 10.1039/D1TB02628C

interconnected scaffolds for surgical applications have also been explored by Hosseini *et al.* to create anisotropic porous microfibrillar scaffolds made of PGA and poly(4-hydroxybutyrate) (P4HB) (436), shown in **Fig. 20D**.

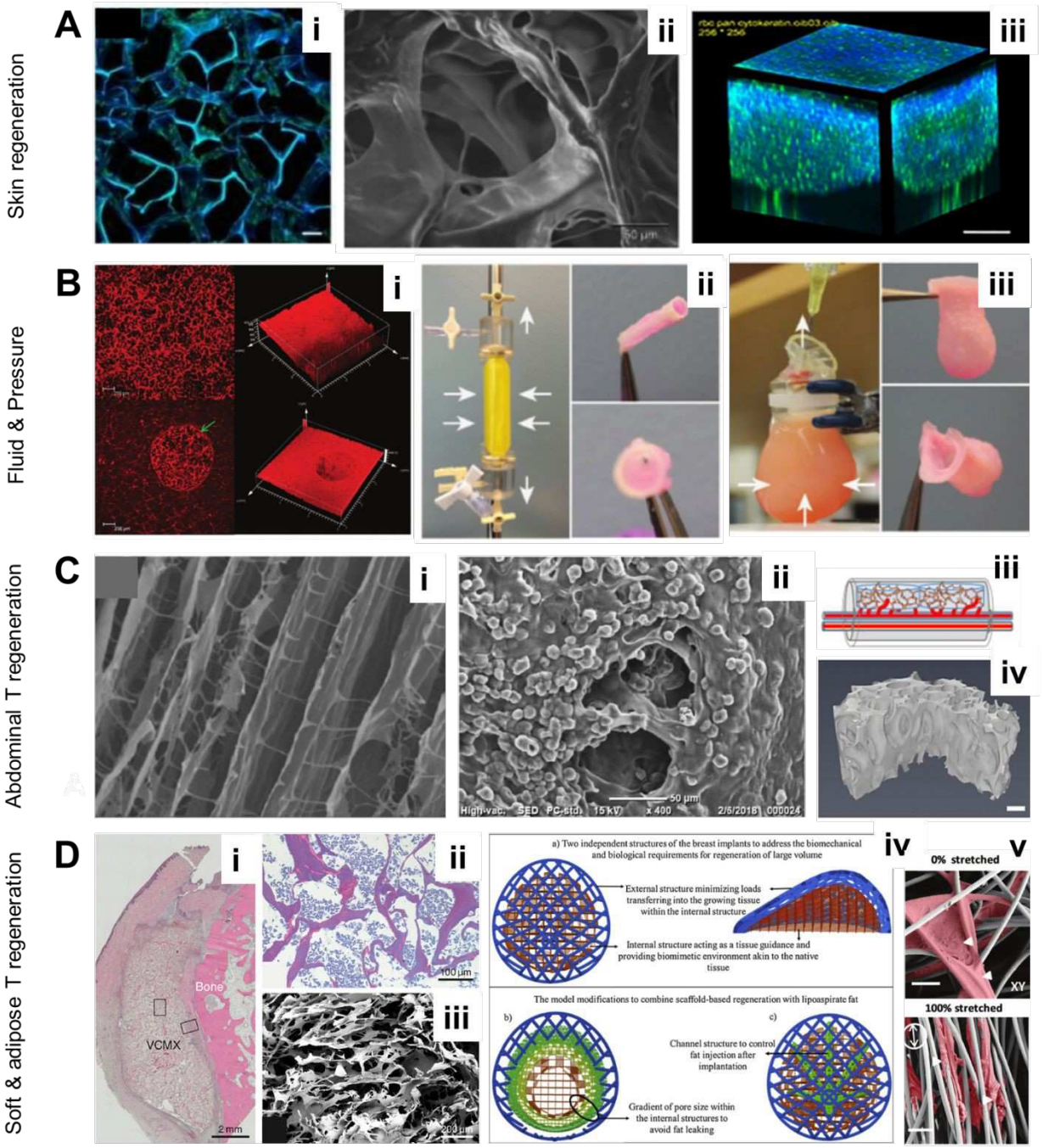

Fig. 20. *Some of the alternative applications of porous materials in reconstruction and tissue regeneration. A) i) Confocal microscopy of HUVEC cells on silk fibroin scaffolds. ii) Preparation of PG2 by a combined particulate leaching/cross linking process. iii) Reconstructed 3D projection image of a 3D microporous regenerated rBC/Gel scaffold. B) i) 3D confocal z-stacks of scaffolds. Green arrows point at 1 mm pores present in the silicone membranes. White arrows point at the edge between the silicone membrane and the fibrin/alginate component. Biomanufacturing tubular and hollow collagen scaffolds: Laboratory setups for creating collagen-based ii) ureter-like tubular, and iii) a bladder-like scaffold (white arrows show collagen condensation toward the internal mould). C) i) SEM of the RP scaffolds showing small interconnections between the collagen lamellae. ii) SEM images*

View Article Online
DOI: 10.1039/D1TB02628C

of the scaffolds based on pectine-A with attached MSCs. iii) Part of a diagram illustrating the method of connecting the human pre-vascularised scaffold to the mouse epigastric pedicle, with the resulting construct (pedicle/scaffold) remaining within the chamber. iv) The X-ray microtomography of porous PCL scaffolds for vaginal TE. D) i) Overview of a paraffin-embedded tissue section stained with Haematoxylin and Eosin showing the VSCM at 4 days after implantation lying parallel to the bone. ii-iii) The resin section illustrates the VSCM pores filled with blood plasma and mainly erythrocytes at 4 h after implantation; complemented by a SEM of the 3D structure of the scaffold. iv) Internal and external structures for large volume breast re-construction. Different designs on internal channels, oriented and graded porous structures are proposed to minimise lipo as-pirate tissue movement and leakage. v) Top: Relaxed and stretched P4HB-PGA scaffolds for surgical applications. Double head arrows show the stretch direction and small arrows show P4HB (false red color) interconnecting PGA fibres. Scale bar: 50 µm. Reproduced from Open Source: Civ (434), D:i-iii (437); with the permission of Elsevier: Aiii (424), Ciii (429), 4iv (435); with the permission of RSC: Ai (67); and with the permission of Wiley: Aii (421), Bi (425), B:ii-iii (431,432), Ci (432), Cii (433), D:iv-v (436).

Abbreviations: *HUVEC: Human Umbilical Vein Endothelial Cells; MSCs: Mesenchymal Cells; PCL: Poly(ε-Caprolactone); PG2: Pullulan/Gelatin; P4HB-PGA: Poly(4-Hydroxybutyrate)-Polyglycolide; rBC/Gel: Bacterial Cellulose-Gelatin; RP: Radial Pore-Oriented; SEM: Scanning Electron Microscopy; TE: Tissue Engineering; VSCM: Volume-Stable Collagen Matrix.*

4.5. Vascular Regeneration

As discussed previously, recent advancements in tissue engineering have allowed the design and manufacture of diverse synthetic and natural materials with both optimal mechanical and chemical properties, and the architecture to promote and enhance cellular development. However, post-implantation difficulties still need to be addressed. One of the main concerns is how tissue engineered constructs can promote and achieve timely vascularisation to enhance their survival *in vivo* (438).

When manufacturing a vascular construct, there are two main aspects to be accounted for: *i*) the size and geometry of the implant (in order to respond to changes in flow/pressure and to cover the required distance) (**Fig. 21A**), and *ii*) the pre-implantation of cells (single or co-culturing techniques) (439). Novel approaches in vascular regeneration include: *i*) traditional seeding techniques plus the use of mechanical stimuli such as tensile strain (440) and perfusion through bioreactors (441,442); or *ii*) cell encapsulation using sol-gel polymers and hydrogels (443). Computational models of the vascularisation mechanism on tailored scaffolds have also allowed researchers to predict the behaviour of such materials in the body (**Fig. 21B**).

PCL has been used in vascular applications due to its biocompatibility, U.S. Food and Drug Administration (FDA) approval, and tuneable biodegradability; its low mechanical properties have been countered by blending it with other polymeric materials such as PHBV (22), PU (444,445), PLA (446,447) collagen (448), chitosan (449), and gelatin (450). For example, PLCL tubular porous constructs were manufactured using solid-liquid phase preparation and freeze drying, and later cultured using cell sheets with hMSCs and endothelial cells (ECs). The cells infiltrated the structure and populated the luminal wall, differentiating into angiogenic lineages (451). Similarly, PCL/Nylon 6 dual was electrospun to create porous tubular structures that positively influenced the cell morphology (fibrous like), attachment and proliferation of endothelial cells (452). **Fig. 21Ci-iii** illustrates a bilayered PCL/PHBV structure where PHBV (**Fig. 21Civ**) has been electrospun to create an inner layer and a PCL (**Fig. 21Cv**) emulsion-templated scaffold forms the external layer. The morphology of the internal and external pores, as well as the thickness of each layer was studied in conjunction with 2-deoxy-D-ribose for improved angiogenesis (22).

A similar study used the size and organization of pores in the surface of vascular grafts, as well as the thickness of the walls, as a measure of enhanced host integration and vascularisation.

View Article Online
DOI: 10.1039/D1TB02628C

The response of the body to a vascular graft wall over time can be observed in **Fig. 21D**, and evidenced *in situ* in **Fig. 21E**. Total blood vessel length, average invasion depth, maximum invasion depth, total number of anastomoses, ratio of successful sprouts, and TBVL per initial sprout were compared (**Fig. 21F**); higher porosities, lower thicknesses, and small-to-medium pore sizes gave the best results (453). These rendered models have also been assessed for cellular and blood vessel infiltration, using agent-based models as toolkits to simulate and understand complex biological systems (454).

3D printing has been used to generate tubular and grid structures using GelMA, sodium alginate, and 4-arm PEG-tetra-acrylate (PEGTA) as a bioink, plus light and calcium chloride as the crosslinking mechanism. Such tubular structures (400–1,000 μm of inner diameter) were bioprinted into 2-, 5-, and 10-layer grids with internal spaces of >1 mm. Both systems were perfused with vascular cells, which attached, proliferated, and matured in the system (455). De Valence *et al*. explored the biological response in the vascular graft wall over time, to understand the internal mechanism of vascularisation (21). Kong *et al*. closely explored early vascularisation of porous polymeric tissue flaps connected directly to a vascular pedicle, with results comparable to the human skin after 1 week of implantation (429).

Odedra *et al*. studied three different ways to distribute growth factors in porous collagen scaffolds, to support vascular regeneration for cardiac applications: perfusion, single point injection, and diffusion, with better results by perfusion, but with an homogeneous distribution of the supplemented media (456). Therefore, they experimented with gradient concentrations of growth factors, seeking to enhance cell migration, promoting cell viability and proliferation for the first couple of days *in vivo*. In a similar way, 2-deoxy-D-ribose and 17*β*-estradiol have been proposed as an alternative to current vascularisation supplements; showing an effective proangiogenic potential in thick (>200 μm) constructs, which usually cannot survive *in vivo* due to the restricted diffusion of oxygen and nutrients (22).

Revascularisation plays a crucial role in bone remodelling, to ensure an adequate supply of oxygen and nutrients. The role of pore size in new blood vessels was studied *in vivo* on biphasic CaP particles; the functional capillary density and the volume of neo-osteo tissue increased as the pore size increased over 28 days, with the best results seen on >200-μm pores (**Fig. 21E**) (457). These results have been supported in other *in vivo* studies, *e.g.*, the treatment of calvarial defects using bioactive glass scaffolds (458), and open porous magnesium scaffolds (459). Interestingly, the 3D-plotted *β*-TCP scaffolds with 100-μm pores showed better vascularisation results for calvarial bones, whilst 400-μm pores proved better for endochondral ossification (460). A robust study on this matter was developed using poly(3-hydroxybutyrate-co-3-hydroxyhexanoate) (PHBHHx) scaffolds, with three different structures: macro pores (porosity 82%, ~300 μm), macro-meso pores (porosity 83.9%, 300-500 μm), and macro-micro-meso pores (porosity 85.95%, 20-50 μm and 300-500 μm). Even though all three structures promoted cell adhesion and proliferation, the 3-level pore version (macro-micro-meso) best accelerated cell metabolism, nutrient transport, and rapid formation of new blood vessels (461).

View Article Online
DOI: 10.1039/D1TB02628C

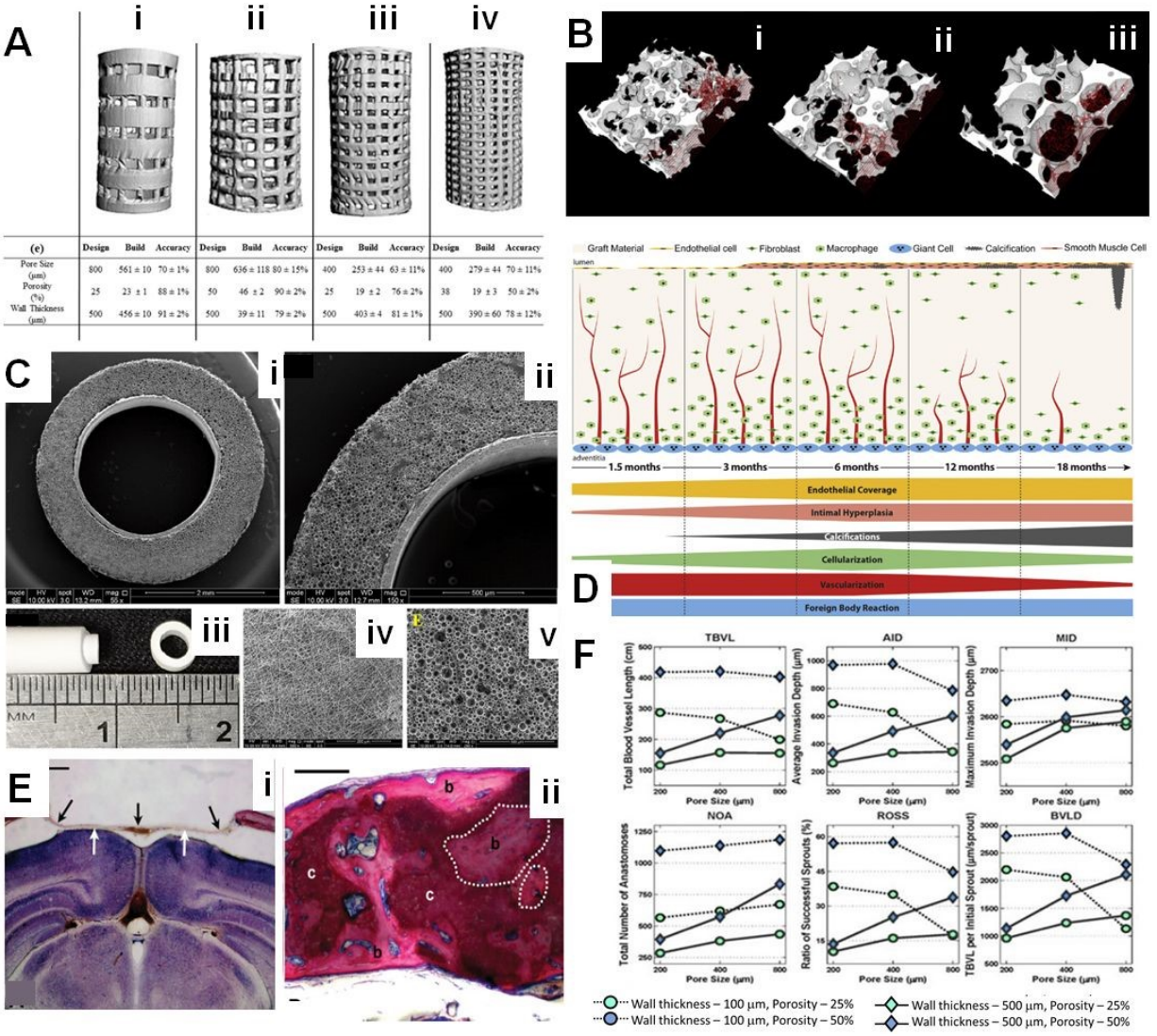

Fig. 21. *A) Micro-CT characterisation of PPF 3D-printed scaffolds: i) 800-μm pores, 25% porosity, ii) 800-μm pores, 50% porosity, iii) 400-μm pores. 25% porosity, iv) 800-μm pores, 38% porosity. B) ABM 3D renderings of heterogeneous scaffold vascularisation after 6 weeks for different pore sizes of i) 150, ii) 275, and iii) 400 mm. Overall scaffold porosity is 80% in all pore sizes. C) (i-ii) SEM image of the cross-section of the bilayer PHBV-PCL tube, iii) Macroscopic image of the bilayer tube, iv) SEM images of the of PHBV electrospun, and v) PCL PolyHIPE. D) Schematic representation of the biological response in the vascular graft wall over time. E) Light micrographs of 300-μm-thick ceramic implant vertical sections through cranial defects, 28 days after surgery. The sections were surface-stained with McNeal's tetrachrome. Ceramic particles (c): brown/red; newly formed bone (b): light pink; pre-existing bone of the calvarium: magenta; grey matter of the brain: blue/violet. i) Control (untreated) defect without implantation of ceramic particles. ii) Ceramic particles with pores in the size range 210–280 μm. Scale bars: i): 1000 μm; ii): 200 μm. F) In silico angiogenesis analysis of polypropylene scaffold designs with two different wall thicknesses and three different pore sizes was evaluated for: TBVL, AID, MID, NOA, ROSS, and TBVLS. Scaffolds with high porosity (50%), wall thickness of 100 μm, and small/medium pore sizes (200–400 μm) had the best values for all metrics. Reproduced from Open Source: C (22); with permission from Elsevier: B (454), D (21); and with permission from Wiley: A & F (453), E (457).*

Abbreviations: *ABM: Agent-Based Modelling; AID: Average Invasion Depth; HIPE: High Internal Phase Emulsion; mCT: Micro-Computed Tomography; MID: Maximum Invasion Depth; NOA: Number Of Anastomoses; PHBV-PCL: Poly(3-Hydroxybutyrate-co-3-Hydroxyvalerate)-Poly(ε-Caprolactone); PPF: Poly(Propylene Fumarate); ROSS: Ratio Of Successful Sprouts; SEM: Scanning Electron Microscopy; TBVL: Total Blood Vessel Length; TBVLS: TBVL Per Initial Sprout.*

View Article Online
DOI: 10.1039/D1TB02628C

4.6. Pharmaceutical Applications

Biomaterials have been used extensively in pharmaceutical applications, greatly benefiting drug discovery, development, and delivery systems. Moreover, the advances in tissues development used in bioprinting are making a breakthrough in the evaluation of drug toxicity, where the goal is to obtain similar results using *in vivo* and *in vitro* testing of new drugs, lowering the number of *in vivo* tests required and the testing phase expenses (462). Additionally, drug-eluting devices, implants with surface drug solutions, 3D-printed tablets with predetermined drug release doses, and anticancer drugs loaded on bioprinted tissues are all revolutionary drug delivery systems available through the development of biomaterials using bioprinting technology (463). This shows only part of the great potential held by biomaterial tissue engineering in personalised medicine (462). Such principles, for example, could be applied to replace conventional chemotherapy by developing personalised tumour models *in vitro*, and creating local drug-delivery systems using cutting-edge printing technologies (463).

The integrated use of bioprinted biomaterials has enhanced both precision and cost-effectiveness for the controlled deposition of drugs, cells, growth factors, and hormones (464,465). Taking these advantages into account, this has resulted in a broader range of applications for porous biomaterials in general (465). To enhance the proliferation, migration, and growth of cells, along with the production of the ECM, it is important to promote the formation of heterogeneities in cell distribution and their biophysical and biochemical properties matrix (464,466). These heterogeneities are created by developing scaffolds with adequate interconnectivity and porosity which subsequently allow for better control of genes, vascularization, and drug delivery (464). The evolution in the field of porous biomaterials is discussed in detail in the following sections, with a special focus on 3D printing/bioprinting for drug delivery; a schematic representation of this technique is shown in **Fig. 22**).

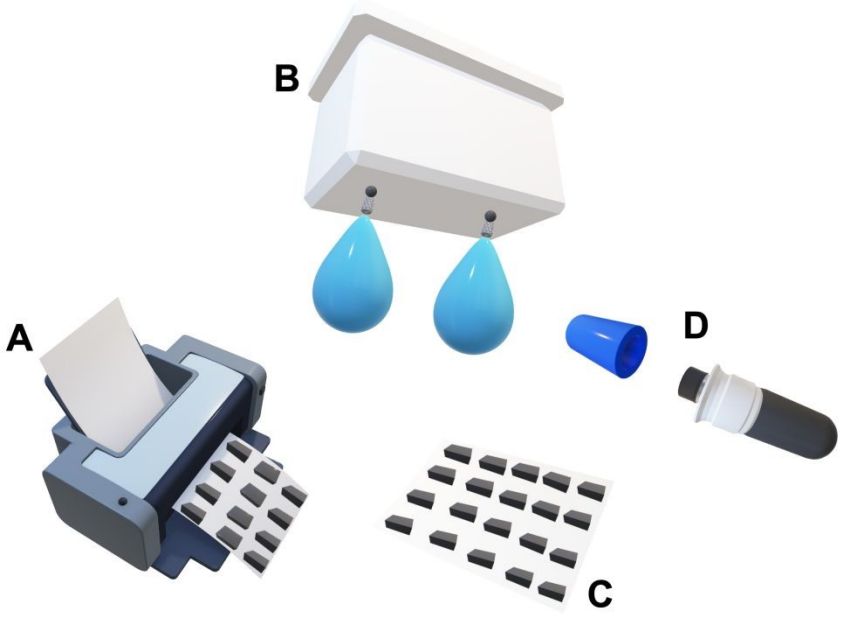

Fig. 22. *Schematic presentation of the concept of pPOD forms A) inkjet printer, B) accurate drug substance formulation ink deposition, C) precise doses of drug substance on a porous paper substrate, and D) doses inserted into capsules (or alternatively, directly fabricated into oral dosage forms) (467).*

View Article Online
DOI: 10.1039/D1TB02628C

Abbreviations: *pPOD: Printable Pharmaceutical Oral Dosage.*

4.6.1. Drug Screening

The ability to predict the effects of a drug is of paramount importance in the pharmaceutical industry, requiring 3D tissue models for drug discovery, development, and delivery systems (468). In the conventional drug discovery pipeline, 2D cell culture is used in the screening phase, followed by animal tests and clinical trials (469). However, native tissues are far more complex than 2D cultures, which generate results that are not representative of the *in vivo* response. It was thus essential to develop advanced models that better replicate the *in vivo* setting to efficiently test and screen drugs and reduce both animal and clinical trials. Moreover, cell-to-cell and cell-to-ECM interactions are usually limited in 2D models, while porous biomaterials offer 3D constructs facilitating cell growth with the correct anatomy (469). Consequently, 3D models for *in vitro* trials are now considered essential for the drug testing phase before proceeding to animal trials (469).

Organ-on-a-chip is an advanced technology that is continuously being developed and applied in *in vitro* experimental platforms and drug screening studies (470). This technology is designed to develop artificial living organs that reproduce the physiological reaction of real organs. By the intentional manipulation of the artificial organ's cells and microenvironment, drug screening could be significantly improved (471). However, many complications are associated with the fabrication of the organ-on-a-chip device (470). The high degree of flexibility and capacity for automation make 3D bioprinting well suited to generate reproducible organ-on-a-chip devices (472). The creation of biosensors and cell-laden microfluidic systems are essential for organ-on-a-chip technology, an area where 3D printing could be successfully applied (473). Additionally, applying bioprinting to fabricate liver, skin, and heart tissue models, as well as microvascular networks, among others, have shown very encouraging results (473). Furthermore, research fields that are mostly based on 2D cell cultures and animal trials, such as oncology research, would significantly benefit from applying 3D bioprinting and mixed technologies (474),(475). This is especially beneficial in light of the ethical concerns of human experimentation, and the general complication of proceeding from animal models to clinical trials in such research fields (476).

Cancer research has also witnessed significant progress when *in vitro* cancer models were 3D-bioprinted (472,477). This allowed the tumour microenvironment to be precisely engineered by spatially controlling cell organization and materials, along with biomolecule organization (477). Moreover, advancement in cancer research was considered tightly connected to further implementation of 3D printing in the field as it addressed many concerns related to tumour microenvironment such as intercellular communication, enzyme kinetics and metastatic progression, as well as cancer cell interaction with adjacent stromal cells (478). It should be noted here that the bioink formulation used for these models must create a microenvironment analogous to *in vivo* tumours especially in terms of cell heterogeneity and biomolecule distribution (479). Thus, cancer associated fibroblasts, immune cells, and endothelial cells should be included in the bioink formulation (480). Since bioprinting is the only technology that allows for such precise tumour microenvironment recreation, it is considered an excellent biofabrication technology for

View Article Online
DOI: 10.1039/D1TB02628C

the advancement of *in vitro* metastasis models, and the discovery of cancer drugs through more efficient drug screening processes (478,479).

4.6.2. Gene Therapy

Gene therapy aims to treat diseases by correcting defective genes or actively transferring therapeutic nucleic acids into the cells, thereby offering the potential to treat previously incurable diseases (481). However, common methods for gene delivery into cells have produced disappointing clinical outcomes, encouraging researchers to develop new approaches for efficient gene transfection into cells (482). One of the novel approaches is the use of polymeric gene carriers with well-defined structural and chemical properties that promote the release, transport, and uptake of plasmids. For example, biodegradable carriers such as chitosan and PLGA showed a positive transfection rate and lower toxicity compared to other non-degradable polymeric carrier matrices (483).

The printing of biomaterials could reform gene therapy as it offers opportunities to transduce and differentiate autologous cells into many lineages in a significantly more efficient manner, using polymeric gene carriers. Nonetheless, studies that report using bioprinting in such applications remain very few (484). When genes are bioprinted in biodegradable microparticles, the rate of vector release to the surrounding cells can be reduced, controlling gene delivery and alleviating the drawbacks of lowering the transfection efficiency and increasing the toxicity associated with the usage of naked nucleic acids (484). One study reported using an inkjet cell printing technique to transfect a plasmid vector as well as deliver cells into bioprinted tissue constructs (482). Both *in vitro* and *in vivo* experiments showed that the transfected genes were expressed in cells, showing the potential of this new technology. Conversely, the focus of the majority of studies has been to utilise 3D bioprinting for non-viral gene therapy such as tissue engineering of bone and cartilage (485). Such studies reported the efficiency of 3D bioprinting for nonviral transfection and *in vivo* expression of proteins when compared to the commonly used approaches (485).

4.6.3. Growth Factor and Drug Delivery

In tissue regeneration, the identification and production of growth factors and recombinant morphogens are of extreme importance. These therapeutic compounds are commonly released and activated by being spatially and temporally controlled through the use of a material carrier, as most effective trials report (486). Challenges still remain in implementing the carrier's manufacturing techniques with mechanisms for the encapsulation and release of growth factors. The use of porous materials is not new to the area, as porous matrices (mainly silica) have been used for decades in the pharmaceutical industry as stabilising agents and to control the rate of drug release (487). Porous biomaterials used as excipients and device platforms have been selected due to their porosity and interconnectivity. Among such, the latest advances in polymer chemistry have opened the path to a group of versatile biocompatible and biodegradable porous materials that can enhance, sustain and control the release of molecules and drugs or interest (488).

This is where 3D bioprinting could potentially make a breakthrough. For example, since it is possible to modify the rate of degradation of alginate through the alteration of its molecular

View Article Online
DOI: 10.1039/D1TB02628C

weight, it has been used in some studies as a bioink to control the release of cell growth factors (489). This study highlighted the potential of biomaterials used in 3D bioprinting in the engineering of microenvironments, and it demonstrated that the release of proteins, mechanical properties, and printability was highly influenced by the alginate's molecular weight, the ionic crosslinker choice, and gelling conditions. In another study, stem cell orientation differentiation was controlled using submicron fibre scaffolds that were patterned with growth factors, to create a primitive muscle tendon-bone unit (490).

Porous biomaterials for compound release applications are evolving to what is termed a "host/guest" system, also referred to as molecular recognition. This term describes the (engineered) preferential interaction between guest compounds (*i.e.*, growth factors, drugs) and the host (porous platforms) (491). Polymers and hydrogels, liposomes and micelles are amongst the most used platforms for drug release (492). For example, porous polystyrene, self-emulsifying beads were explored for a controlled release of loratadine, offering an alternative approach for the administration of drugs that suffer limited oral bioavailability (493). Similarly, mesoporous silica-based biomaterials have been shown to be capable of enhancing the dissolution of anticancer drugs associated with poor solubility, therefore improving their availability and efficiency (494).

As indicated in the previously reported studies, the development of biomaterials for 3D bioprinting holds the potential to create a breakthrough in the fields of pharmacy and regenerative medicine. However, the limitations of 3D bioprinting still need to be addressed for this process, for fabricating fully functional organs, which is the ultimate aim in the field. One future direction will be the use of cells that are patient-specific for cancer treatments (personalised medicine). Another horizon for 3D-bioprinting progress is the potential to employ bioink formulations based on hydrogels that are stimuli-responsive thus creating dynamic tumour models (477). The use of robotic bioprinting in surgeries is another future perspective that could make it possible to build bioengineered tissues for humans (484).

5. Conclusions

A wide variety of natural and synthetic materials have been proposed as biomaterials. During the process of attempting to mimic host tissues and organs, biomaterial scientists have developed porous and interconnected scaffolds that ensure nutrients and cells can travel through the structure promoting the formation of new tissues and thus healing and restoring body mechanisms.

Porous materials can be characterised according to their bulk properties (*e.g.*, tensile and compressive strengths, rheological properties); their pore features (*e.g.*, size, orientation, geometry) and interconnectivity (*e.g.*, porosity, internal phase volume); and their behaviour when interacting with body tissues (*e.g.*, biocompatibility, bioactivity, tissue conductivity/inductivity, biodegradation). Further optimization of the manufacturing techniques will lead to successful materials which can ultimately satisfy the requirements of all involved in the clinical applications (material scientists, surgeons, and patients).

View Article Online
DOI: 10.1039/D1TB02628C

Materials such as metals excel for their ability to maintain shape and bear the load from external forces, even though they are usually bioinert and non-degradable. However, challenges remain in the duration of their structural stability and their effect in the tissue remodelling process. Similarly, polymer chemistry has advanced to a level of control on the molecular weights and chain heterogeneity that allowed for the creation of polymer solutions (including hydrogels) that are reactive to external or internal stimuli, self-assembling and crosslinking at ideal conditions or as a result of chemical cues that can be observed *in vivo* (497). Challenges remaining in this field include addressing the *i*) logistic details of purification, sterilisation and packaging, and *ii*) ensuring full biocompatibility of the materials from the moment they are implanted, to their full degradation when this occurs. Finally, ceramics and glasses have found a new avenue as co-materials with polymers and metals. They contain mineral components naturally found in the body, where they perform as catalysts, inducers/inhibitors, stabilisers or supplements that can be in long contact with the body tissues or resorbed. However, opportunities for improvement remain in their load-bearing capacity, inherent brittleness and the development of suitable and scalable processing strategies (498,499).

The fabrication and manufacturing of porous biomaterials focuses on producing high-fidelity structures that mimic *in vivo* environments. As no method is universal, techniques should be chosen to better accommodate both the material properties, and the intended applications. For example, salt and emulsion templating have been extensively used with polymers and hydrogels for the creation of well-defined pores, up to the nanometer-level. This cost-effective technique uses a variety of materials as bulk and sacrificial materials, enabling the internal geometries and interconnectivities to be tuned and controlled. The latest studies aim to reduce and eliminate the use of solvents and other compounds that could impact negatively on the biocompatibility of the constructs *in vitro* and *in vivo*. Freeze-drying is a similar technique that focuses on the phase characteristics of the material, and easily creates porous structures with attractive geometrical and fractal patterns. As priorly mentioned, it is however limited by long drying/purification processes, and the use of cytotoxic solvents. A hybrid alternative for such situations is electrospinning, which still works with a diverse range of materials and reduces the use of solvents, whilst enhancing the production of oriented fibres with tailored porosities.

Patterning techniques have been proposed that further enhance the 3D design and functionality by offering chemical treatments on the surface of materials that can ameliorate the biomaterial-host body interactions. Such methodologies, even if expensive, can be applied to numerous material surfaces, significantly benefiting the clinical performances of biomaterials.

Finally, bioprinting techniques offer a unique opportunity to play with the design and functionality, from the nanometre- to the macroscale level. Their operation has been adapted to almost all blends of materials and have also introduced the possibility of including cellular bodies in the printing process, opening the door to hybrid techniques that create well-controlled environments that satisfy the host body needs during and after implantation. However, at this time, such technologies are costly and require long development times, thus limiting their availability and direct applications.

As reported in this extensive review, there is a massive interest in the development of biomaterials that fulfil the requirements of cell entities and tissues, supporting their healing and

View Article Online
DOI: 10.1039/D1TB02628C

regeneration, or even replacing them. A balance between the choice of porous biomaterials and the manufacturing techniques will allow such specifications to be satisfied. The creativity and innovation committed to these efforts has allowed the field of biomaterials science to grow exponentially in the last century and undoubtedly, we can expect that to continue, specifically in the areas linked to cancer, diabetes, immunology, cardiac and liver pathologies, among others.

Acknowledgment

We acknowledge funding from the Royal Society International Exchange (IESR3183215).

View Article Online
DOI: 10.1039/D1TB02628C

References

1. Tiwari A, Nordin AN. Advanced Biomaterials and Biodevices. John Wiley & Sons; 2014. 576 p.

2. Farid SBH. Bioceramics: For Materials Science and Engineering. Woodhead Publishing; 2018. 226 p.

3. Mays TJ. A new classification of pore sizes. Stud Surf Sci Catal [Internet]. 2007; Available from: https://researchportal.bath.ac.uk/en/publications/a-new-classification-of-pore-sizes

4. Sobral JM, Caridade SG, Sousa RA, Mano JF, Reis RL. Three-dimensional plotted scaffolds with controlled pore size gradients: Effect of scaffold geometry on mechanical performance and cell seeding efficiency. Acta Biomater. 2011 Mar;7(3):1009–18.

5. Butscher A, Bohner M, Doebelin N, Hofmann S, Müller R. New depowdering-friendly designs for three-dimensional printing of calcium phosphate bone substitutes. Acta Biomater. 2013 Nov;9(11):9149–58.

6. Babaie E, Bhaduri SB. Fabrication Aspects of Porous Biomaterials in Orthopedic Applications: A Review. ACS Biomater Sci Eng. 2018 Jan 8;4(1):1–39.

7. Abbasi N, Hamlet S, Love RM, Nguyen N-T. Porous scaffolds for bone regeneration. Journal of Science: Advanced Materials and Devices. 2020 Mar 1;5(1):1–9.

8. Pałka K, Pokrowiecki R. Porous titanium implants: A review. Adv Eng Mater. 2018 May;20(5):1700648.

9. Mediaswanti K, Wen C, Ivanova E, Berndt C, Malherbe F, Pham V, et al. A review on bioactive porous metallic biomaterials. J Biomim Biomater Tissue Eng. 2013;18(1):1–8.

10. Aldemir Dikici B, Claeyssens F. Basic Principles of Emulsion Templating and Its Use as an Emerging Manufacturing Method of Tissue Engineering Scaffolds. Front Bioeng Biotechnol. 2020 Aug 12;8:875.

11. Ashby MF, Johnson K. Materials and Design: The Art and Science of Material Selection in Product Design. Butterworth-Heinemann; 2013. 416 p.

12. T. Balaganapathi, B. KaniAmuthan, S.Vinoth, P. Thilakan. Synthesis, characterization and dye adsorption studies of porous brookite and mixed brookite with rutile TiO2 using PEG assisted sol-gel synthesis process _ Elsevier Enhanced Reader.pdf [Internet]. 2017. Available from: https://www.sciencedirect.com/science/article/pii/S0025540816313307?via%3Dihub

13. Tian F, Zhang S, Zhai M, Sui J, Lan X, Gao J. Thermal properties of nano-sized polyethylene glycol confined in silica gels for latent heat storage. Thermochim Acta. 2017 Sep 10;655:211–8.

14. Constantinides C, Basnett P, Lukasiewicz B, Carnicer R, Swider E, Majid QA, et al. In Vivo Tracking and H/F Magnetic Resonance Imaging of Biodegradable

View Article Online
DOI: 10.1039/D1TB02628C

Polyhydroxyalkanoate/Polycaprolactone Blend Scaffolds Seeded with Labeled Cardiac Stem Cells. ACS Appl Mater Interfaces. 2018 Aug 1;10(30):25056–68.

15. Wei X, Gao Q, Xie C, Gu C, Liang T, Wan H, et al. Extracellular recordings of bionic engineered cardiac tissue based on a porous scaffold and microelectrode arrays [Internet]. Vol. 11, Analytical Methods. 2019. p. 5872–9. Available from: http://dx.doi.org/10.1039/c9ay01888c

16. Rose JB, Sidney LE, Patient J, White LJ, Dua HS, El Haj AJ, et al. In vitro evaluation of electrospun blends of gelatin and PCL for application as a partial thickness corneal graft. J Biomed Mater Res A. 2019 Apr;107(4):828–38.

17. Paul K, Darzi S, Mcphee G, Del Borgo M, Werkmeister JA, Gargett CE, et al. 3D Bioprinted Endometrial Stem Cells on Melt Electrospun PCL Meshes for Pelvic Floor Application Promote Anti-Inflammatory Responses in Mice [Internet]. SSRN Electronic Journal. Available from: http://dx.doi.org/10.2139/ssrn.3387674

18. Piai JF, da Silva MA, Martins A, Torres AB, Faria S, Reis RL, et al. Chondroitin sulfate immobilization at the surface of electrospun nanofiber meshes for cartilage tissue regeneration approaches [Internet]. Vol. 403, Applied Surface Science. 2017. p. 112–25. Available from: http://dx.doi.org/10.1016/j.apsusc.2016.12.135

19. Li Y, Liu Y, Xun X, Zhang W, Xu Y, Gu D. Three-Dimensional Porous Scaffolds with Biomimetic Microarchitecture and Bioactivity for Cartilage Tissue Engineering. ACS Appl Mater Interfaces. 2019 Oct 9;11(40):36359–70.

20. Yang F, Murugan R, Wang S, Ramakrishna S. Electrospinning of nano/micro scale poly(L-lactic acid) aligned fibers and their potential in neural tissue engineering. Biomaterials. 2005 May;26(15):2603–10.

21. de Valence S, Tille J-C, Mugnai D, Mrowczynski W, Gurny R, Möller M, et al. Long term performance of polycaprolactone vascular grafts in a rat abdominal aorta replacement model. Biomaterials. 2012 Jan;33(1):38–47.

22. Dikici S, Mangır N, Claeyssens F, Yar M, MacNeil S. Exploration of 2-deoxy-D-ribose and 17β-Estradiol as alternatives to exogenous VEGF to promote angiogenesis in tissue-engineered constructs. Regen Med. 2019 Mar;14(3):179–97.

23. Whitely M, Rodriguez-Rivera G, Waldron C, Mohiuddin S, Cereceres S, Sears N, et al. Porous PolyHIPE microspheres for protein delivery from an injectable bone graft. Acta Biomater. 2019 Jul 15;93:169–79.

24. Rodríguez-Contreras A, Guillem-Marti J, Lopez O, Manero JM, Ruperez E. Antimicrobial PHAs coatings for solid and porous tantalum implants. Colloids Surf B Biointerfaces. 2019 Oct 1;182:110317.

25. Yin H-M, Li X, Wang P, Ren Y, Liu W, Xu J-Z, et al. Role of HA and BG in engineering poly(ε-caprolactone) porous scaffolds for accelerating cranial bone regeneration. J Biomed Mater Res A. 2019 Mar;107(3):654–62.

View Article Online
DOI: 10.1039/D1TB02628C

26. Sangkert S, Meesane J, Kamonmattayakul S, Chai WL. Modified silk fibroin scaffolds with collagen/decellularized pulp for bone tissue engineering in cleft palate: Morphological structures and biofunctionalities. Mater Sci Eng C Mater Biol Appl. 2016 Jan 1;58:1138–49.

27. Bartnikowski M, Vaquette C, Ivanovski S. Workflow for highly porous resorbable custom 3D printed scaffolds using medical grade polymer for large volume alveolar bone regeneration. Clin Oral Implants Res. 2020 May;31(5):431–41.

28. Chang B, Ahuja N, Ma C, Liu X. Injectable scaffolds: Preparation and application in dental and craniofacial regeneration [Internet]. Vol. 111, Materials Science and Engineering: R: Reports. 2017. p. 1–26. Available from: http://dx.doi.org/10.1016/j.mser.2016.11.001

29. Pashneh-Tala S, Owen R, Bahmaee H, Rekštyte S, Malinauskas M, Claeyssens F. Synthesis, characterization and 3D micro-structuring via 2-photon polymerization of poly(glycerol sebacate)-methacrylate-an elastomeric degradable polymer. Frontiers in Physics [Internet]. 2018 May 8 [cited 2021 Feb 16];6. Available from: http://eprints.whiterose.ac.uk/131337/

30. Sencadas V, Sadat S, Silva DM. Mechanical performance of elastomeric PGS scaffolds under dynamic conditions. J Mech Behav Biomed Mater. 2020 Feb;102:103474.

31. Aldemir Dikici B, Sherborne C, Reilly GC, Claeyssens F. Emulsion templated scaffolds manufactured from photocurable polycaprolactone. Polymer . 2019 Jun 26;175:243–54.

32. Li J, Liu X, Crook JM, Wallace GG. Development of a porous 3D graphene-PDMS scaffold for improved osseointegration [Internet]. Vol. 159, Colloids and Surfaces B: Biointerfaces. 2017. p. 386–93. Available from: http://dx.doi.org/10.1016/j.colsurfb.2017.07.087

33. Montazerian H, Mohamed MGA, Montazeri MM, Kheiri S, Milani AS, Kim K, et al. Permeability and mechanical properties of gradient porous PDMS scaffolds fabricated by 3D-printed sacrificial templates designed with minimal surfaces. Acta Biomater. 2019 Sep 15;96:149–60.

34. Quirós-Solano WF, Gaio N, Stassen OMJA, Arik YB, Silvestri C, Van Engeland NCA, et al. Microfabricated tuneable and transferable porous PDMS membranes for Organs-on-Chips. Sci Rep. 2018 Sep 10;8(1):13524.

35. Bettinger CJ. Biodegradable elastomers for tissue engineering and cell-biomaterial interactions. Macromol Biosci. 2011 Apr 8;11(4):467–82.

36. Chen Q, Liang S, Thouas GA. Elastomeric biomaterials for tissue engineering. Prog Polym Sci. 2013 Mar 1;38(3):584–671.

37. Le Fer G, Becker ML. 4D Printing of Resorbable Complex Shape-Memory Poly(propylene fumarate) Star Scaffolds. ACS Appl Mater Interfaces. 2020 May 20;12(20):22444–52.

38. James N, Philip J, Jayakrishnan A. Polyurethanes with radiopaque properties [Internet]. Vol. 27, Biomaterials. 2006. p. 160–6. Available from: http://dx.doi.org/10.1016/j.biomaterials.2005.05.099

View Article Online
DOI: 10.1039/D1TB02628C

39. Cai S, Sun Y-C, Ren J, Naguib HE. Toward the low actuation temperature of flexible shape memory polymer composites with room temperature deformability via induced plasticizing effect. J Mater Chem B Mater Biol Med. 2017 Nov 28;5(44):8845–53.

40. Wischke C, Neffe AT, Steuer S, Lendlein A. Evaluation of a degradable shape-memory polymer network as matrix for controlled drug release. J Control Release. 2009 Sep 15;138(3):243–50.

41. Dalton E, Chai Q, Shaw MW, McKenzie TJ, Mullins ES, Ayres N. Hydrogel-coated polyurethane/urea shape memory polymer foams. J Polym Sci A Polym Chem. 2019 Jul;57(13):1389–95.

42. Serrano MC, Ameer GA. Recent insights into the biomedical applications of shape-memory polymers. Macromol Biosci. 2012 Sep;12(9):1156–71.

43. Boire TC, Himmel LE, Yu F, Guth CM, Dollinger BR, Werfel TA, et al. Effect of pore size and spacing on neovascularization of a biodegradble shape memory polymer perivascular wrap. J Biomed Mater Res A. 2021 Mar;109(3):272–88.

44. Zhang D, George OJ, Petersen KM, Jimenez-Vergara AC, Hahn MS, Grunlan MA. A bioactive "self-fitting" shape memory polymer scaffold with potential to treat cranio-maxillo facial bone defects. Acta Biomater. 2014 Nov;10(11):4597–605.

45. Xie R, Hu J, Hoffmann O, Zhang Y, Ng F, Qin T, et al. Self-fitting shape memory polymer foam inducing bone regeneration: A rabbit femoral defect study. Biochim Biophys Acta Gen Subj. 2018 Apr;1862(4):936–45.

46. Schlotter NE. Raman Spectroscopy [Internet]. Comprehensive Polymer Science and Supplements. 1989. p. 469–97. Available from: http://dx.doi.org/10.1016/b978-0-08-096701-1.00021-5

47. Xue N, Wang D, Liu C, Ke Z, Elia P, Li T, et al. A biodegradable porous silicon and polymeric hybrid probe for electrical neural signal recording. Sens Actuators B Chem. 2018 Nov 1;272:314–23.

48. Yasin MN, Brooke RK, Rudd S, Chan A, Chen W-T, Waterhouse GIN, et al. 3-Dimensionally ordered macroporous PEDOT ion-exchange resins prepared by vapor phase polymerization for triggered drug delivery: Fabrication and characterization. Electrochim Acta. 2018 Apr 10;269:560–70.

49. Guex AG, Puetzer JL, Armgarth A, Littmann E, Stavrinidou E, Giannelis EP, et al. Highly porous scaffolds of PEDOT:PSS for bone tissue engineering. Acta Biomater. 2017 Oct 15;62:91–101.

50. Xu J, Xu J, Moon H, Sintim HO, Lee H. Zwitterionic Porous Conjugated Polymers as a Versatile Platform for Antibiofouling Implantable Bioelectronics. ACS Appl Polym Mater. 2020 Feb 14;2(2):528–36.

51. Zhang BGX, Spinks GM, Gorkin R 3rd, Sangian D, Di Bella C, Quigley AF, et al. In vivo

View Article Online
DOI: 10.1039/D1TB02628C

biocompatibility of porous and non-porous polypyrrole based trilayered actuators. J Mater Sci Mater Med. 2017 Sep 27;28(11):172.

52. Sarvari R, Massoumi B, Zareh A, Beygi-Khosrowshahi Y, Agbolaghi S. Porous conductive and biocompatible scaffolds on the basis of polycaprolactone and polythiophene for scaffolding [Internet]. Vol. 77, Polymer Bulletin. 2020. p. 1829–46. Available from: http://dx.doi.org/10.1007/s00289-019-02732-z

53. Solanki NG, Tahsin M, Shah AV, Serajuddin ATM. Formulation of 3D Printed Tablet for Rapid Drug Release by Fused Deposition Modeling: Screening Polymers for Drug Release, Drug-Polymer Miscibility and Printability. J Pharm Sci. 2018 Jan;107(1):390–401.

54. Shamaeli E, Alizadeh N. Functionalized gold nanoparticle-polypyrrole nanobiocomposite with high effective surface area for electrochemical/pH dual stimuli-responsive smart release of insulin. Colloids Surf B Biointerfaces. 2015 Feb 1;126:502–9.

55. Wang J, Yang P, Cao M, Kong N, Yang W, Sun S, et al. A novel graphene nanodots inlaid porous gold electrode for electrochemically controlled drug release. Talanta. 2016 Jan 15;147:184–92.

56. Xia B, Wang B, Shi J, Zhang Y, Zhang Q, Chen Z, et al. Photothermal and biodegradable polyaniline/porous silicon hybrid nanocomposites as drug carriers for combined chemo-photothermal therapy of cancer. Acta Biomater. 2017 Mar 15;51:197–208.

57. Pramanik N, Dutta K, Basu RK, Kundu PP. Aromatic π-Conjugated Curcumin on Surface Modified Polyaniline/Polyhydroxyalkanoate Based 3D Porous Scaffolds for Tissue Engineering Applications. ACS Biomater Sci Eng. 2016 Dec 12;2(12):2365–77.

58. Shoichet MS. Polymer Scaffolds for Biomaterials Applications [Internet]. Vol. 43, Macromolecules. 2010. p. 581–91. Available from: http://dx.doi.org/10.1021/ma901530r

59. Rea I, Terracciano M, De Stefano L. Synthetic vs Natural: Diatoms Bioderived Porous Materials for the Next Generation of Healthcare Nanodevices. Adv Healthc Mater [Internet]. 2017 Feb;6(3). Available from: http://dx.doi.org/10.1002/adhm.201601125

60. Moura CS, Silva JC, Faria S, Fernandes PR, da Silva CL, Cabral JMS, et al. Chondrogenic differentiation of mesenchymal stem/stromal cells on 3D porous poly (ε-caprolactone) scaffolds: Effects of material alkaline treatment and chondroitin sulfate supplementation. J Biosci Bioeng. 2020 Jun;129(6):756–64.

61. Osmond M, Bernier SM, Pantcheva MB, Krebs MD. Collagen and collagen-chondroitin sulfate scaffolds with uniaxially aligned pores for the biomimetic, three dimensional culture of trabecular meshwork cells. Biotechnol Bioeng. 2017 Apr;114(4):915–23.

62. Yu X, Qian G, Chen S, Xu D, Zhao X, Du C. A tracheal scaffold of gelatin-chondroitin sulfate-hyaluronan-polyvinyl alcohol with orientated porous structure. Carbohydr Polym. 2017 Mar 1;159:20–8.

63. Billiet T, Gevaert E, De Schryver T, Cornelissen M, Dubruel P. The 3D printing of gelatin

View Article Online
DOI: 10.1039/D1TB02628C

methacrylamide cell-laden tissue-engineered constructs with high cell viability. Biomaterials. 2014 Jan;35(1):49–62.

64. Liu S, Sun X, Wang T, Chen S, Zeng C-G, Xie G, et al. Nano-fibrous and ladder-like multi-channel nerve conduits: Degradation and modification by gelatin. Mater Sci Eng C Mater Biol Appl. 2018 Feb 1;83:130–42.

65. Bosio VE, Brown J, Rodriguez MJ, Kaplan DL. Biodegradable Porous Silk Microtubes for Tissue Vascularization. J Mater Chem B Mater Biol Med. 2017;5(6):1227–35.

66. Yao D, Qian Z, Zhou J, Peng G, Zhou G, Liu H, et al. Facile incorporation of REDV into porous silk fibroin scaffolds for enhancing vascularization of thick tissues. Mater Sci Eng C Mater Biol Appl. 2018 Dec 1;93:96–105.

67. Li X, You R, Luo Z, Chen G, Li M. Silk fibroin scaffolds with a micro-/nano-fibrous architecture for dermal regeneration. J Mater Chem B Mater Biol Med. 2016 May 7;4(17):2903–12.

68. Wang Y, Xu R, Luo G, Lei Q, Shu Q, Yao Z, et al. Biomimetic fibroblast-loaded artificial dermis with "sandwich" structure and designed gradient pore sizes promotes wound healing by favoring granulation tissue formation and wound re-epithelialization. Acta Biomater. 2016 Jan;30:246–57.

69. Linderman SW, Shen H, Yoneda S, Jayaram R, Tanes ML, Sakiyama-Elbert SE, et al. Effect of connective tissue growth factor delivered via porous sutures on the proliferative stage of intrasynovial tendon repair. J Orthop Res. 2018 Jul;36(7):2052–63.

70. Chantre CO, Gonzalez GM, Ahn S, Cera L, Campbell PH, Hoerstrup SP, et al. Porous Biomimetic Hyaluronic Acid and Extracellular Matrix Protein Nanofiber Scaffolds for Accelerated Cutaneous Tissue Repair. ACS Appl Mater Interfaces. 2019 Dec 11;11(49):45498–510.

71. Vepari C, Kaplan DL. Silk as a Biomaterial. Prog Polym Sci. 2007;32(8-9):991–1007.

72. Sundback C, Hadlock T, Cheney M, Vacanti J. Manufacture of porous polymer nerve conduits by a novel low-pressure injection molding process. Biomaterials. 2003 Feb;24(5):819–30.

73. Hsu S-H, Chang W-C, Yen C-T. Novel flexible nerve conduits made of water-based biodegradable polyurethane for peripheral nerve regeneration. J Biomed Mater Res A. 2017 May;105(5):1383–92.

74. Agrawal CM, Athanasiou KA. Technique to control pH in vicinity of biodegrading PLA-PGA implants. J Biomed Mater Res. 1997 Summer;38(2):105–14.

75. Wang G-W, Yang H, Wu W-F, Zhang P, Wang J-Y. Design and optimization of a biodegradable porous zein conduit using microtubes as a guide for rat sciatic nerve defect repair. Biomaterials. 2017 Jul;131:145–59.

76. Wang S, Guan S, Wang J, Liu H, Liu T, Ma X, et al. Fabrication and characterization of

View Article Online
DOI: 10.1039/D1TB02628C

conductive poly (3,4-ethylenedioxythiophene) doped with hyaluronic acid/poly (l-lactic acid) composite film for biomedical application. J Biosci Bioeng. 2017 Jan;123(1):116–25.

77. Bhatnagar D, Bushman JS, Murthy NS, Merolli A, Kaplan HM, Kohn J. Fibrin glue as a stabilization strategy in peripheral nerve repair when using porous nerve guidance conduits. J Mater Sci Mater Med. 2017 May;28(5):79.

78. Affatato S, Freccero N, Taddei P. The biomaterials challenge: A comparison of polyethylene wear using a hip joint simulator. J Mech Behav Biomed Mater. 2016 Jan;53:40–8.

79. Martínez Rodríguez J, Renou SJ, Guglielmotti MB, Olmedo DG. Tissue response to porous high density polyethylene as a three-dimensional scaffold for bone tissue engineering: An experimental study. J Biomater Sci Polym Ed. 2019 Apr;30(6):486–99.

80. Bhaskar B, Owen R, Bahmaee H, Wally Z, Sreenivasa Rao P, Reilly GC. Composite porous scaffold of PEG/PLA support improved bone matrix deposition in vitro compared to PLA-only scaffolds. Journal of Biomedical Materials Research - Part A. 2018;106(5):1334–40.

81. Bui HT, Prawel DA, Harris KL, Li E, James SP. Development and Fabrication of Vapor Cross-Linked Hyaluronan-Polyethylene Interpenetrating Polymer Network as a Biomaterial. ACS Appl Mater Interfaces. 2019 May 29;11(21):18930–41.

82. Van Hoof L, Verbrugghe P, Verbeken E, Treasure T, Famaey N, Meuris B, et al. Support of the aortic wall: a histological study in sheep comparing a macroporous mesh with low-porosity vascular graft of the same polyethylene terephthalate material [Internet]. Vol. 25, Interactive CardioVascular and Thoracic Surgery. 2017. p. 89–95. Available from: http://dx.doi.org/10.1093/icvts/ivx009

83. Lermontov SA, Malkova AN, Sipyagina NA, Straumal EA, Maksimkin AV, Kolesnikov EA, et al. Properties of highly porous aerogels prepared from ultra-high molecular weight polyethylene [Internet]. Vol. 182, Polymer. 2019. p. 121824. Available from: http://dx.doi.org/10.1016/j.polymer.2019.121824

84. Senatov FS, Chubrik AV, Maksimkin AV, Kolesnikov EA, Salimon AI. Comparative analysis of structure and mechanical properties of porous PEEK and UHMWPE biomimetic scaffolds. Mater Lett. 2019 Mar 15;239:63–6.

85. Heymann F, von Trotha K-T, Preisinger C, Lynen-Jansen P, Roeth AA, Geiger M, et al. Polypropylene mesh implantation for hernia repair causes myeloid cell-driven persistent inflammation. JCI Insight [Internet]. 2019 Jan 24;4(2). Available from: http://dx.doi.org/10.1172/jci.insight.123862

86. Mangir N, Dikici BA, Chapple CR, MacNeil S. Landmarks in vaginal mesh development: polypropylene mesh for treatment of SUI and POP [Internet]. Vol. 16, Nature Reviews Urology. 2019. p. 675–89. Available from: http://dx.doi.org/10.1038/s41585-019-0230-2

87. Hu W, Zhang Z, Zhu L, Wen Y, Zhang T, Ren P, et al. Combination of Polypropylene Mesh and in Situ Injectable Mussel-Inspired Hydrogel in Laparoscopic Hernia Repair for Preventing Post-Surgical Adhesions in the Piglet Model. ACS Biomater Sci Eng. 2020 Mar 9;6(3):1735–

View Article Online
DOI: 10.1039/D1TB02628C

43.

88. Beavers KR, Werfel TA, Shen T, Kavanaugh TE, Kilchrist KV, Mares JW, et al. Porous Silicon and Polymer Nanocomposites for Delivery of Peptide Nucleic Acids as Anti-MicroRNA Therapies. Adv Mater. 2016 Sep;28(36):7984–92.

89. Dabrowski ML, Jenkins D, Cosgriff-Hernandez E, Stubenrauch C. Methacrylate-based polymer foams with controllable connectivity, pore shape, pore size and polydispersity. Phys Chem Chem Phys. 2019 Dec 18;22(1):155–68.

90. Sherborne C, Owen R, Reilly GC, Claeyssens F. Light-based additive manufacturing of PolyHIPEs: Controlling the surface porosity for 3D cell culture applications [Internet]. Vol. 156, Materials & Design. 2018. p. 494–503. Available from: http://dx.doi.org/10.1016/j.matdes.2018.06.061

91. Kelly CN, Miller AT, Hollister SJ, Guldberg RE, Gall K. Design and structure--function characterization of 3D printed synthetic porous biomaterials for tissue engineering. Adv Healthc Mater. 2018;7(7):1701095.

92. Zhang YS, Khademhosseini A. Advances in engineering hydrogels. Science [Internet]. 2017 May 5;356(6337). Available from: http://dx.doi.org/10.1126/science.aaf3627

93. Zoratto N, Matricardi P. Semi-IPN- and IPN-Based Hydrogels. Adv Exp Med Biol. 2018;1059:155–88.

94. Ying G-L, Jiang N, Maharjan S, Yin Y-X, Chai R-R, Cao X, et al. Aqueous Two-Phase Emulsion Bioink-Enabled 3D Bioprinting of Porous Hydrogels. Adv Mater. 2018 Dec;30(50):e1805460.

95. Drury JL, Mooney DJ. Hydrogels for tissue engineering: scaffold design variables and applications. Biomaterials. 2003 Nov;24(24):4337–51.

96. Caliari SR, Vega SL, Kwon M, Soulas EM, Burdick JA. Dimensionality and spreading influence MSC YAP/TAZ signaling in hydrogel environments. Biomaterials. 2016 Oct;103:314–23.

97. Engler AJ, Discher DE. Rationally engineered advances in cancer research. APL Bioeng. 2018 Sep;2(3):031601.

98. DeForest CA, Anseth KS. Advances in bioactive hydrogels to probe and direct cell fate. Annu Rev Chem Biomol Eng. 2012 Apr 17;3:421–44.

99. Bott K, Upton Z, Schrobback K, Ehrbar M, Hubbell JA, Lutolf MP, et al. The effect of matrix characteristics on fibroblast proliferation in 3D gels. Biomaterials. 2010 Nov;31(32):8454–64.

100. Van Den Bulcke AI, Bogdanov B, De Rooze N, Schacht EH, Cornelissen M, Berghmans H. Structural and rheological properties of methacrylamide modified gelatin hydrogels. Biomacromolecules. 2000 Spring;1(1):31–8.

View Article Online
DOI: 10.1039/D1TB02628C

101. Yue K, Li X, Schrobback K, Sheikhi A, Annabi N, Leijten J, et al. Structural analysis of photocrosslinkable methacryloyl-modified protein derivatives. Biomaterials. 2017 Sep;139:163–71.

102. Miri AK, Hosseinabadi HG, Cecen B, Hassan S, Zhang YS. Permeability mapping of gelatin methacryloyl hydrogels. Acta Biomater. 2018 Sep 1;77:38–47.

103. You F, Wu X, Zhu N, Lei M, Eames BF, Chen X. 3D Printing of Porous Cell-Laden Hydrogel Constructs for Potential Applications in Cartilage Tissue Engineering. ACS Biomater Sci Eng. 2016 Jul 11;2(7):1200–10.

104. You F, Wu X, Chen X. 3D printing of porous alginate/gelatin hydrogel scaffolds and their mechanical property characterization [Internet]. Vol. 66, International Journal of Polymeric Materials and Polymeric Biomaterials. 2017. p. 299–306. Available from: http://dx.doi.org/10.1080/00914037.2016.1201830

105. Senior JJ, Cooke ME, Grover LM, Smith AM. Fabrication of complex hydrogel structures using suspended layer additive manufacturing (SLAM). Adv Funct Mater. 2019 Dec;29(49):1904845.

106. Zhu Y, Hideyoshi S, Jiang H, Matsumura Y, Dziki JL, LoPresti ST, et al. Injectable, porous, biohybrid hydrogels incorporating decellularized tissue components for soft tissue applications. Acta Biomater. 2018 Jun;73:112–26.

107. Paukkonen H, Kunnari M, Laurén P, Hakkarainen T, Auvinen V-V, Oksanen T, et al. Nanofibrillar cellulose hydrogels and reconstructed hydrogels as matrices for controlled drug release. Int J Pharm. 2017 Oct 30;532(1):269–80.

108. Ying G, Jiang N, Parra-Cantu C, Tang G, Zhang J, Wang H, et al. Bioprinted Injectable Hierarchically Porous Gelatin Methacryloyl Hydrogel Constructs with Shape-Memory Properties. Adv Funct Mater [Internet]. 2020 Sep;30. Available from: http://dx.doi.org/10.1002/adfm.202003740

109. Ying G, Manríquez J, Wu D, Zhang J, Jiang N, Maharjan S, et al. An open-source handheld extruder loaded with pore-forming bioink for in situ wound dressing. Materials Today Bio. 2020;8:100074.

110. Qin X-S, Wang M, Li W, Zhang YS. Biosurfactant-Stabilized Micropore-Forming GelMA Inks Enable Improved Usability for 3D Printing Applications [Internet]. Regenerative Engineering and Translational Medicine. 2022. Available from: http://dx.doi.org/10.1007/s40883-022-00250-5

111. Norouzi SK, Shamloo A. Bilayered heparinized vascular graft fabricated by combining electrospinning and freeze drying methods. Mater Sci Eng C Mater Biol Appl. 2019 Jan 1;94:1067–76.

112. Di Luca A, Longoni A, Criscenti G, - A. Surface energy and stiffness discrete gradients in additive manufactured scaffolds for osteochondral regeneration Related content Toward mimicking the bone structure: design of novel hierarchical scaffolds with a tailored radial

View Article Online
DOI: 10.1039/D1TB02628C

porosity gradient. 2016; Available from: http://dx.doi.org/10.1088/1758-5090/8/1/015014

113. Fang J, Yong Q, Zhang K, Sun W, Yan S, Cui L, et al. Novel injectable porous poly(γ-benzyl-l-glutamate) microspheres for cartilage tissue engineering: preparation and evaluation. J Mater Chem B Mater Biol Med. 2015 Feb 14;3(6):1020–31.

114. Chau M, De France KJ, Kopera B, Machado VR, Rosenfeldt S, Reyes L, et al. Composite Hydrogels with Tunable Anisotropic Morphologies and Mechanical Properties. Chem Mater. 2016 May 24;28(10):3406–15.

115. Liu PS, Chen GF. Applications of Porous Ceramics [Internet]. Porous Materials. 2014. p. 303–44. Available from: http://dx.doi.org/10.1016/b978-0-12-407788-1.00006-x

116. Hench LL. Bioactive ceramics. Ann N Y Acad Sci. 1988;523:54–71.

117. Thomas S, Balakrishnan P, Sreekala MS. Fundamental Biomaterials: Polymers. Woodhead Publishing; 2018. 352 p.

118. Pearce G. Introduction to membranes: Filtration for water and wastewater treatment [Internet]. Vol. 44, Filtration & Separation. 2007. p. 24–7. Available from: http://dx.doi.org/10.1016/s0015-1882(07)70052-6

119. Ismail AF, Matsuura T. Progress in transport theory and characterization method of Reverse Osmosis (RO) membrane in past fifty years [Internet]. Vol. 434, Desalination. 2018. p. 2–11. Available from: http://dx.doi.org/10.1016/j.desal.2017.09.028

120. Johnson D, Lynch R, Marshall C, Mead K, Hirst D. Aerosol Generation by Modern Flush Toilets. Aerosol Sci Technol. 2013;47(9):1047–57.

121. Pinto J, Morselli D, Bernardo V, Notario B, Fragouli D, Rodriguez-Perez MA, et al. Nanoporous PMMA foams with templated pore size obtained by localized in situ synthesis of nanoparticles and CO2 foaming [Internet]. Vol. 124, Polymer. 2017. p. 176–85. Available from: http://dx.doi.org/10.1016/j.polymer.2017.07.067

122. Liu W, Nie C, Li W, Ao Z, Wang S, An T. Oily sludge derived carbons as peroxymonosulfate activators for removing aqueous organic pollutants: Performances and the key role of carbonyl groups in electron-transfer mechanism. J Hazard Mater. 2021 Jul 15;414:125552.

123. Sang L-C, Coppens M-O. Effects of surface curvature and surface chemistry on the structure and activity of proteins adsorbed in nanopores. Phys Chem Chem Phys. 2011 Apr 14;13(14):6689–98.

124. Pereira L, Pereira R, Pereira MFR, van der Zee FP, Cervantes FJ, Alves MM. Thermal modification of activated carbon surface chemistry improves its capacity as redox mediator for azo dye reduction. J Hazard Mater. 2010 Nov 15;183(1-3):931–9.

125. Jones JR, Ehrenfried LM, Hench LL. Optimising bioactive glass scaffolds for bone tissue engineering. Biomaterials. 2006 Mar;27(7):964–73.

View Article Online
DOI: 10.1039/D1TB02628C

126. Vlasea M, Shanjani Y, Bothe A, Kandel R, Toyserkani E. A combined additive manufacturing and micro-syringe deposition technique for realization of bio-ceramic structures with micro-scale channels [Internet]. Vol. 68, The International Journal of Advanced Manufacturing Technology. 2013. p. 2261–9. Available from: http://dx.doi.org/10.1007/s00170-013-4839-7

127. Vakifahmetoglu C, Zeydanli D, Ozalp VC, Borsa BA, Soraru GD. Hierarchically porous polymer derived ceramics: A promising platform for multidrug delivery systems [Internet]. Vol. 140, Materials & Design. 2018. p. 37–44. Available from: http://dx.doi.org/10.1016/j.matdes.2017.11.047

128. He Q, Shi J. Mesoporous silica nanoparticle based nano drug delivery systems: synthesis, controlled drug release and delivery, pharmacokinetics and biocompatibility [Internet]. Vol. 21, Journal of Materials Chemistry. 2011. p. 5845. Available from: http://dx.doi.org/10.1039/c0jm03851b

129. Kwon S, Singh RK, Perez RA, Abou Neel EA, Kim H-W, Chrzanowski W. Silica-based mesoporous nanoparticles for controlled drug delivery. J Tissue Eng. 2013 Sep 3;4:2041731413503357.

130. Sayed E, Haj-Ahmad R, Ruparelia K, Arshad MS, Chang M-W, Ahmad Z. Porous Inorganic Drug Delivery Systems-a Review. AAPS PharmSciTech. 2017 Jul;18(5):1507–25.

131. Tamayo A, Mazo MA, Veiga MD, Ruiz-Caro R, Notario-Pérez F, Rubio J. Drug kinetics release from Eudragit - Tenofovir@SiOC tablets. Mater Sci Eng C Mater Biol Appl. 2017 Jun 1;75:1097–105.

132. Ye J, He J, Wang C, Yao K, Gou Z. Copper-containing mesoporous bioactive glass coatings on orbital implants for improving drug delivery capacity and antibacterial activity. Biotechnol Lett. 2014 May;36(5):961–8.

133. Cesarano J, Dellinger JG, Saavedra MP, Gill DD, Jamison RD, Grosser BA, et al. Customization of Load-Bearing Hydroxyapatite Lattice Scaffolds [Internet]. Vol. 2, International Journal of Applied Ceramic Technology. 2005. p. 212–20. Available from: http://dx.doi.org/10.1111/j.1744-7402.2005.02026.x

134. Montazerian M, Zanotto ED. Chapter 2. Bioactive Glass-ceramics: Processing, Properties and Applications [Internet]. Bioactive Glasses. p. 27–60. Available from: http://dx.doi.org/10.1039/9781782622017-00027

135. Hench LL. The story of Bioglass. J Mater Sci Mater Med. 2006 Nov;17(11):967–78.

136. Carta D, Knowles JC, Guerry P, Smith ME, Newport RJ. Sol–gel synthesis and structural characterisation of P2O5–B2O3–Na2O glasses for biomedical applications. J Mater Chem. 2008 Dec 8;19(1):150–8.

137. Hoppe A, Güldal NS, Boccaccini AR. A review of the biological response to ionic dissolution products from bioactive glasses and glass-ceramics. Biomaterials. 2011 Apr;32(11):2757–74.

View Article Online
DOI: 10.1039/D1TB02628C

138. Magyari K, Gruian C, Varga B, Ciceo-Lucacel R, Radu T, Steinhoff H-J, et al. Addressing the optimal silver content in bioactive glass systems in terms of BSA adsorption. J Mater Chem B Mater Biol Med. 2014 Sep 21;2(35):5799–808.

139. Lucacel RC, Ponta O, Licarete E, Radu T, Simon V. Synthesis, structure, bioactivity and biocompatibility of melt-derived P2O5-CaO-B2O3-K2O-MoO3 glasses. J Non-Cryst Solids. 2016 May 1;439:67–73.

140. Magyari K, Stefan R, Vulpoi A, Baia L. Bioactivity evolution of calcium-free borophosphate glass with addition of titanium dioxide. J Non-Cryst Solids. 2015 Feb 15;410:112–7.

141. Liang W, Tu Y, Zhou H, Liu C, Rüssel C. Borophosphate glass-ceramic scaffolds by a sodium silicate bonding process [Internet]. Vol. 357, Journal of Non-Crystalline Solids. 2011. p. 958–62. Available from: http://dx.doi.org/10.1016/j.jnoncrysol.2010.07.068

142. Brandão SM, Schellini SA, Moraes AD, Padovani CR, Pellizzon CH, Peitl O, et al. Biocompatibility analysis of bioglass® 45S5 and biosilicate® implants in the rabbit eviscerated socket. Orbit. 2012 Jun;31(3):143–9.

143. Eqtesadi S, Motealleh A, Miranda P, Lemos A, Rebelo A, Ferreira JMF. A simple recipe for direct writing complex 45S5 Bioglass® 3D scaffolds. Mater Lett. 2013 Feb 15;93:68–71.

144. Handel M, Hammer TR, Nooeaid P, Boccaccini AR, Hoefer D. 45S5-Bioglass(®)-based 3D-scaffolds seeded with human adipose tissue-derived stem cells induce in vivo vascularization in the CAM angiogenesis assay. Tissue Eng Part A. 2013 Dec;19(23-24):2703–12.

145. Rezwan K, Chen QZ, Blaker JJ, Boccaccini AR. Biodegradable and bioactive porous polymer/inorganic composite scaffolds for bone tissue engineering. Biomaterials. 2006 Jun;27(18):3413–31.

146. Hall SR, Walsh D, Green D, Oreffo R, Mann S. A novel route to highly porous bioactive silica gels [Internet]. Vol. 13, Journal of Materials Chemistry. 2003. p. 186–90. Available from: http://dx.doi.org/10.1039/b209300f

147. Tang W, Lin D, Yu Y, Niu H, Guo H, Yuan Y, et al. Bioinspired trimodal macro/micro/nano-porous scaffolds loading rhBMP-2 for complete regeneration of critical size bone defect. Acta Biomater. 2016 Mar 1;32:309–23.

148. Lei B, Shin K-H, Moon Y-W, Noh D-Y, Koh Y-H, Jin Y, et al. Synthesis and bioactivity of sol-gel derived porous, bioactive glass microspheres using chitosan as novel biomolecular template. J Am Ceram Soc. 2012 Jan;95(1):30–3.

149. Qian J, Kang Y, Wei Z, Zhang W. Fabrication and characterization of biomorphic 45S5 bioglass scaffold from sugarcane [Internet]. Vol. 29, Materials Science and Engineering: C. 2009. p. 1361–4. Available from: http://dx.doi.org/10.1016/j.msec.2008.11.004

150. Zheng K, Bortuzzo JA, Liu Y, Li W, Pischetsrieder M, Roether J, et al. Bio-templated

View Article Online
DOI: 10.1039/D1TB02628C

bioactive glass particles with hierarchical macro-nano porous structure and drug delivery capability. Colloids Surf B Biointerfaces. 2015 Nov 1;135:825–32.

151. Fan T-X, Chow S-K, Zhang D. Biomorphic mineralization: From biology to materials [Internet]. Vol. 54, Progress in Materials Science. 2009. p. 542–659. Available from: http://dx.doi.org/10.1016/j.pmatsci.2009.02.001

152. Luo H, Ji D, Li W, Xiao J, Li C, Xiong G, et al. Constructing a highly bioactive 3D nanofibrous bioglass scaffold via bacterial cellulose-templated sol-gel approach [Internet]. Vol. 176, Materials Chemistry and Physics. 2016. p. 1–5. Available from: http://dx.doi.org/10.1016/j.matchemphys.2016.03.029

153. Boccaccini AR, Notingher I, Maquet V, Jérôme R. Bioresorbable and bioactive composite materials based on polylactide foams filled with and coated by Bioglass particles for tissue engineering applications. J Mater Sci Mater Med. 2003 May;14(5):443–50.

154. Chen QZ, Thompson ID, Boccaccini AR. 45S5 Bioglass®-derived glass–ceramic scaffolds for bone tissue engineering [Internet]. Vol. 27, Biomaterials. 2006. p. 2414–25. Available from: http://dx.doi.org/10.1016/j.biomaterials.2005.11.025

155. Bretcanu O, Samaille C, Boccaccini AR. Simple methods to fabricate Bioglass®-derived glass–ceramic scaffolds exhibiting porosity gradient. J Mater Sci. 2008 Jun 1;43(12):4127–34.

156. Zhang K, Washburn NR, Simon CG Jr. Cytotoxicity of three-dimensionally ordered macroporous sol-gel bioactive glass (3DOM-BG). Biomaterials. 2005 Aug;26(22):4532–9.

157. Minaberry Y, Jobbágy M. Macroporous Bioglass Scaffolds Prepared by Coupling Sol–Gel with Freeze Drying. Chem Mater. 2011 May 10;23(9):2327–32.

158. Onna D, Minaberry Y, Jobbágy M. Hierarchical bioglass scaffolds: introducing the "milky way" for templated bioceramics. J Mater Chem B Mater Biol Med. 2015 Apr 21;3(15):2971–7.

159. Chen G-Q, Wu Q. The application of polyhydroxyalkanoates as tissue engineering materials. Biomaterials. 2005 Nov;26(33):6565–78.

160. Manavitehrani I, Fathi A, Badr H, Daly S, Negahi Shirazi A, Dehghani F. Biomedical Applications of Biodegradable Polyesters. Polymers [Internet]. 2016 Jan 16;8(1). Available from: http://dx.doi.org/10.3390/polym8010020

161. Paşcu EI, Stokes J, McGuinness GB. Electrospun composites of PHBV, silk fibroin and nano-hydroxyapatite for bone tissue engineering. Mater Sci Eng C Mater Biol Appl. 2013 Dec 1;33(8):4905–16.

162. Pires LSO, Fernandes MHFV, de Oliveira JMM. Biofabrication of glass scaffolds by 3D printing for tissue engineering. Int J Adv Manuf Technol. 2018 Oct 1;98(9):2665–76.

163. Wu C, Luo Y, Cuniberti G, Xiao Y, Gelinsky M. Three-dimensional printing of

View Article Online
DOI: 10.1039/D1TB02628C

hierarchical and tough mesoporous bioactive glass scaffolds with a controllable pore architecture, excellent mechanical strength and mineralization ability. Acta Biomater. 2011 Jun;7(6):2644–50.

164. Poh PSP, Hutmacher DW, Stevens MM, Woodruff MA. Fabrication and in vitro characterization of bioactive glass composite scaffolds for bone regeneration. Biofabrication. 2013 Dec;5(4):045005.

165. Langstaff S, Sayer M, Smith TJ, Pugh SM. Resorbable bioceramics based on stabilized calcium phosphates. Part II: evaluation of biological response. Biomaterials. 2001 Jan;22(2):135–50.

166. Duta L, Popescu AC. Current Status on Pulsed Laser Deposition of Coatings from Animal-Origin Calcium Phosphate Sources. Coat World. 2019 May 24;9(5):335.

167. Ginebra MP, Traykova T, Planell JA. Calcium phosphate cements as bone drug delivery systems: a review. J Control Release. 2006 Jun 28;113(2):102–10.

168. Surmenev RA, Surmeneva MA, Ivanova AA. Significance of calcium phosphate coatings for the enhancement of new bone osteogenesis--a review. Acta Biomater. 2014 Feb;10(2):557–79.

169. LeGeros RZ, Lin S, Rohanizadeh R, Mijares D, LeGeros JP. Biphasic calcium phosphate bioceramics: preparation, properties and applications. J Mater Sci Mater Med. 2003 Mar;14(3):201–9.

170. Oriá AP, Neto FAD, Laus JL, Dos Santos LA, Piza ET, Brunelli AT, et al. Evaluation of a double-setting alpha-tricalcium phosphate cement in eviscerated rabbit eyes. Ophthal Plast Reconstr Surg. 2006 Mar;22(2):126–30.

171. van Blitterswijk CA, Hesseling SC, Grote JJ, Koerten HK, de Groot K. The biocompatibility of hydroxyapatite ceramic: a study of retrieved human middle ear implants. J Biomed Mater Res. 1990 Apr;24(4):433–53.

172. Habraken W, Habibovic P, Epple M, Bohner M. Calcium phosphates in biomedical applications: materials for the future? Mater Today. 2016 Mar 1;19(2):69–87.

173. Ripamonti U. The morphogenesis of bone in replicas of porous hydroxyapatite obtained from conversion of calcium carbonate exoskeletons of coral. J Bone Joint Surg Am. 1991 Jun;73(5):692–703.

174. Barba A, Diez-Escudero A, Maazouz Y, Rappe K, Espanol M, Montufar EB, et al. Osteoinduction by Foamed and 3D-Printed Calcium Phosphate Scaffolds: Effect of Nanostructure and Pore Architecture. ACS Appl Mater Interfaces. 2017 Dec 6;9(48):41722–36.

175. Zhu Y, Wang M, Zhang Y, Zeng J, Omari-Siaw E, Yu J, et al. In Vitro Release and Bioavailability of Silybin from Micelle-Templated Porous Calcium Phosphate Microparticles. AAPS PharmSciTech. 2016 Oct;17(5):1232–9.

View Article Online
DOI: 10.1039/D1TB02628C

176. Barba A, Diez-Escudero A, Espanol M, Bonany M, Sadowska JM, Guillem-Marti J, et al. Impact of Biomimicry in the Design of Osteoinductive Bone Substitutes: Nanoscale Matters. ACS Appl Mater Interfaces. 2019 Mar 6;11(9):8818–30.

177. Aranaz I, Martínez-Campos E, Moreno-Vicente C, Civantos A, García-Arguelles S, Del Monte F. Macroporous Calcium Phosphate/Chitosan Composites Prepared via Unidirectional Ice Segregation and Subsequent Freeze-Drying. Materials [Internet]. 2017 May 8;10(5). Available from: http://dx.doi.org/10.3390/ma10050516

178. Gan D, Liu M, Xu T, Wang K, Tan H, Lu X. Chitosan/biphasic calcium phosphate scaffolds functionalized with BMP-2-encapsulated nanoparticles and RGD for bone regeneration. J Biomed Mater Res A. 2018 Oct;106(10):2613–24.

179. Jin S, Li J, Wang J, Jiang J, Zuo Y, Li Y, et al. Electrospun silver ion-loaded calcium phosphate/chitosan antibacterial composite fibrous membranes for guided bone regeneration. Int J Nanomedicine. 2018 Aug 10;13:4591–605.

180. Panzavolta S, Gualandi C, Fiorani A, Bracci B, Focarete ML, Bigi A. Fast Coprecipitation of Calcium Phosphate Nanoparticles inside Gelatin Nanofibers by Tricoaxial Electrospinning [Internet]. Vol. 2016, Journal of Nanomaterials. 2016. p. 1–7. Available from: http://dx.doi.org/10.1155/2016/4235235

181. Costa Machado G, García-Tuñón E, Bell RV, Alini M, Saiz E, Peroglio M. Calcium phosphate substrates with emulsion-derived roughness: Processing, characterisation and interaction with human mesenchymal stem cells. J Eur Ceram Soc. 2018 Mar 1;38(3):949–61.

182. TenHuisen KS, Brown PW. Formation of calcium-deficient hydroxyapatite from alpha-tricalcium phosphate. Biomaterials. 1998 Dec;19(23):2209–17.

183. Raymond S, Maazouz Y, Montufar EB, Perez RA, González B, Konka J, et al. Accelerated hardening of nanotextured 3D-plotted self-setting calcium phosphate inks. Acta Biomater. 2018 Jul 15;75:451–62.

184. Zhang K, Fan Y, Dunne N, Li X. Effect of microporosity on scaffolds for bone tissue engineering. Regen Biomater. 2018 Mar;5(2):115–24.

185. Novotna L, Kucera L, Hampl A, Drdlik D, Cihlar J Jr, Cihlar J. Biphasic calcium phosphate scaffolds with controlled pore size distribution prepared by in-situ foaming. Mater Sci Eng C Mater Biol Appl. 2019 Feb 1;95:363–70.

186. Aveic S, Davtalab R, Vogt M, Weber M, Buttler P, Tonini GP, et al. Calcium phosphate scaffolds with defined interconnecting channel structure provide a mimetic 3D niche for bone marrow metastasized tumor cell growth. Acta Biomater. 2019 Apr 1;88:527–39.

187. Farzadi A, Solati-Hashjin M, Asadi-Eydivand M, Abu Osman NA. Effect of layer thickness and printing orientation on mechanical properties and dimensional accuracy of 3D printed porous samples for bone tissue engineering. PLoS One. 2014 Sep 18;9(9):e108252.

View Article Online
DOI: 10.1039/D1TB02628C

188. de Lacerda Schickert S, van den Beucken JJJP, Leeuwenburgh SCG, Jansen JA. Pre-Clinical Evaluation of Biological Bone Substitute Materials for Application in Highly Loaded Skeletal Sites. Biomolecules [Internet]. 2020 Jun 9;10(6). Available from: http://dx.doi.org/10.3390/biom10060883

189. Tang Z, Li X, Tan Y, Fan H, Zhang X. The material and biological characteristics of osteoinductive calcium phosphate ceramics. Regen Biomater. 2018 Feb;5(1):43–59.

190. LeGeros RZ. Biodegradation and bioresorption of calcium phosphate ceramics. Clin Mater. 1993;14(1):65–88.

191. Yaylaoğlu MB, Korkusuz P, Ors U, Korkusuz F, Hasirci V. Development of a calcium phosphate-gelatin composite as a bone substitute and its use in drug release. Biomaterials. 1999 Apr;20(8):711–9.

192. Marques CF, Perera FH, Marote A, Ferreira S, Vieira SI, Olhero S, et al. Biphasic calcium phosphate scaffolds fabricated by direct write assembly: Mechanical, anti-microbial and osteoblastic properties. J Eur Ceram Soc. 2017 Jan 1;37(1):359–68.

193. Ogilvie A, Frank RM, Benqué EP, Gineste M, Heughebaert M, Hemmerle J. The biocompatibility of hydroxyapatite implanted in the human periodontium. J Periodontal Res. 1987 Jul;22(4):270–83.

194. Roohani-Esfahani S-I, Nouri-Khorasani S, Lu Z, Appleyard R, Zreiqat H. The influence hydroxyapatite nanoparticle shape and size on the properties of biphasic calcium phosphate scaffolds coated with hydroxyapatite-PCL composites. Biomaterials. 2010 Jul;31(21):5498–509.

195. Suneetha M, Rao KM, Han SS. Mussel-Inspired Cell/Tissue-Adhesive, Hemostatic Hydrogels for Tissue Engineering Applications. ACS Omega. 2019 Jul 31;4(7):12647–56.

196. Chen S, Shi Y, Zhang X, Ma J. Biomimetic synthesis of Mg-substituted hydroxyapatite nanocomposites and three-dimensional printing of composite scaffolds for bone regeneration. J Biomed Mater Res A. 2019 Nov;107(11):2512–21.

197. Milovac D, Weigand I, Kovacic M, Ivankovic M, Ivankovic H. Highly porous hydroxyapatite derived from cuttlefish bone as tio2 catalyst support [Internet]. Vol. 12, Processing and Application of Ceramics. 2018. p. 136–42. Available from: http://dx.doi.org/10.2298/pac1802136m

198. Farokhi M, Mottaghitalab F, Samani S, Shokrgozar MA, Kundu SC, Reis RL, et al. Silk fibroin/hydroxyapatite composites for bone tissue engineering. Biotechnol Adv. 2018 Jan;36(1):68–91.

199. Lee H, Jang T-S, Song J, Kim H-E, Jung H-D. The Production of Porous Hydroxyapatite Scaffolds with Graded Porosity by Sequential Freeze-Casting. Materials [Internet]. 2017 Mar 31;10(4). Available from: http://dx.doi.org/10.3390/ma10040367

200. Cox SC, Thornby JA, Gibbons GJ, Williams MA, Mallick KK. 3D printing of porous

View Article Online
DOI: 10.1039/D1TB02628C

hydroxyapatite scaffolds intended for use in bone tissue engineering applications. Materials Science and Engineering C. 2015 Feb;47:237–47.

201. Roy TD, Simon JL, Ricci JL, Rekow ED, Thompson VP, Parsons JR. Performance of degradable composite bone repair products made via three-dimensional fabrication techniques. J Biomed Mater Res. 2003 Aug 1;66A(2):283–91.

202. Gbureck U, Vorndran E, Müller FA, Barralet JE. Low temperature direct 3D printed bioceramics and biocomposites as drug release matrices. 2007; Available from: http://dx.doi.org/10.1016/j.jconrel.2007.06.022

203. Han L, Jiang Y, Lv C, Gan D, Wang K, Ge X, et al. Mussel-inspired hybrid coating functionalized porous hydroxyapatite scaffolds for bone tissue regeneration. Colloids Surf B Biointerfaces. 2019 Jul 1;179:470–8.

204. Fihri A, Len C, Varma RS, Solhy A. Hydroxyapatite: A review of syntheses, structure and applications in heterogeneous catalysis. Coord Chem Rev. 2017 Sep 15;347:48–76.

205. Xiao D, Guo T, Yang F, Feng G, Shi F, Li J, et al. In situ formation of nanostructured calcium phosphate coatings on porous hydroxyapatite scaffolds using a hydrothermal method and the effect on mesenchymal stem cell behavior. Ceram Int. 2017 Jan 1;43(1, Part B):1588–96.

206. Wilson J. 1 - Metallic biomaterials: State of the art and new challenges. In: Balakrishnan P, M S S, Thomas S, editors. Fundamental Biomaterials: Metals. Woodhead Publishing; 2018. p. 1–33.

207. Ping D. Review on ω Phase in Body-Centered Cubic Metals and Alloys. Acta Metall Sin . 2014 Feb 1;27(1):1–11.

208. Pelton AR, Dicello J, Miyazaki S. Optimisation of processing and properties of medical grade Nitinol wire [Internet]. Vol. 9, Minimally Invasive Therapy & Allied Technologies. 2000. p. 107–18. Available from: http://dx.doi.org/10.3109/13645700009063057

209. Thandapani G, Radha E, Jayashri J, Annie Kamala Florence J, Sudha PN. 4 - Bioactive metallic surfaces for bone tissue engineering. In: Balakrishnan P, M S S, Thomas S, editors. Fundamental Biomaterials: Metals. Woodhead Publishing; 2018. p. 79–110.

210. Crovace AM, Lacitignola L, Forleo DM, Staffieri F, Francioso E, Di Meo A, et al. 3D Biomimetic Porous Titanium (TiAlV ELI) Scaffolds for Large Bone Critical Defect Reconstruction: An Experimental Study in Sheep. Animals (Basel) [Internet]. 2020 Aug 11;10(8). Available from: http://dx.doi.org/10.3390/ani10081389

211. Witte F, Kaese V, Haferkamp H, Switzer E, Meyer-Lindenberg A, Wirth CJ, et al. In vivo corrosion of four magnesium alloys and the associated bone response. Biomaterials. 2005 Jun;26(17):3557–63.

212. Li Z, Gu X, Lou S, Zheng Y. The development of binary Mg-Ca alloys for use as biodegradable materials within bone. Biomaterials. 2008 Apr;29(10):1329–44.

View Article Online
DOI: 10.1039/D1TB02628C

213. Peuster M, Wohlsein P, Brügmann M, Ehlerding M, Seidler K, Fink C, et al. A novel approach to temporary stenting: degradable cardiovascular stents produced from corrodible metal-results 6-18 months after implantation into New Zealand white rabbits. Heart. 2001 Nov;86(5):563–9.

214. Balamurugan A, Rajeswari S, Balossier G, Rebelo AHS, Ferreira JMF. Corrosion aspects of metallic implants - An overview [Internet]. Vol. 59, Materials and Corrosion. 2008. p. 855–69. Available from: http://dx.doi.org/10.1002/maco.200804173

215. Dewidar MM, Khalil KA, Lim JK. Processing and mechanical properties of porous 316L stainless steel for biomedical applications [Internet]. Vol. 17, Transactions of Nonferrous Metals Society of China. 2007. p. 468–73. Available from: http://dx.doi.org/10.1016/s1003-6326(07)60117-4

216. Braic M, Balaceanu M, Braic V, Vladescu A, Pavelescu G, Albulescu M. Synthesis and characterization of TiN, TiAlN and TiN/TiAlN biocompatible coatings. Surf Coat Technol. 2005 Oct 1;200(1):1014–7.

217. Begum Z, Poonguzhali A, Basu R, Sudha C, Shaikh H, Subba Rao RV, et al. Studies of the tensile and corrosion fatigue behaviour of austenitic stainless steels. Corros Sci. 2011 Apr 1;53(4):1424–32.

218. Han C, Yao Y, Cheng X, Luo J, Luo P, Wang Q, et al. Electrophoretic Deposition of Gentamicin-Loaded Silk Fibroin Coatings on 3D-Printed Porous Cobalt-Chromium-Molybdenum Bone Substitutes to Prevent Orthopedic Implant Infections. Biomacromolecules. 2017 Nov 13;18(11):3776–87.

219. Mantripragada VP, Lecka-Czernik B, Ebraheim NA, Jayasuriya AC. An overview of recent advances in designing orthopedic and craniofacial implants. J Biomed Mater Res A. 2013 Nov;101(11):3349–64.

220. Li JP, de Wijn JR, Van Blitterswijk CA, de Groot K. Porous Ti6Al4V scaffold directly fabricating by rapid prototyping: preparation and in vitro experiment. Biomaterials. 2006 Mar;27(8):1223–35.

221. Brailovski V, Prokoshkin S, Gauthier M, Inaekyan K, Dubinskiy S, Petrzhik M, et al. Bulk and porous metastable beta Ti–Nb–Zr(Ta) alloys for biomedical applications. Materials Science and Engineering: C. 2011 Apr 8;31(3):643–57.

222. Nakai M, Niinomi M, Zhao X, Zhao X. Self-adjustment of Young's modulus in biomedical titanium alloys during orthopaedic operation [Internet]. Vol. 65, Materials Letters. 2011. p. 688–90. Available from: http://dx.doi.org/10.1016/j.matlet.2010.11.006

223. Zhao X, Niinomi M, Nakai M, Hieda J. Beta type Ti-Mo alloys with changeable Young's modulus for spinal fixation applications. Acta Biomater. 2012 May;8(5):1990–7.

224. Gorgin Karaji Z, Speirs M, Dadbakhsh S, Kruth J-P, Weinans H, Zadpoor AA, et al. Additively Manufactured and Surface Biofunctionalized Porous Nitinol. ACS Appl Mater Interfaces. 2017 Jan 18;9(2):1293–304.

View Article Online
DOI: 10.1039/D1TB02628C

225. Hermawan H, Dubé D, Mantovani D. Degradable metallic biomaterials: design and development of Fe-Mn alloys for stents. J Biomed Mater Res A. 2010 Apr;93(1):1–11.

226. MM Porter JM. It's tough to be strong: Advances in bioinspired structural ceramic based materials. Am Ceram Soc Bull. 93(5):81–24.

227. Johnson DW, Sherborne C, Didsbury MP, Pateman C, Cameron NR, Claeyssens F. Macrostructuring of Emulsion-templated Porous Polymers by 3D Laser Patterning. Adv Mater. 2013;25(23):3178–81.

228. Huczko A. Template-based synthesis of nanomaterials. Appl Phys A. 2000;70:365–76.

229. Andrieux S, Drenckhan W, Stubenrauch C. Highly ordered biobased scaffolds: From liquid to solid foams [Internet]. Vol. 126, Polymer. 2017. p. 425–31. Available from: http://dx.doi.org/10.1016/j.polymer.2017.04.031

230. Wang C, Jiang W, Zuo W, Han G, Zhang Y. Effect of heat-transfer capability on micropore structure of freeze-drying alginate scaffold. Mater Sci Eng C Mater Biol Appl. 2018 Dec 1;93:944–9.

231. Offeddu GS, Ashworth JC, Cameron RE, Oyen ML. Structural determinants of hydration, mechanics and fluid flow in freeze-dried collagen scaffolds. Acta Biomater. 2016 Sep 1;41:193–203.

232. Krieghoff J, Picke A-K, Salbach-Hirsch J, Rother S, Heinemann C, Bernhardt R, et al. Increased pore size of scaffolds improves coating efficiency with sulfated hyaluronan and mineralization capacity of osteoblasts. Biomater Res. 2019 Dec 18;23:26.

233. Tan S, Gu J, Han SC, Lee D-W, Kang K. Design and fabrication of a non-clogging scaffold composed of semi-permeable membrane [Internet]. Vol. 142, Materials & Design. 2018. p. 229–39. Available from: http://dx.doi.org/10.1016/j.matdes.2018.01.033

234. Kim JH, Lee SB, Kim SJ, Lee YM. Rapid temperature/pH response of porous alginate-g-poly(N- isopropylacrylamide) hydrogels. Polymer . 2002;43:7549–58.

235. Chan AW, Neufeld RJ. Modeling the controllable pH-responsive swelling and pore size of networked alginate based biomaterials. Biomaterials. 2009 Oct;30(30):6119–29.

236. Janoušková O, Přádný M, Vetrík M, Chylíková Krumbholcová E, Michálek J, Dušková Smrčková M. Biomimetic modification of dual porosity poly(2-hydroxyethyl methacrylate) hydrogel scaffolds-porosity and stem cell growth evaluation. Biomed Mater. 2019 Jul 15;14(5):055004.

237. Mangione MR, Giacomazza D, Bulone D, Martorana V, Cavallaro G, San Biagio PL. K(+) and Na(+) effects on the gelation properties of kappa-Carrageenan. Biophys Chem. 2005 Feb 1;113(2):129–35.

238. Cho YS, Hong MW, Kim YY, Cho Y-S. Assessment of cell proliferation in salt-leaching using powder (SLUP) scaffolds with penetrated macro-pores [Internet]. Vol. 131, Journal of

View Article Online
DOI: 10.1039/D1TB02628C

Applied Polymer Science. 2014. Available from: http://dx.doi.org/10.1002/app.40240

239. Mohanty S, Sanger K, Heiskanen A, Trifol J, Szabo P, Dufva M, et al. Fabrication of scalable tissue engineering scaffolds with dual-pore microarchitecture by combining 3D printing and particle leaching. Mater Sci Eng C Mater Biol Appl. 2016 Apr 1;61:180–9.

240. Jakus AE, Geisendorfer NR, Lewis PL, Shah RN. 3D-printing porosity: A new approach to creating elevated porosity materials and structures. Acta Biomater. 2018 May;72:94–109.

241. Pashneh-Tala S, Moorehead R, Claeyssens F. Hybrid manufacturing strategies for tissue engineering scaffolds using methacrylate functionalised poly(glycerol sebacate) [Internet]. Vol. 34, Journal of Biomaterials Applications. 2020. p. 1114–30. Available from: http://dx.doi.org/10.1177/0885328219898385

242. Armstrong JPK, Burke M, Carter BM, Davis SA, Perriman AW. 3D Bioprinting Using a Templated Porous Bioink. Adv Healthc Mater. 2016 Jul;5(14):1724–30.

243. Bechara SL, Judson A, Popat KC. Template synthesized poly(ε-caprolactone) nanowire surfaces for neural tissue engineering [Internet]. Vol. 31, Biomaterials. 2010. p. 3492–501. Available from: http://dx.doi.org/10.1016/j.biomaterials.2010.01.084

244. Liu B, Hu X. Chapter 1 - Hollow Micro- and Nanomaterials: Synthesis and Applications. In: Zhao Q, editor. Advanced Nanomaterials for Pollutant Sensing and Environmental Catalysis. Elsevier; 2020. p. 1–38. (Micro and Nano Technologies).

245. Sjoblom J. Emulsions and Emulsion Stability: Surfactant Science Series/61. CRC Press; 2005. 688 p.

246. Donderwinkel I, van Hest JCM, Cameron NR. Bio-inks for 3D bioprinting: recent advances and future prospects [Internet]. Vol. 8, Polymer Chemistry. 2017. p. 4451–71. Available from: http://dx.doi.org/10.1039/c7py00826k

247. Zhou S, Bismarck A, Steinke JHG. Ion-responsive alginate based macroporous injectable hydrogel scaffolds prepared by emulsion templating. J Mater Chem B Mater Biol Med. 2013 Oct 7;1(37):4736–45.

248. Schipani R, Nolan DR, Lally C, Kelly DJ. Integrating finite element modelling and 3D printing to engineer biomimetic polymeric scaffolds for tissue engineering. Connect Tissue Res. 2020 Mar;61(2):174–89.

249. Murphy AR, Ghobrial I, Jamshidi P, Laslett A, O'Brien CM, Cameron NR. Tailored emulsion-templated porous polymer scaffolds for iPSC-derived human neural precursor cell culture. Polym Chem. 2017 Nov 7;8(43):6617–27.

250. Nottelet B, Pektok E, Mandracchia D, Tille J-C, Walpoth B, Gurny R, et al. Factorial design optimization and in vivo feasibility of poly(epsilon-caprolactone)-micro- and nanofiber-based small diameter vascular grafts. J Biomed Mater Res A. 2009 Jun 15;89(4):865–75.

251. Dikici BA, Dikici S, Reilly GC, Macneil S, Claeyssens F. materials A Novel Bilayer

View Article Online
DOI: 10.1039/D1TB02628C

Polycaprolactone Membrane for Guided Bone Regeneration: Combining Electrospinning and Emulsion Templating. 2019; Available from: http://dx.doi.org/10.3390/ma12162643

252. Owen R, Sherborne C, Paterson T, Green NH, Reilly GC, Claeyssens F. Emulsion templated scaffolds with tunable mechanical properties for bone tissue engineering. J Mech Behav Biomed Mater. 2016 Feb;54:159–72.

253. Sears NA, Dhavalikar PS, Cosgriff-Hernandez EM. Emulsion Inks for 3D Printing of High Porosity Materials. Macromol Rapid Commun. 2016;37(16):1369–74.

254. Hsiao LC, Badruddoza AZM, Cheng L-C, Doyle PS. 3D printing of self-assembling thermoresponsive nanoemulsions into hierarchical mesostructured hydrogels. Soft Matter. 2017 Feb 7;13(5):921–9.

255. Song Y, Sauret A, Cheung Shum H. All-aqueous multiphase microfluidics. Biomicrofluidics. 2013 Dec 27;7(6):61301–61301.

256. Gurevitch I, Silverstein MS. Polymerized pickering HIPEs: Effects of synthesis parameters on porous structure: Polymerized Pickering HIPEs. J Polym Sci A Polym Chem. 2010 Apr 1;48(7):1516–25.

257. Haugh MG, Murphy CM, O'Brien FJ. Novel Freeze-Drying Methods to Produce a Range of Collagen–Glycosaminoglycan Scaffolds with Tailored Mean Pore Sizes [Internet]. Vol. 16, Tissue Engineering Part C: Methods. 2010. p. 887–94. Available from: http://dx.doi.org/10.1089/ten.tec.2009.0422

258. Fissore D, Pisano R, Barresi AA. Process analytical technology for monitoring pharmaceuticals freeze-drying – A comprehensive review. Drying Technol. 2018 Nov 18;36(15):1839–65.

259. Den Brok MWJ, Nuijen B, Lutz C, Opitz H-G, Beijnen JH. Pharmaceutical Development of a Lyophilised Dosage Form for the Investigational Anticancer Agent Imexon Using Dimethyl Sulfoxide as Solubilising and Stabilising Agent. J Pharm Sci. 2005 May 1;94(5):1101–14.

260. Teagarden DL, Petre WJ, Gold PM. Stabilized prostaglandin E1 [Internet]. US Patent. 5741523, 1998 [cited 2021 Feb 17]. Available from: https://patentimages.storage.googleapis.com/62/b7/3e/d6ff6e662730b7/US5741523.pdf

261. de Waard H, De Beer T, Hinrichs WLJ, Vervaet C, Remon J-P, Frijlink HW. Controlled crystallization of the lipophilic drug fenofibrate during freeze-drying: elucidation of the mechanism by in-line Raman spectroscopy. AAPS J. 2010 Dec;12(4):569–75.

262. Haseley P, Oetjen G-W. Freeze-Drying. John Wiley & Sons; 2018. 440 p.

263. Shukla S. Freeze drying process: A review. International journal of pharmaceutical sciences and research. 2011;2(12):3061.

264. Hou Q, Grijpma DW, Feijen J. Preparation of interconnected highly porous polymeric

View Article Online
DOI: 10.1039/D1TB02628C

structures by a replication and freeze-drying process. Journal of Biomedical Materials Research Part B: Applied Biomaterials: An Official Journal of The Society for Biomaterials, The Japanese Society for Biomaterials, and The Australian Society for Biomaterials and the Korean Society for Biomaterials. 2003;67(2):732–40.

265. Schugens C, Maquet V, Grandfils C, Jerome R, Teyssie P. Biodegradable and macroporous polylactide implants for cell transplantation: 1. Preparation of macroporous polylactide supports by solid-liquid phase separation [Internet]. Vol. 37, Polymer. 1996. p. 1027–38. Available from: http://dx.doi.org/10.1016/0032-3861(96)87287-9

266. Wu X, Liu Y, Li X, Wen P, Zhang Y, Long Y, et al. Preparation of aligned porous gelatin scaffolds by unidirectional freeze-drying method [Internet]. Vol. 6, Acta Biomaterialia. 2010. p. 1167–77. Available from: http://dx.doi.org/10.1016/j.actbio.2009.08.041

267. Mikos AG, Lyman MD, Freed LE, Langer R. Wetting of poly(L-lactic acid) and poly(DL-lactic-co-glycolic acid) foams for tissue culture. Biomaterials. 1994 Jan;15(1):55–8.

268. Gao J, Niklason L, Langer R. Surface hydrolysis of poly(glycolic acid) meshes increases the seeding density of vascular smooth muscle cells. J Biomed Mater Res. 1998 Dec 5;42(3):417–24.

269. Yang J, Shi G, Bei J, Wang S, Cao Y, Shang Q, et al. Fabrication and surface modification of macroporous poly(L-lactic acid) and poly(L-lactic-co-glycolic acid) (70/30) cell scaffolds for human skin fibroblast cell culture [Internet]. Vol. 62, Journal of Biomedical Materials Research. 2002. p. 438–46. Available from: http://dx.doi.org/10.1002/jbm.10318

270. Chen G, Okamura A, Sugiyama K, Wozniak MJ, Kawazoe N, Sato S, et al. Surface modification of porous scaffolds with nanothick collagen layer by centrifugation and freeze-drying. Journal of Biomedical Materials Research Part B: Applied Biomaterials: An Official Journal of The Society for Biomaterials, The Japanese Society for Biomaterials, and The Australian Society for Biomaterials and the Korean Society for Biomaterials. 2009;90(2):864–72.

271. Curtis A, Wilkinson C. Topographical control of cells. Biomaterials. 1997 Dec;18(24):1573–83.

272. Flemming RG, Murphy CJ, Abrams GA, Goodman SL, Nealey PF. Effects of synthetic micro- and nano-structured surfaces on cell behavior. Biomaterials. 1999 Mar;20(6):573–88.

273. Falconnet D, Csucs G, Grandin HM, Textor M. Surface engineering approaches to micropattern surfaces for cell-based assays. Biomaterials. 2006 Jun;27(16):3044–63.

274. Ram M, Paulo Davim J. Advanced Applications in Manufacturing Engineering. Woodhead Publishing; 2018. 278 p.

275. He W, Gonsalves KE, Batina N, Poker DB, Alexander E, Hudson M. Micro/nanomachining of Polymer Surface for Promoting Osteoblast Cell Adhesion. Biomed Microdevices. 2003 Jun 1;5(2):101–8.

View Article Online
DOI: 10.1039/D1TB02628C

276. Charest JL, King WP. Engineering Biomaterial Interfaces Through Micro and Nano-Patterning [Internet]. BioNanoFluidic MEMS. p. 251–77. Available from: http://dx.doi.org/10.1007/978-0-387-46283-7_10

277. Broers AN, Hoole ACF, Ryan JM. Electron beam lithography—Resolution limits. Microelectron Eng. 1996 Sep 1;32(1):131–42.

278. Bhatia SN, Yarmush ML, Toner M. Controlling cell interactions by micropatterning in co-cultures: hepatocytes and 3T3 fibroblasts. J Biomed Mater Res. 1997 Feb;34(2):189–99.

279. Rundqvist J, Hoh JH, Haviland DB. Directed immobilization of protein-coated nanospheres to nanometer-scale patterns fabricated by electron beam lithography of poly(ethylene glycol) self-assembled monolayers. Langmuir. 2006 May 23;22(11):5100–7.

280. Bryant SJ, Cuy JL, Hauch KD, Ratner BD. Photo-patterning of porous hydrogels for tissue engineering. Biomaterials. 2007 Jul;28(19):2978–86.

281. Myung D, Koh W, Bakri A, Zhang F, Marshall A, Ko J, et al. Design and fabrication of an artificial cornea based on a photolithographically patterned hydrogel construct. Biomed Microdevices. 2007 Dec;9(6):911–22.

282. Jing W, Chunxi Y, Yizao W, Honglin L, Fang H, Kerong D, et al. Laser Patterning of Bacterial Cellulose Hydrogel and its Modification With Gelatin and Hydroxyapatite for Bone Tissue Engineering. Soft Mater. 2013 Apr 1;11(2):173–80.

283. Kawahara T. Formation of Saturated Solitons in a Nonlinear Dispersive System with Instability and Dissipation. Phys Rev Lett. 1983 Aug 1;51(5):381–3.

284. Niaounakis M. Biopolymers: Processing and Products. William Andrew; 2014. 616 p.

285. Ul Ahad I, Bartnik A, Fiedorowicz H, Kostecki J, Korczyc B, Ciach T, et al. Surface modification of polymers for biocompatibility via exposure to extreme ultraviolet radiation. J Biomed Mater Res A. 2014;102(9):3298–310.

286. Park GE, Pattison MA, Park K, Webster TJ. Accelerated chondrocyte functions on NaOH-treated PLGA scaffolds. Biomaterials. 2005 Jun;26(16):3075–82.

287. Wang S, Cui W, Bei J. Bulk and surface modifications of polylactide. Anal Bioanal Chem. 2005 Feb;381(3):547–56.

288. Zhu Y, Gao C, Liu X, Shen J. Surface modification of polycaprolactone membrane via aminolysis and biomacromolecule immobilization for promoting cytocompatibility of human endothelial cells. Biomacromolecules. 2002 Nov;3(6):1312–9.

289. Zhu Y, Gao C, Liu Y, Shen J. Endothelial cell functions in vitro cultured on poly (L-lactic acid) membranes modified with different methods. Journal of Biomedical Materials Research Part A: An Official Journal of The Society for Biomaterials, The Japanese Society for Biomaterials, and The Australian Society for Biomaterials and the Korean Society for Biomaterials. 2004;69(3):436–43.

View Article Online
DOI: 10.1039/D1TB02628C

290. Morent R, De Geyter N, Desmet T, Dubruel P, Leys C. Plasma surface modification of biodegradable polymers: A review: Plasma surface modification of biodegradable polymers: A review. Plasma Process Polym. 2011 Mar 22;8(3):171–90.

291. Baier RE. Surface properties influencing biological adhesion. Adhesion in biological systems. 1970;15–48.

292. Rasal RM, Janorkar AV, Hirt DE. Poly(lactic acid) modifications. Prog Polym Sci. 2010 Mar 1;35(3):338–56.

293. McCord MG, Hwang YJ, Qiu Y, Hughes LK, Bourham MA. Surface analysis of cotton fabrics fluorinated in radio-frequency plasma. J Appl Polym Sci. 2003 May 23;88(8):2038–47.

294. Molina R, Erra P, Julià L, Bertran E. Free Radical Formation in Wool Fibers Treated by Low Temperature Plasma. Text Res J. 2003 Nov 1;73(11):955–9.

295. Marcandalli B, Riccardi C. Plasma treatments of fibres and textiles [Internet]. Plasma Technologies for Textiles. 2007. p. 282–300. Available from: http://dx.doi.org/10.1533/9781845692575.2.282

296. Fabbri P, Messori M. 5 - Surface Modification of Polymers: Chemical, Physical, and Biological Routes. In: Jasso-Gastinel CF, Kenny JM, editors. Modification of Polymer Properties. William Andrew Publishing; 2017. p. 109–30.

297. Castilho M, Moseke C, Ewald A, Gbureck U, Groll J, Pires I, et al. Direct 3D powder printing of biphasic calcium phosphate scaffolds for substitution of complex bone defects. Biofabrication. 2014 Mar;6(1):015006.

298. Bertol LS, Schabbach R, Loureiro Dos Santos LA. Different post-processing conditions for 3D bioprinted α-tricalcium phosphate scaffolds. J Mater Sci Mater Med. 2017 Sep 15;28(10):168.

299. Hochleitner G. Advancing melt electrospinning writing for fabrication of biomimetic structures [Internet]. Universität Würzburg; 2018. Available from: https://opus.bibliothek.uni-wuerzburg.de/export/index/bibtex/searchtype/authorsearch/referee/J%C3%BCrgen+Groll/start/0/rows/10/subjectfq/3D+printing

300. Lins LC, Wianny F, Livi S, Dehay C, Duchet-Rumeau J, Gérard J-F. Effect of polyvinylidene fluoride electrospun fiber orientation on neural stem cell differentiation. J Biomed Mater Res B Appl Biomater. 2017 Nov;105(8):2376–93.

301. Liu R, Becer CR, Screen HRC. Guided Cell Attachment via Aligned Electrospinning of Glycopolymers. Macromol Biosci. 2018 Dec;18(12):e1800293.

302. Mohamadi F, Ebrahimi-Barough S, Reza Nourani M, Ali Derakhshan M, Goodarzi V, Sadegh Nazockdast M, et al. Electrospun nerve guide scaffold of poly(ε-caprolactone)/collagen/nanobioglass: an in vitro study in peripheral nerve tissue engineering.

View Article Online
DOI: 10.1039/D1TB02628C

J Biomed Mater Res A. 2017 Jul;105(7):1960–72.

303. Augustine R, Nethi SK, Kalarikkal N, Thomas S, Patra CR. Electrospun polycaprolactone (PCL) scaffolds embedded with europium hydroxide nanorods (EHNs) with enhanced vascularization and cell proliferation for tissue engineering applications. J Mater Chem B Mater Biol Med. 2017 Jun 28;5(24):4660–72.

304. Raic A, Friedrich F, Kratzer D, Bieback K, Lahann J, Lee-Thedieck C. Potential of electrospun cationic BSA fibers to guide osteogenic MSC differentiation via surface charge and fibrous topography. Sci Rep. 2019 Dec 27;9(1):20003.

305. Kang Y, Chen P, Shi X, Zhang G, Wang C. Multilevel structural stereocomplex polylactic acid/collagen membranes by pattern electrospinning for tissue engineering. Polymer . 2018 Nov 7;156:250–60.

306. Tian L, Prabhakaran MP, Hu J, Chen M, Besenbacher F, Ramakrishna S. Synergistic effect of topography, surface chemistry and conductivity of the electrospun nanofibrous scaffold on cellular response of PC12 cells. Colloids Surf B Biointerfaces. 2016 Sep 1;145:420–9.

307. Jeong SI, Burns NA, Bonino CA, Kwon IK, Khan SA, Alsberg E. Improved cell infiltration of highly porous 3D nanofibrous scaffolds formed by combined fiber-fiber charge repulsions and ultra-sonication. J Mater Chem B Mater Biol Med. 2014;2(46):8116–22.

308. Nam J, Huang Y, Agarwal S, Lannutti J. Improved cellular infiltration in electrospun fiber via engineered porosity. Tissue Eng. 2007 Sep 9;13(9):2249–57.

309. Chen H, Peng Y, Wu S, Tan LP. Electrospun 3D fibrous scaffolds for chronic wound repair. Materials [Internet]. 2016;9(4). Available from: http://dx.doi.org/10.3390/ma9040272

310. Wu Y, Qin Y, Wang Z, Wang J, Zhang C, Li C, et al. The regeneration of macro-porous electrospun poly(ε-caprolactone) vascular graft during long-term in situ implantation. J Biomed Mater Res B Appl Biomater. 2018 May;106(4):1618–27.

311. Vaquette C, Cooper-White JJ. Increasing electrospun scaffold pore size with tailored collectors for improved cell penetration. Acta Biomater. 2011 Jun;7(6):2544–57.

312. Jiang J, Li Z, Wang H, Wang Y, Carlson MA, Teusink MJ, et al. Expanded 3D Nanofiber Scaffolds: Cell Penetration, Neovascularization, and Host Response. Adv Healthc Mater. 2016 Dec;5(23):2993–3003.

313. Chen H, Malheiro A de BFB, van Blitterswijk C, Mota C, Wieringa PA, Moroni L. Direct Writing Electrospinning of Scaffolds with Multidimensional Fiber Architecture for Hierarchical Tissue Engineering. ACS Appl Mater Interfaces. 2017 Nov 8;9(44):38187–200.

314. Adhikari SP, Pant HR, Mousa HM, Lee J, Kim HJ, Park CH, et al. Synthesis of high porous electrospun hollow TiO2 nanofibers for bone tissue engineering application. J Ind Eng Chem . 2016 Mar 25;35:75–82.

315. He F-L, Li D-W, He J, Liu Y-Y, Ahmad F, Liu Y-L, et al. A novel layer-structured scaffold

View Article Online
DOI: 10.1039/D1TB02628C

with large pore sizes suitable for 3D cell culture prepared by near-field electrospinning. Mater Sci Eng C Mater Biol Appl. 2018 May 1;86:18–27.

316. Malda J, Visser J, Melchels FP, Jüngst T, Hennink WE, Dhert WJA, et al. 25th anniversary article: Engineering hydrogels for biofabrication. Adv Mater. 2013 Sep 25;25(36):5011–28.

317. Zhang YS, Yue K, Aleman J, Moghaddam KM, Bakht SM, Yang J, et al. 3D Bioprinting for Tissue and Organ Fabrication. Ann Biomed Eng. 2017 Jan;45(1):148–63.

318. Heinrich MA, Liu W, Jimenez A, Yang J, Akpek A, Liu X, et al. 3D Bioprinting: from Benches to Translational Applications. Small. 2019;15(23):1–47.

319. Li W, Mille LS, Robledo JA, Uribe T, Huerta V, Zhang YS. Recent Advances in Formulating and Processing Biomaterial Inks for Vat Polymerization-Based 3D Printing. Adv Healthc Mater. 2020 Aug;9(15):e2000156.

320. Hull CW. Apparatus for production of three-dimensional objects by stereolithography. Date of Patent: Mar. 1986;11.

321. Klimek L, Klein HM, Schneider W, Mösges R, Schmelzer B, Voy ED. Stereolithographic modelling for reconstructive head surgery. Acta Otorhinolaryngol Belg. 1993;47(3):329–34.

322. Raman R, Bhaduri B, Mir M, Shkumatov A, Lee MK, Popescu G, et al. Bioprinting: High-Resolution Projection Microstereolithography for Patterning of Neovasculature (Adv. Healthcare Mater. 5/2016) [Internet]. Vol. 5, Advanced Healthcare Materials. 2016. p. 622–622. Available from: http://dx.doi.org/10.1002/adhm.201670025

323. Bahnini I, Rivette M, Rechia A, Siadat A, Elmesbahi A. Additive manufacturing technology: the status, applications, and prospects [Internet]. Vol. 97, The International Journal of Advanced Manufacturing Technology. 2018. p. 147–61. Available from: http://dx.doi.org/10.1007/s00170-018-1932-y

324. Guzzi EA, Tibbitt MW. Additive Manufacturing of Precision Biomaterials. Adv Mater. 2020 Apr;32(13):e1901994.

325. Zhu W. 3D Printing of Functional Biomaterials for Tissue Modeling. 2016. 125 p.

326. Kadry H, Wadnap S, Xu C, Ahsan F. Digital light processing (DLP) 3D-printing technology and photoreactive polymers in fabrication of modified-release tablets. Eur J Pharm Sci. 2019 Jul 1;135:60–7.

327. Boland T, Wilson WC Jr, Xu T. Ink-jet printing of viable cells [Internet]. US Patent. 7051654, 2006 [cited 2021 Sep 2]. Available from: https://patentimages.storage.googleapis.com/c9/0b/a6/f62484b5d9521a/US7051654.pdf

328. Boland T, Xu T, Damon B, Cui X. Application of inkjet printing to tissue engineering. Biotechnol J. 2006 Sep;1(9):910–7.

329. Gao G, Schilling AF, Hubbell K, Yonezawa T, Truong D, Hong Y, et al. Improved

View Article Online
DOI: 10.1039/D1TB02628C

properties of bone and cartilage tissue from 3D inkjet-bioprinted human mesenchymal stem cells by simultaneous deposition and photocrosslinking in PEG-GelMA [Internet]. Vol. 37, Biotechnology Letters. 2015. p. 2349–55. Available from: http://dx.doi.org/10.1007/s10529-015-1921-2

330. Mandrycky C, Wang Z, Kim K, Kim D-H. 3D bioprinting for engineering complex tissues. Biotechnol Adv. 2016 Jul;34(4):422–34.

331. Wilson WC Jr, Boland T. Cell and organ printing 1: protein and cell printers. Anat Rec A Discov Mol Cell Evol Biol. 2003 Jun;272(2):491–6.

332. Yoon S, Park JA, Lee H-R, Yoon WH, Hwang DS, Jung S. Bioprinting: Inkjet-Spray Hybrid Printing for 3D Freeform Fabrication of Multilayered Hydrogel Structures (Adv. Healthcare Mater. 14/2018) [Internet]. Vol. 7, Advanced Healthcare Materials. 2018. p. 1870055. Available from: http://dx.doi.org/10.1002/adhm.201870055

333. Duocastella M, Colina M, Fernández-Pradas JM, Serra P, Morenza JL. Study of the laser-induced forward transfer of liquids for laser bioprinting [Internet]. Vol. 253, Applied Surface Science. 2007. p. 7855–9. Available from: http://dx.doi.org/10.1016/j.apsusc.2007.02.097

334. Guillemot F, Souquet A, Catros S, Guillotin B. Laser-assisted cell printing: principle, physical parameters versus cell fate and perspectives in tissue engineering [Internet]. Vol. 5, Nanomedicine. 2010. p. 507–15. Available from: http://dx.doi.org/10.2217/nnm.10.14

335. Ali M, Pages E, Ducom A, Fontaine A, Guillemot F. Controlling laser-induced jet formation for bioprinting mesenchymal stem cells with high viability and high resolution [Internet]. Vol. 6, Biofabrication. 2014. p. 045001. Available from: http://dx.doi.org/10.1088/1758-5082/6/4/045001

336. Murphy SV, Atala A. 3D bioprinting of tissues and organs. Nat Biotechnol. 2014 Aug;32(8):773–85.

337. Zein I, Hutmacher DW, Tan KC, Teoh SH. Fused deposition modeling of novel scaffold architectures for tissue engineering applications. Biomaterials. 2002 Feb;23(4):1169–85.

338. Ozbolat IT, Hospodiuk M. Current advances and future perspectives in extrusion-based bioprinting [Internet]. Vol. 76, Biomaterials. 2016. p. 321–43. Available from: http://dx.doi.org/10.1016/j.biomaterials.2015.10.076

339. Fielding GA, Bandyopadhyay A, Bose S. Effects of silica and zinc oxide doping on mechanical and biological properties of 3D printed tricalcium phosphate tissue engineering scaffolds. Dent Mater. 2012 Feb;28(2):113–22.

340. Sun D, Chang C, Li S, Lin L. Near-field electrospinning. Nano Lett. 2006 Apr;6(4):839–42.

341. Bisht GS, Canton G, Mirsepassi A, Kulinsky L, Oh S, Dunn-Rankin D, et al. Controlled continuous patterning of polymeric nanofibers on three-dimensional substrates using low-voltage near-field electrospinning. Nano Lett. 2011 Apr 13;11(4):1831–7.

View Article Online
DOI: 10.1039/D1TB02628C

342. An BW, Kim K, Lee H, Kim S-Y, Shim Y, Lee D-Y, et al. High-Resolution Printing of 3D Structures Using an Electrohydrodynamic Inkjet with Multiple Functional Inks. Adv Mater. 2015 Aug 5;27(29):4322–8.

343. de Ruijter M, Hrynevich A, Haigh JN, Hochleitner G, Castilho M, Groll J, et al. Out-of-Plane 3D-Printed Microfibers Improve the Shear Properties of Hydrogel Composites. Small [Internet]. 2018 Feb;14(8). Available from: http://dx.doi.org/10.1002/smll.201702773

344. Khaled A-RA, Vafai K. The role of porous media in modeling flow and heat transfer in biological tissues [Internet]. Vol. 46, International Journal of Heat and Mass Transfer. 2003. p. 4989–5003. Available from: http://dx.doi.org/10.1016/s0017-9310(03)00301-6

345. Tsai M-H, Haung C-F, Shyu S-S, Chou Y-R, Lin M-H, Peng P-W, et al. Surface modification induced phase transformation and structure variation on the rapidly solidified recast layer of titanium. Mater Charact. 2015 Aug 1;106:463–9.

346. Ran Q, Yang W, Hu Y, Shen X, Yu Y, Xiang Y, et al. Osteogenesis of 3D printed porous Ti6Al4V implants with different pore sizes. J Mech Behav Biomed Mater. 2018 Aug;84:1–11.

347. Reznikov N, Boughton OR, Ghouse S, Weston AE, Collinson L, Blunn GW, et al. Individual response variations in scaffold-guided bone regeneration are determined by independent strain- and injury-induced mechanisms. Biomaterials. 2019 Feb;194:183–94.

348. Ashammakhi N, Wimpenny I, Nikkola L, Yang Y. Electrospinning: Methods and development of biodegradable nanofibres for drug release [Internet]. Vol. 5, Journal of Biomedical Nanotechnology. 2009. p. 1–19. Available from: http://dx.doi.org/10.1166/jbn.2009.1003

349. Jeong J, Kim JH, Shim JH, Hwang NS, Heo CY. Bioactive calcium phosphate materials and applications in bone regeneration. Biomater Res. 2019 Jan 14;23:4.

350. Inzana JA, Olvera D, Fuller SM, Kelly JP, Graeve OA, Schwarz EM, et al. 3D printing of composite calcium phosphate and collagen scaffolds for bone regeneration. Biomaterials. 2014 Apr;35(13):4026–34.

351. Shi H, Yang S, Zeng S, Liu X, Zhang J, Zhang J, et al. Enhanced angiogenesis of biodegradable iron-doped octacalcium phosphate/poly(lactic-co-glycolic acid) scaffold for potential cancerous bone regeneration [Internet]. Vol. 15, Applied Materials Today. 2019. p. 100–14. Available from: http://dx.doi.org/10.1016/j.apmt.2019.01.002

352. Lai Y, Cao H, Wang X, Chen S, Zhang M, Wang N, et al. Porous composite scaffold incorporating osteogenic phytomolecule icariin for promoting skeletal regeneration in challenging osteonecrotic bone in rabbits. Biomaterials. 2018 Jan;153:1–13.

353. Becker ST, Bolte H, Krapf O, Seitz H, Douglas T, Sivananthan S, et al. Endocultivation: 3D printed customized porous scaffolds for heterotopic bone induction. Oral Oncol [Internet]. 2009 Nov;45(11). Available from: http://dx.doi.org/10.1016/j.oraloncology.2009.07.004

View Article Online
DOI: 10.1039/D1TB02628C

354. Zhang J, Zhao S, Zhu Y, Huang Y, Zhu M, Tao C, et al. Three-dimensional printing of strontium-containing mesoporous bioactive glass scaffolds for bone regeneration. Acta Biomater. 2014;10(5):2269–81.

355. Tamburaci S, Tihminlioglu F. Novel poss reinforced chitosan composite membranes for guided bone tissue regeneration. J Mater Sci Mater Med. 2017 Dec 1;29(1):1.

356. Petersen A, Princ A, Korus G, Ellinghaus A, Leemhuis H, Herrera A, et al. A biomaterial with a channel-like pore architecture induces endochondral healing of bone defects. Nat Commun. 2018 Oct 25;9(1):4430.

357. Zhang W, Feng C, Yang G, Li G, Ding X, Wang S, et al. 3D-printed scaffolds with synergistic effect of hollow-pipe structure and bioactive ions for vascularized bone regeneration [Internet]. Vol. 135, Biomaterials. 2017. p. 85–95. Available from: http://dx.doi.org/10.1016/j.biomaterials.2017.05.005

358. Hedayati R, Janbaz S, Sadighi M, Mohammadi-Aghdam M, Zadpoor AA. How does tissue regeneration influence the mechanical behavior of additively manufactured porous biomaterials? J Mech Behav Biomed Mater. 2017 Jan;65:831–41.

359. Bly RA, Bhrany AD, Murakami CS, Sie KCY. Microtia Reconstruction [Internet]. Vol. 24, Facial Plastic Surgery Clinics of North America. 2016. p. 577–91. Available from: http://dx.doi.org/10.1016/j.fsc.2016.06.011

360. Beck JC. The Anatomy, psychology, diagnosis and treatment of congenital malformation and absence of the ear. Laryngoscope. 1925;35(11).

361. Dormer KJ, Gan RZ. Biomaterials for implantable middle ear hearing devices. Otolaryngol Clin North Am. 2001 Apr;34(2):289–97.

362. Zim SA. Microtia reconstruction: an update. Curr Opin Otolaryngol Head Neck Surg. 2003 Aug;11(4):275–81.

363. Cao Y, Vacanti JP, Paige KT, Upton J, Vacanti CA. Transplantation of chondrocytes utilizing a polymer-cell construct to produce tissue-engineered cartilage in the shape of a human ear. Plast Reconstr Surg. 1997 Aug;100(2):297–302; discussion 303–4.

364. Xue J, Feng B, Zheng R, Lu Y, Zhou G, Liu W, et al. Engineering ear-shaped cartilage using electrospun fibrous membranes of gelatin/polycaprolactone. Biomaterials. 2013 Apr;34(11):2624–31.

365. O'Sullivan NA, Kobayashi S, Ranka MP, Zaleski KL, Yaremchuk MJ, Bonassar LJ, et al. Adhesion and integration of tissue engineered cartilage to porous polyethylene for composite ear reconstruction. J Biomed Mater Res B Appl Biomater. 2015 Jul;103(5):983–91.

366. Zhao X, Bichara DA, Zhou L, Kulig KM, Tseng A, Bowley CM, et al. Conditions for seeding and promoting neo-auricular cartilage formation in a fibrous collagen scaffold [Internet]. Vol. 43, Journal of Cranio-Maxillofacial Surgery. 2015. p. 382–9. Available from: http://dx.doi.org/10.1016/j.jcms.2014.12.007

View Article Online
DOI: 10.1039/D1TB02628C

367. Reiffel AJ, Kafka C, Hernandez KA, Popa S, Perez JL, Zhou S, et al. High-fidelity tissue engineering of patient-specific auricles for reconstruction of pediatric microtia and other auricular deformities. PLoS One. 2013 Feb 20;8(2):e56506.

368. Kang N, Liu X, Yan L, Wang Q, Cao Y, Xiao R. Different ratios of bone marrow mesenchymal stem cells and chondrocytes used in tissue-engineered cartilage and its application for human ear-shaped substitutes in vitro. Cells Tissues Organs. 2013;198(5):357–66.

369. Liao HT, Zheng R, Liu W, Zhang WJ, Cao Y, Zhou G. Prefabricated, ear-shaped cartilage tissue engineering by scaffold-free porcine chondrocyte membrane. Plast Reconstr Surg. 2015 Feb;135(2):313e – 321e.

370. Chen W-H, Liu H-Y, Tsai C-Y, Wu C-C, Wei H-J, Liu A, et al. The Potential Use of Platelet-Rich Plasma to Reconstruct the Microtia Chondrocyte in Human Auricular Cartilage Regeneration. J Nanomater [Internet]. 2015 May 18 [cited 2021 Feb 18];2015. Available from: https://www.hindawi.com/journals/jnm/2015/250615/

371. Martínez Ávila H, Feldmann E-M, Pleumeekers MM, Nimeskern L, Kuo W, de Jong WC, et al. Novel bilayer bacterial nanocellulose scaffold supports neocartilage formation in vitro and in vivo. Biomaterials. 2015 Mar;44:122–33.

372. Morrison KA, Cohen BP, Asanbe O, Dong X, Harper A, Bonassar LJ, et al. Optimizing cell sourcing for clinical translation of tissue engineered ears. Biofabrication. 2016 Dec 5;9(1):015004.

373. Nimeskern L, Martínez Ávila H, Sundberg J, Gatenholm P, Müller R, Stok KS. Mechanical evaluation of bacterial nanocellulose as an implant material for ear cartilage replacement. J Mech Behav Biomed Mater. 2013 Jun;22:12–21.

374. Walser J, Stok KS, Caversaccio MD, Ferguson SJ. Direct electrospinning of 3D auricle-shaped scaffolds for tissue engineering applications. Biofabrication. 2016 May 12;8(2):025007.

375. Lee J-S, Kim BS, Seo D, Park JH, Cho D-W. Three-Dimensional Cell Printing of Large-Volume Tissues: Application to Ear Regeneration. Tissue Eng Part C Methods. 2017 Mar;23(3):136–45.

376. Schroeder MJ, Lloyd MS. Tissue Engineering Strategies for Auricular Reconstruction. J Craniofac Surg. 2017 Nov;28(8):2007–11.

377. Lin AJ, Bernstein JL, Spector JA. Ear Reconstruction and 3D Printing: Is It Reality? Current Surgery Reports. 2018 Feb 1;6(2):4.

378. Ruszymah BHI, Chua KH, Mazlyzam AL, Aminuddin BS. Formation of tissue engineered composite construct of cartilage and skin using high density polyethylene as inner scaffold in the shape of human helix. Int J Pediatr Otorhinolaryngol. 2011 Jun;75(6):805–10.

379. Iyer K, Dearman BL, Wagstaff MJD, Greenwood JE. A Novel Biodegradable Polyurethane

View Article Online
DOI: 10.1039/D1TB02628C

Matrix for Auricular Cartilage Repair: An In Vitro and In Vivo Study. J Burn Care Res. 2016 Jul;37(4):e353–64.

380. Lee J-S, Hong JM, Jung JW, Shim J-H, Oh J-H, Cho D-W. 3D printing of composite tissue with complex shape applied to ear regeneration. Biofabrication. 2014 Jun;6(2):024103.

381. Jung JW, Lee J-S, Cho D-W. Computer-aided multiple-head 3D printing system for printing of heterogeneous organ/tissue constructs. Sci Rep. 2016 Feb 22;6:21685.

382. Park JY, Choi Y-J, Shim J-H, Park JH, Cho D-W. Development of a 3D cell printed structure as an alternative to autologs cartilage for auricular reconstruction. J Biomed Mater Res B Appl Biomater. 2017 Jul;105(5):1016–28.

383. Zhou G, Jiang H, Yin Z, Liu Y, Zhang Q, Zhang C, et al. In Vitro Regeneration of Patient-specific Ear-shaped Cartilage and Its First Clinical Application for Auricular Reconstruction. EBioMedicine. 2018 Feb;28:287–302.

384. Sterodimas A, de Faria J. Human auricular tissue engineering in an immunocompetent animal model. Aesthet Surg J. 2013 Feb;33(2):283–9.

385. Zopf DA, Flanagan CL, Mitsak AG, Brennan JR, Hollister SJ. Pore architecture effects on chondrogenic potential of patient-specific 3-dimensionally printed porous tissue bioscaffolds for auricular tissue engineering. Int J Pediatr Otorhinolaryngol. 2018 Nov;114:170–4.

386. Kasyanov VA, F D A, Parfenov VA, Kudan EV, Bulanova EA, Khesuani YD, et al. Development and Implantation of a Biocompatible Auricular Prosthesis [Internet]. Vol. 49, Biomedical Engineering. 2016. p. 327–30. Available from: http://dx.doi.org/10.1007/s10527-016-9559-5

387. Visser J, Peters B, Burger TJ, Boomstra J, Dhert WJA, Melchels FPW, et al. Biofabrication of multi-material anatomically shaped tissue constructs. Biofabrication. 2013 Sep;5(3):035007.

388. Otto IA, Melchels FPW, Zhao X, Randolph MA, Kon M, Breugem CC, et al. Auricular reconstruction using biofabrication-based tissue engineering strategies. Biofabrication. 2015 Jul 22;7(3):032001.

389. Cervantes TM, Bassett EK, Tseng A, Kimura A, Roscioli N, Randolph MA, et al. Design of composite scaffolds and three-dimensional shape analysis for tissue-engineered ear. J R Soc Interface. 2013 Oct 6;10(87):20130413.

390. Cohen BP, Hooper RC, Puetzer JL, Nordberg R, Asanbe O, Hernandez KA, et al. Long-Term Morphological and Microarchitectural Stability of Tissue-Engineered, Patient-Specific Auricles In Vivo. Tissue Eng Part A. 2016 Mar;22(5-6):461–8.

391. Lee JM, Sultan MT, Kim SH, Kumar V, Yeon YK, Lee OJ, et al. Artificial Auricular Cartilage Using Silk Fibroin and Polyvinyl Alcohol Hydrogel. Int J Mol Sci [Internet]. 2017 Aug 4;18(8). Available from: http://dx.doi.org/10.3390/ijms18081707

View Article Online
DOI: 10.1039/D1TB02628C

392. Bichara DA, O'Sullivan N-A, Pomerantseva I, Zhao X, Sundback CA, Vacanti JP, et al. The tissue-engineered auricle: past, present, and future. Tissue Eng Part B Rev. 2012 Feb;18(1):51–61.

393. Shasti M, Jacquet R, McClellan P, Yang J, Matsushima S, Isogai N, et al. Effects of FGF-2 and OP-1 in vitro on donor source cartilage for auricular reconstruction tissue engineering. Int J Pediatr Otorhinolaryngol. 2014 Mar;78(3):416–22.

394. Lin C-H, Yang I-C, Tsai C-H, Fang H-W, Ma H. Auricular Tissue Engineering Using Osteogenic Differentiation of Adipose Stem Cells with Small Intestine Submucosa. Plast Reconstr Surg. 2017 Aug;140(2):297–305.

395. Liu J, Li L, Suo H, Yan M, Yin J, Fu J. 3D printing of biomimetic multi-layered GelMA/nHA scaffold for osteochondral defect repair. Mater Des. 2019 Jun 5;171:107708.

396. Castilho M, Mouser V, Chen M, Malda J, Ito K. Bi-layered micro-fibre reinforced hydrogels for articular cartilage regeneration. Acta Biomater. 2019 Sep 1;95:297–306.

397. Lin H-Y, Tsai W-C, Chang S-H. Collagen-PVA aligned nanofiber on collagen sponge as bi-layered scaffold for surface cartilage repair. J Biomater Sci Polym Ed. 2017 May;28(7):664–78.

398. Mow VC, Kuei SC, Lai WM, Armstrong CG. Biphasic Creep and Stress Relaxation of Articular Cartilage in Compression: Theory and Experiments. J Biomech Eng. 1980 Feb 1;102(1):73–84.

399. Eftekhari A, Maleki Dizaj S, Sharifi S, Salatin S, Rahbar Saadat Y, Zununi Vahed S, et al. The Use of Nanomaterials in Tissue Engineering for Cartilage Regeneration; Current Approaches and Future Perspectives. Int J Mol Sci [Internet]. 2020 Jan 14;21(2). Available from: http://dx.doi.org/10.3390/ijms21020536

400. Olubamiji AD, Izadifar Z, Si JL, Cooper DML, Eames BF, Chen DXB. Modulating mechanical behaviour of 3D-printed cartilage-mimetic PCL scaffolds: influence of molecular weight and pore geometry. Biofabrication. 2016 Jun 22;8(2):025020.

401. Vishwanath V, Pramanik K, Biswas A. Optimization and evaluation of silk fibroin-chitosan freeze-dried porous scaffolds for cartilage tissue engineering application. J Biomater Sci Polym Ed. 2016 Mar 11;27(7):657–74.

402. Kankala RK, Lu F-J, Liu C-G, Zhang S-S, Chen A-Z, Wang S-B. Effect of Icariin on Engineered 3D-Printed Porous Scaffolds for Cartilage Repair. Materials [Internet]. 2018 Aug 9;11(8). Available from: http://dx.doi.org/10.3390/ma11081390

403. Wise JK, Yarin AL, Megaridis CM, Cho M. Chondrogenic differentiation of human mesenchymal stem cells on oriented nanofibrous scaffolds: engineering the superficial zone of articular cartilage. Tissue Eng Part A. 2009 Apr;15(4):913–21.

404. Chen W, Wang C, Gao Y, Wu Y, Wu G, Shi X, et al. Incorporating chitin derived glucosamine sulfate into nanofibers via coaxial electrospinning for cartilage regeneration.

View Article Online
DOI: 10.1039/D1TB02628C

Carbohydr Polym. 2020 Feb 1;229:115544.

405. Chen P, Xia C, Mo J, Mei S, Lin X, Fan S. Interpenetrating polymer network scaffold of sodium hyaluronate and sodium alginate combined with berberine for osteochondral defect regeneration. Mater Sci Eng C Mater Biol Appl. 2018 Oct 1;91:190–200.

406. Zhao P, Deng C, Xu H, Tang X, He H, Lin C, et al. Fabrication of photo-crosslinked chitosan- gelatin scaffold in sodium alginate hydrogel for chondrocyte culture. Biomed Mater Eng. 2014;24(1):633–41.

407. Lu H, Ko Y-G, Kawazoe N, Chen G. Cartilage tissue engineering using funnel-like collagen sponges prepared with embossing ice particulate templates. Biomaterials. 2010 Aug;31(22):5825–35.

408. Luo L, Eswaramoorthy R, Mulhall KJ, Kelly DJ. Decellularization of porcine articular cartilage explants and their subsequent repopulation with human chondroprogenitor cells. J Mech Behav Biomed Mater. 2015 Mar;55:21–31.

409. Zhang J, Wang J, Zhang H, Lin J, Ge Z, Zou X. Macroporous interpenetrating network of polyethylene glycol (PEG) and gelatin for cartilage regeneration. Biomed Mater. 2016 Jun 15;11(3):035014.

410. Etxabide A, Ribeiro RDC, Guerrero P, Ferreira AM, Stafford GP, Dalgarno K, et al. Lactose-crosslinked fish gelatin-based porous scaffolds embedded with tetrahydrocurcumin for cartilage regeneration. Int J Biol Macromol. 2018 Oct 1;117:199–208.

411. Izzo D, Palazzo B, Scalera F, Gullotta F, Lapesa V, Scialla S, et al. Chitosan scaffolds for cartilage regeneration: influence of different ionic crosslinkers on biomaterial properties. International Journal of Polymeric Materials and Polymeric Biomaterials. 2019 Oct 13;68(15):936–45.

412. Rajzer I, Kurowska A, Jabłoński A, Jatteau S, Śliwka M, Ziąbka M, et al. Layered gelatin/PLLA scaffolds fabricated by electrospinning and 3D printing- for nasal cartilages and subchondral bone reconstruction. Mater Des. 2018 Oct 5;155:297–306.

413. Piai V, Anderson KL, Lin JJ, Dewar C, Parvizi J, Dronkers NF, et al. Direct brain recordings reveal hippocampal rhythm underpinnings of language processing. Proc Natl Acad Sci U S A. 2016 Oct 4;113(40):11366–71.

414. Furth ME, Atala A. Chapter 6 - Tissue Engineering: Future Perspectives. In: Lanza R, Langer R, Vacanti J, editors. Principles of Tissue Engineering (Fourth Edition). Boston: Academic Press; 2014. p. 83–123.

415. Chapple CR, MacNeil S. The use of implanted materials for treating women with pelvic organ prolapse and stress urinary incontinence. Curr Opin Urol. 2019 Jul;29(4):431–6.

416. Pan S, Zhong Y, Shan Y, Liu X, Xiao Y, Shi H. Selection of the optimum 3D-printed pore and the surface modification techniques for tissue engineering tracheal scaffold in vivo reconstruction. J Biomed Mater Res A. 2019 Feb;107(2):360–70.

View Article Online
DOI: 10.1039/D1TB02628C

417. Hsieh T-Y, Dedhia R, Cervenka B, Tollefson TT. 3D Printing: current use in facial plastic and reconstructive surgery. Curr Opin Otolaryngol Head Neck Surg. 2017 Aug;25(4):291–9.

418. Sun H, Hu C, Zhou C, Wu L, Sun J, Zhou X, et al. 3D printing of calcium phosphate scaffolds with controlled release of antibacterial functions for jaw bone repair. Mater Des. 2020 Apr 1;189:108540.

419. Jessop ZM, Al-Sabah A, Gardiner MD, Combellack E, Hawkins K, Whitaker IS. 3D bioprinting for reconstructive surgery: Principles, applications and challenges. J Plast Reconstr Aesthet Surg. 2017 Sep;70(9):1155–70.

420. Intini C, Elviri L, Cabral J, Mros S, Bergonzi C, Bianchera A, et al. 3D-printed chitosan-based scaffolds: An in vitro study of human skin cell growth and an in-vivo wound healing evaluation in experimental diabetes in rats. Carbohydr Polym. 2018 Nov 1;199:593–602.

421. Cheng N, Jeschke MG, Sheikholeslam M, Datu A-K, Oh HH, Amini-Nik S. Promotion of dermal regeneration using pullulan/gelatin porous skin substitute. J Tissue Eng Regen Med. 2019 Nov;13(11):1965–77.

422. Xiong S, Zhang X, Lu P, Wu Y, Wang Q, Sun H, et al. A Gelatin-sulfonated Silk Composite Scaffold based on 3D Printing Technology Enhances Skin Regeneration by Stimulating Epidermal Growth and Dermal Neovascularization. Sci Rep. 2017 Jun 27;7(1):4288.

423. Joseph B, Augustine R, Kalarikkal N, Thomas S, Seantier B, Grohens Y. Recent advances in electrospun polycaprolactone based scaffolds for wound healing and skin bioengineering applications. Materials Today Communications. 2019 Jun 1;19:319–35.

424. Khan S, Ul-Islam M, Ikram M, Islam SU, Ullah MW, Israr M, et al. Preparation and structural characterization of surface modified microporous bacterial cellulose scaffolds: A potential material for skin regeneration applications in vitro and in vivo. Int J Biol Macromol. 2018 Oct 1;117:1200–10.

425. Sharma V, Kohli N, Moulding D, Afolabi H, Hook L, Mason C, et al. Design of a Novel Two-Component Hybrid Dermal Scaffold for the Treatment of Pressure Sores. Macromol Biosci [Internet]. 2017 Nov;17(11). Available from: http://dx.doi.org/10.1002/mabi.201700185

426. El-Serafi AT, El-Serafi IT, Elmasry M, Steinvall I, Sjöberg F. Skin regeneration in three dimensions, current status, challenges and opportunities. Differentiation. 2017 Jul;96:26–9.

427. Yin J, Zhang D, Xiang Y, Wei P, Yang Z, Wang Z, et al. The influence of cross-sectional morphology on the compressive resistance of polymeric nerve conduits. Polymer . 2018 Jul 18;148:93–100.

428. Shor E, Merdler U, Brosh I, Shoham S, Levenberg S. Induced neuro-vascular interactions robustly enhance functional attributes of engineered neural implants. Biomaterials. 2018 Oct;180:1–11.

View Article Online
DOI: 10.1039/D1TB02628C

429. Kong AM, Yap KK, Lim SY, Marre D, Pébay A, Gerrand Y-W, et al. Bio-engineering a tissue flap utilizing a porous scaffold incorporating a human induced pluripotent stem cell-derived endothelial cell capillary network connected to a vascular pedicle. Acta Biomater. 2019 May 30;94:281–94.

430. Singh A, Lee D, Jeong H, Yu C, Li J, Fang CH, et al. Tissue-Engineered Neo-Urinary Conduit from Decellularized Trachea. Tissue Eng Part A. 2018 Oct;24(19-20):1456–67.

431. Singh A, Lee D, Sopko N, Matsui H, Sabnekar P, Liu X, et al. Biomanufacturing Seamless Tubular and Hollow Collagen Scaffolds with Unique Design Features and Biomechanical Properties. Adv Healthc Mater [Internet]. 2017 Mar;6(5). Available from: http://dx.doi.org/10.1002/adhm.201601136

432. Eastwood MP, Daamen WF, Joyeux L, Pranpanus S, Rynkevic R, Hympanova L, et al. Providing direction improves function: Comparison of a radial pore-orientated acellular collagen scaffold to clinical alternatives in a surgically induced rabbit diaphragmatic tissue defect model. J Tissue Eng Regen Med. 2018 Nov;12(11):2138–50.

433. Kulikouskaya V, Kraskouski A, Hileuskaya K, Zhura A, Tratsyak S, Agabekov V. Fabrication and characterization of pectin-based three-dimensional porous scaffolds suitable for treatment of peritoneal adhesions. J Biomed Mater Res A. 2019 Aug;107(8):1814–23.

434. Sartoneva R, Kuismanen K, Juntunen M, Karjalainen S, Hannula M, Kyllönen L, et al. Porous poly-l-lactide-co-ε-caprolactone scaffold: a novel biomaterial for vaginal tissue engineering. R Soc Open Sci. 2018 Aug;5(8):180811.

435. Mohseni M, Bas O, Castro NJ, Schmutz B, Hutmacher DW. Additive biomanufacturing of scaffolds for breast reconstruction. Additive Manufacturing. 2019 Dec 1;30:100845.

436. Hosseini V, Evrova O, Hoerstrup SP, Vogel V. A Simple Modification Method to Obtain Anisotropic and Porous 3D Microfibrillar Scaffolds for Surgical and Biomedical Applications. Small [Internet]. 2018 Jan;14(4). Available from: http://dx.doi.org/10.1002/smll.201702650

437. Caballé-Serrano J, Zhang S, Ferrantino L, Simion M, Chappuis V, Bosshardt DD. Tissue Response to a Porous Collagen Matrix Used for Soft Tissue Augmentation. Materials [Internet]. 2019 Nov 11;12(22). Available from: http://dx.doi.org/10.3390/ma12223721

438. Auger FA, Gibot L, Lacroix D. The pivotal role of vascularization in tissue engineering. Annu Rev Biomed Eng. 2013 Aug 29;15:177–200.

439. Ben-Shaul S, Landau S, Levenberg S. Implanted scaffolds: Pre-ordered vessels halt ischaemia [Internet]. Vol. 1, Nature Biomedical Engineering. 2017. Available from: http://dx.doi.org/10.1038/s41551-017-0089

440. Rosenfeld D, Landau S, Shandalov Y, Raindel N, Freiman A, Shor E, et al. Morphogenesis of 3D vascular networks is regulated by tensile forces. Proc Natl Acad Sci U S A. 2016 Mar 22;113(12):3215–20.

View Article Online
DOI: 10.1039/D1TB02628C

441. Lin S, Mequanint K. Bioreactor-induced mesenchymal progenitor cell differentiation and elastic fiber assembly in engineered vascular tissues. Acta Biomater. 2017 Sep 1;59:200–9.

442. Ball O, Nguyen B-NB, Placone JK, Fisher JP. 3D Printed Vascular Networks Enhance Viability in High-Volume Perfusion Bioreactor. Ann Biomed Eng. 2016 Dec;44(12):3435–45.

443. Tresoldi C, Pacheco DP, Formenti E, Pellegata AF, Mantero S, Petrini P. Shear-resistant hydrogels to control permeability of porous tubular scaffolds in vascular tissue engineering. Mater Sci Eng C Mater Biol Appl. 2019 Dec;105:110035.

444. Jirofti N, Mohebbi-Kalhori D, Samimi A, Hadjizadeh A, Kazemzadeh GH. Small-diameter vascular graft using co-electrospun composite PCL/PU nanofibers. Biomed Mater. 2018 Aug 6;13(5):055014.

445. Guo F, Wang N, Wang L, Hou L, Ma L, Liu J, et al. An electrospun strong PCL/PU composite vascular graft with mechanical anisotropy and cyclic stability. J Mater Chem A Mater Energy Sustain [Internet]. 2015 Feb;3. Available from: http://dx.doi.org/10.1039/C4TA06845A

446. Stefani I, Cooper-White JJ. Development of an in-process UV-crosslinked, electrospun PCL/aPLA-co-TMC composite polymer for tubular tissue engineering applications. Acta Biomater. 2016 Mar 8;36:231–40.

447. Li C, Wang F, Douglas G, Zhang Z, Guidoin R, Wang L. Comprehensive mechanical characterization of PLA fabric combined with PCL to form a composite structure vascular graft. J Mech Behav Biomed Mater. 2016 Dec 15;69:39–49.

448. Park S, Kim J, Lee M-K, Park C, Jung H-D, Kim H-E, et al. Fabrication of strong, bioactive vascular grafts with PCL/collagen and PCL/silica bilayers for small-diameter vascular applications. Mater Des. 2019;181:108079.

449. Yao Y, Wang J, Cui Y, Xu R, Wang Z, Zhang J, et al. Effect of sustained heparin release from PCL/chitosan hybrid small-diameter vascular grafts on anti-thrombogenic property and endothelialization. Acta Biomater. 2014 Mar 4;10(6):2739–49.

450. Li Z, Zhou P, Zhou F, Zhao Y, Ren L, Yuan X. Antimicrobial eugenol-loaded electrospun membranes of poly(ε-caprolactone)/gelatin incorporated with REDV for vascular graft applications. Colloids Surf B Biointerfaces. 2018;162:335–44.

451. Pangesty AI, Arahira T, Todo M. Development and characterization of hybrid tubular structure of PLCL porous scaffold with hMSCs/ECs cell sheet. J Mater Sci Mater Med. 2017 Sep 15;28(10):165.

452. Abdal-hay A, Memic A, Hussein KH, Oh YS, Fouad M, Al-Jassir FF, et al. Rapid fabrication of highly porous and biocompatible composite textile tubular scaffold for vascular tissue engineering. Eur Polym J. 2017;96:27–43.

453. Wang MO, Vorwald CE, Dreher ML, Mott EJ, Cheng M-H, Cinar A, et al. Evaluating 3D-

View Article Online
DOI: 10.1039/D1TB02628C

Printed Biomaterials as Scaffolds for Vascularized Bone Tissue Engineering. Adv Mater. 2015;27(1):138–44.

454. Mehdizadeh H, Sumo S, Bayrak ES, Brey EM, Cinar A. Three-dimensional modeling of angiogenesis in porous biomaterial scaffolds. Biomaterials. 2013 Apr;34(12):2875–87.

455. Jia W, Gungor-Ozkerim PS, Zhang YS, Yue K, Zhu K, Liu W, et al. Direct 3D bioprinting of perfusable vascular constructs using a blend bioink. Biomaterials. 2016 Aug 2;106:58–68.

456. Odedra D, Chiu LLY, Shoichet M, Radisic M. Endothelial cells guided by immobilized gradients of vascular endothelial growth factor on porous collagen scaffolds. Acta Biomater. 2011;7(8):3027–35.

457. Klenke FM, Liu Y, Yuan H, Hunziker EB, Siebenrock KA, Hofstetter W. Impact of pore size on the vascularization and osseointegration of ceramic bone substitutes in vivo. J Biomed Mater Res A. 2008 Jun 1;85(3):777–86.

458. Lin Y, Xiao W, Liu X, Bal BS, Bonewald LF, Rahaman MN. Long-term bone regeneration, mineralization and angiogenesis in rat calvarial defects implanted with strong porous bioactive glass (13–93) scaffolds. J Non-Cryst Solids. 2016;432:120–9.

459. Cheng M-Q, Wahafu T, Jiang G-F, Liu W, Qiao Y-Q, Peng X-C, et al. A novel open-porous magnesium scaffold with controllable microstructures and properties for bone regeneration. Sci Rep. 2016 Apr 13;6:24134.

460. Diao J, Ding H, Huang M, Fu X, Zou F, Li T, et al. Bone Defect Model Dependent Optimal Pore Sizes of 3D-Plotted Beta-Tricalcium Phosphate Scaffolds for Bone Regeneration. Small Methods. 2019;3(11):1900237.

461. Liu Y, Yang S, Cao L, Zhang X, Wang J, Liu C. Facilitated vascularization and enhanced bone regeneration by manipulation hierarchical pore structure of scaffolds. Materials Science and Engineering: C. 2020;110:110622.

462. Bishop ES, Mostafa S, Pakvasa M, Luu HH, Lee MJ, Wolf JM, et al. 3-D bioprinting technologies in tissue engineering and regenerative medicine: Current and future trends. Genes Dis. 2017 Nov 22;4(4):185–95.

463. Vijayavenkataraman S, Yan W-C, Lu WF, Wang C-H, Fuh JYH. 3D bioprinting of tissues and organs for regenerative medicine. Adv Drug Deliv Rev. 2018 Jul 7;132:296–332.

464. Aljohani W, Ullah MW, Zhang X, Yang G. Bioprinting and its applications in tissue engineering and regenerative medicine. Int J Biol Macromol. 2017 Sep 21;107(Pt A):261–75.

465. Derakhshanfar S, Mbeleck R, Xu K, Zhang X, Zhong W, Xing M. 3D bioprinting for biomedical devices and tissue engineering: A review of recent trends and advances. Bioactive Materials. 2018;3(2):144–56.

466. Trachtenberg JE, Kasper FK, Mikos AG. Chapter 22 - Polymer Scaffold Fabrication. In: Lanza R, Langer R, Vacanti J, editors. Principles of Tissue Engineering (Fourth Edition).

View Article Online
DOI: 10.1039/D1TB02628C

Fourth Edition. Boston: Academic Press; 2014. p. 423–40.

467. Sandler N, Määttänen A, Ihalainen P, Kronberg L, Meierjohann A, Viitala T, et al. Inkjet printing of drug substances and use of porous substrates-towards individualized dosing. J Pharm Sci. 2011 Mar 1;100(8):3386–95.

468. Peng W, Datta P, Ayan B, Ozbolat V, Sosnoski D, Ozbolat IT. 3D bioprinting for drug discovery and development in pharmaceutics. Acta Biomater. 2017;57:26–46.

469. Peng W, Unutmaz D, Ozbolat IT. Bioprinting towards Physiologically Relevant Tissue Models for Pharmaceutics. Trends Biotechnol. 2016 Jun 10;34(9):722–32.

470. Yang Q, Lian Q, Xu F. Perspective: Fabrication of integrated organ-on-a-chip via bioprinting. Biomicrofluidics. 2017 May 9;11(3):031301.

471. Yi H-G, Lee H, Cho D-W. 3D Printing of Organs-On-Chips. Bioengineering (Basel) [Internet]. 2017 Jan 25;4(1). Available from: http://dx.doi.org/10.3390/bioengineering4010010

472. Zhang YS, Khademhosseini A. Engineering in vitro human tissue models through bio-design and manufacturing [Internet]. Vol. 3, Bio-Design and Manufacturing. 2020. p. 155–9. Available from: http://dx.doi.org/10.1007/s42242-020-00080-w

473. Park J, Jang J, Kang H-W. 3D Bioprinting and its application to organ-on-a-chip. Microelectron Eng [Internet]. 2018 Aug;200. Available from: http://dx.doi.org/10.1016/j.mee.2018.08.004

474. Li J, Parra-Cantu C, Wang Z, Zhang YS. Improving Bioprinted Volumetric Tumor Microenvironments In Vitro. Trends Cancer Res. 2020 Sep;6(9):745–56.

475. Liu T, Delavaux C, Zhang YS. 3D bioprinting for oncology applications. J 3D Print Med. 2019 Jun;3(2):55–8.

476. Charbe N, McCarron PA, Tambuwala MM. Three-dimensional bio-printing: A new frontier in oncology research. World J Clin Oncol. 2017 Feb 10;8(1):21–36.

477. Samavedi S, Joy N. 3D printing for the development of in vitro cancer models. Current Opinion in Biomedical Engineering. 2017;2:35–42.

478. Albritton JL, Miller JS. 3D bioprinting: improving in vitro models of metastasis with heterogeneous tumor microenvironments. Dis Model Mech. 2017 Jan 1;10(1):3–14.

479. Knowlton S, Joshi A, Yenilmez B, Ozbolat I, Chua K, Khademhosseini A, et al. Advancing cancer research using bioprinting for tumor-on-a-chip platforms. International Journal of Bioprinting [Internet]. 2016 Jun;2. Available from: http://dx.doi.org/10.18063/IJB.2016.02.003

480. Junttila MR, de Sauvage FJ. Influence of tumour micro-environment heterogeneity on therapeutic response. Nature. 2013 Sep 19;501(7467):346–54.

View Article Online
DOI: 10.1039/D1TB02628C

481. Kumar S, Kumari R, Sharma V. Coevolution mechanisms that adapt viruses to genetic code variations implemented in their hosts. J Genet. 2016 Mar;95(1):3–12.

482. Xu T, Rohozinski J, Zhao W, Moorefield EC, Atala A, Yoo JJ. Inkjet-mediated gene transfection into living cells combined with targeted delivery. Tissue Eng Part A. 2009 Jan;15(1):95–101.

483. Han S-O, Mahato RI, Sung YK, Kim SW. Development of Biomaterials for Gene Therapy [Internet]. Vol. 2, Molecular Therapy. 2000. p. 302–17. Available from: http://dx.doi.org/10.1006/mthe.2000.0142

484. Ozbolat IT. 10 - Future Trends. In: Ozbolat IT, editor. 3D Bioprinting. Oxford: Academic Press; 2017. p. 313–36.

485. Loozen L, Wegman F, Öner F, Dhert W, Alblas J. Porous bioprinted constructs in BMP-2 non-viral gene therapy for bone tissue engineering. J Mater Chem B Mater Biol Med [Internet]. 2013 Nov;1. Available from: http://dx.doi.org/10.1039/C3TB21093F

486. Lee K, Silva EA, Mooney DJ. Growth factor delivery-based tissue engineering: general approaches and a review of recent developments. J R Soc Interface. 2010 Aug 18;8(55):153–70.

487. Unger K, Rupprecht H, Valentin B, Kircher W. The use of porous and surface modified silicas as drug delivery and stabilizing agents [Internet]. Vol. 9, Drug Development and Industrial Pharmacy. 1983. p. 69–91. Available from: http://dx.doi.org/10.3109/03639048309048546

488. Parra-Nieto J, Del Cid MAG, de Cárcer IA, Baeza A. Inorganic Porous Nanoparticles for Drug Delivery in Antitumoral Therapy. Biotechnol J. 2021 Feb;16(2):e2000150.

489. Freeman FE, Kelly DJ. Tuning Alginate Bioink Stiffness and Composition for Controlled Growth Factor Delivery and to Spatially Direct MSC Fate within Bioprinted Tissues. Sci Rep. 2017 Dec 6;7(1):17042.

490. Ker EDF, Nain AS, Weiss LE, Wang J, Suhan J, Amon CH, et al. Bioprinting of growth factors onto aligned sub-micron fibrous scaffolds for simultaneous control of cell differentiation and alignment. Biomaterials. 2011 Aug 5;32(32):8097–107.

491. Braegelman AS, Webber MJ. Integrating Stimuli-Responsive Properties in Host-Guest Supramolecular Drug Delivery Systems. Theranostics. 2019 May 15;9(11):3017–40.

492. Ahuja G, Pathak K. Porous carriers for controlled/modulated drug delivery. Indian J Pharm Sci. 2009 Nov;71(6):599–607.

493. Patil P, Paradkar A. Porous polystyrene beads as carriers for self-emulsifying system containing loratadine. AAPS PharmSciTech. 2006 Mar 24;7(1):E28.

494. Lu J, Liong M, Sherman S, Xia T, Kovochich M, Nel AE, et al. Mesoporous Silica Nanoparticles for Cancer Therapy: Energy-Dependent Cellular Uptake and Delivery of

View Article Online
DOI: 10.1039/D1TB02628C

Paclitaxel to Cancer Cells. NanoBiotechnology. 2007 May 1;3(2):89–95.

495. Fu J, Su Y, Qin Y-X, Zheng Y, Wang Y, Zhu D. Evolution of metallic cardiovascular stent materials: A comparative study among stainless steel, magnesium and zinc. Biomaterials. 2020 Feb;230:119641.

496. Current status and future direction of metallic and polymeric materials for advanced vascular stents. Prog Mater Sci. 2022 May 1;126:100922.

497. Kowalski PS, Bhattacharya C, Afewerki S, Langer R. Smart Biomaterials: Recent Advances and Future Directions. ACS Biomater Sci Eng. 2018 Nov 12;4(11):3809–17.

498. Kaur G, Kumar V, Baino F, Mauro JC, Pickrell G, Evans I, et al. Mechanical properties of bioactive glasses, ceramics, glass-ceramics and composites: State-of-the-art review and future challenges. Mater Sci Eng C Mater Biol Appl. 2019 Nov;104:109895.

499. Punj S, Singh J, Singh K. Ceramic biomaterials: Properties, state of the art and future prospectives [Internet]. Vol. 47, Ceramics International. 2021. p. 28059–74. Available from: http://dx.doi.org/10.1016/j.ceramint.2021.06.238